

THESIS

UNDRAINED SHEAR BEHAVIOR OF MIXED MINE WASTE ROCK AND TAILINGS

Submitted by

Matteus M. P. Hamade

Department of Civil and Environmental Engineering

In partial fulfillment of the requirements

For the Degree of Master of Science

Colorado State University

Fort Collins, Colorado

Spring 2017

Masters Committee:

Advisor: Christopher A. Bareither

Joseph Scalia IV  
Jerry F. Magloughlin

Copyright by Matteus Hamade 2017

All Rights Reserved

## ABSTRACT

### UNDRAINED SHEAR BEHAVIOR OF MIXED MINE WASTE ROCK AND TAILINGS

The objective of this study was to evaluate the effect of variability in mixture ratio ( $R$ ) and tailings composition on shear behavior and shear strength of mixed mine waste rock and tailings (WR&T). Crushed gravel was used as a synthetic waste rock (SWR), and mixtures of sand, silt, and clay were used to create two synthetic mine tailings: average synthetic tailings (AST) and fine synthetic tailings (FST). Mixtures of WR&T were prepared with varying  $R$  to represent coarse-dominated structures to fine-dominated structures, as well as  $R = R_{opt}$ , which represents an optimal mixture ratio where tailings “just fill” void space of the waste rock. Pure SWR, pure tailings, and WR&T mixtures containing AST and FST were tested in consolidated-undrained triaxial compression at target effective confining stresses ( $\sigma'_c$ ) of 10, 50, and 100 kPa. The SWR and WR&T triaxial specimens were 150 mm in diameter by 300 mm tall, whereas the AST and FST specimens were 38 mm in diameter by 76 mm tall.

Dilative, strain-hardening behavior was observed for all triaxial tests on pure SWR, whereas contractive, strain-softening behavior was observed for all triaxial tests on pure FST. Triaxial tests on pure AST exhibited both dilative, strain-hardening behavior and contractive, strain-softening behavior; contractive behavior was observed for AST specimens that contained larger initial void ratios ( $e$ ) after consolidation. Waste rock and tailings mixtures that had coarse-dominated structures exhibited comparable undrained shear behavior to pure SWR. Fine-dominated WR&T mixtures exhibited undrained shear behavior that was more similar to the pure tailings; however, the addition of waste rock to tailings was observed to mitigate some contractive behavior as the addition of waste rock to tailings increased the tendency of the WR&T mixtures to exhibit dilative response. Mixtures prepared to target  $R_{opt}$  exhibited dilative, strain-hardening behavior. An analysis of flow behavior indicated that the addition of waste rock

to tailings to create WR&T mixtures improved flow behavior of pure tailings to a limited- or no-flow behavior that improves resistance against static liquefaction.

Shear strength parameters for all materials were calculated based on stress paths in  $p'$ - $q$  space reaching the failure line ( $K_f$  Line). Pure materials yielded effective tangent friction angle ( $\phi'_t$ ) of  $38^\circ$  for AST,  $39^\circ$  for FST, and  $41^\circ$  for SWR. The AST mixture with  $R \approx R_{opt}$  yielded  $\phi'_t = 48^\circ$ , which was the largest  $\phi'_t$  of all mixtures. Fine-dominated structures of AST (i.e.,  $R < R_{opt}$ ) yielded  $\phi'_t = 44^\circ$ . This increase in  $\phi'_t$  relative to the pure AST was attributed to the additional frictional resistance between the silty-sand AST and the SWR. The FST WR&T mixtures were only fine-dominated structures as all specimens yielded  $R < R_{opt}$ . The effective stress friction angle increased from  $32^\circ$  for FST mixtures prepared at  $R = 1.7$  to  $38^\circ$  for  $R = 2.5$ . The lower  $\phi'_t$  for the FST mixtures relative to the pure FST was attributed to looser tailings (i.e., higher void ratio) compared to the pure tailings specimens.

A steady-state analysis was performed with the assistance of mixture theory to determine if a single steady state line (SSL) could be relevant for WR&T mixtures that was independent of mixture ratio. Results showed that the use of equivalent void ratios for the steady-state analysis of mixtures provide a reasonable prediction of undrained shear behavior of mixtures. The analysis on AST mixtures demonstrates the effectiveness of equivalent void ratios both for fine- and coarse-dominated structures. The FST mixtures also supports the effectiveness of fine-dominated equivalent void ratios for assessing undrained shear behavior of mixtures. The steady state analysis supports the use of a single SSL for mixtures based on pure tailings and the use of equivalent void ratios that are both independent of  $R$ .

## ACKNOWLEDGEMENTS

I would like to express my appreciation to everyone that cooperated, directly and indirectly in the completion of this work. This thesis represents not only an academic and professional achievement, but also a time of personal growth.

Direct influence of Dr. Bareither since day one was crucial to the completion of this work. I would like to thank him for his patience and guidance, both academically and personally. My colleagues of the Geo-Group at CSU showed me that it is possible to develop strong friendships within the work environment. I appreciate the company and motivation provided by my friends in the office. Special thanks to Mohammad Gorakhki, Zhengguang Tian, Aliena Debelak, Saman Solemanian, and Shahin Ghazizadeh for their sustained company and support from the beginning to the end of this journey. I would also like to show my appreciation to all the people that recently joined the Geo-Group, your presence brought new life to the office. I have deep appreciation for all the professors of CSU, especially Dr. Shackelford and Dr. Scalia, for making classes so engaging by lecturing with excitement and interest. I would also like to thank Dr. Magloughlin for serving on my graduate committee.

I also want to thank those people within my social realm that may not have been directly involved in this research. Special thanks to Afonso de Lara, Salvador Lurbe, and Mirella Ortiz, your friendship made this experience unforgettable. Finally, and most importantly, I would like to thank my parents and my brother for showing their true support and love for me to achieve my personal goals.

## TABLE OF CONTENTS

	Page
ABSTRACT .....	ii
ACKNOWLEDGEMENTS .....	iv
TABLE OF CONTENTS .....	v
LIST OF TABLES .....	vii
LIST OF FIGURES .....	viii
LIST OF SYMBOLS .....	xi
CHAPTER 1: INTRODUCTION .....	1
1.1 Problem Statement .....	1
1.2 Research Objectives and Tasks .....	2
CHAPTER 2: BACKGROUND .....	4
2.1 Mine Waste .....	4
2.1.1 Waste Rock .....	4
2.1.2 Mine Tailings .....	5
2.2 Mixture Theory .....	7
2.2.1 Mixture Void Ratios .....	8
2.2.2 Previous Studies on Co-Mixed WR&T .....	10
2.3 Undrained Shear Behavior .....	11
CHAPTER 3: MATERIALS AND METHODS .....	20
3.1 Synthetic Waste Rock .....	20
3.2 Mine Tailings .....	21
3.3 Triaxial Compression Testing .....	22
3.3.1 Tailings Specimen Preparation .....	23
3.3.2 Specimen Preparation for Waste Rock and Waste Mixtures .....	24
3.3.3 Isotropic Consolidation .....	25
CHAPTER 4: RESULTS & DISCUSSION .....	33
4.1 Shear Behavior .....	33
4.1.1 Pure Materials .....	33
4.1.2 Waste Rock and Tailings Mixtures .....	36
4.2 Shear Strength .....	40
4.2.1 Evaluation and Definition of Failure .....	40

4.2.2 Shear Strength of Pure Waste Materials .....	41
4.2.3 Average Synthetic Tailings Mixture.....	42
4.2.4 Fine Synthetic Tailings Mixture .....	44
4.3 Steady State Analysis .....	45
4.3.1 Pure Materials .....	45
4.3.2 Waste Rock and Tailings Mixtures.....	47
CHAPTER 5: SUMMARY, CONCLUSION, AND FUTURE WORK.....	72
5.1 Summary and Conclusion.....	72
5.2 Future Research .....	73
REFERENCES .....	75
APPENDIX A: SAMPLE VOID RATIO CALCULATION.....	79

## LIST OF TABLES

Table 3.1. Summary of waste rock and tailings physical characteristics and classification.....	27
Table 4.1. Summary of tests parameters and results for pure materials. Failure criterion of reaching $K_f$ line was used to determine the effective friction angle and test parameters at failure. ....	51
Table 4.2. Summary of tests parameters and results for mixtures. Failure criterion of reaching $K_f$ line was used to determine the effective friction angle and test parameters at failure. ....	52
Table 4.3. Void ratio at initial conditions and at steady state with equivalent void ratios and parameters used in calculation. ....	53

## LIST OF FIGURES

Fig. 2.1.	Range and average particle-size distributions for mine tailings and waste rock compiled from Qiu and Segó (2001), Morris and Williams (2005), Khalili et al. (2005), Wickland and Wilson (2005), Wickland et al. (2006) Busnière (2007), Khalili et al. (2010), and Wickland et al. (2010). .....	15
Fig. 2.2.	Typical curve for rheology measurement of a non-Newtonian fluid in Bingham regime. Curve shows increase of strength with increase on concentration. For this study, concentration was chosen targeting initial strength gain, or paste tailings.....	16
Fig. 2.3.	Particle structure of co-mixed waste rock and tailings for different mixture ratios, $R$ . Adapted from Wickland et al. (2006). .....	17
Fig. 2.4.	Schematics of three possible undrained shear flow behaviors for (a) deviator stress ( $\Delta\sigma$ ) versus axial strain ( $\epsilon_a$ ), (b) effective stress paths, and (c) excess pore water pressure ( $u_e$ ) versus axial strain ( $\epsilon_a$ ). Modified from Bobei et al. (2009). .....	18
Fig. 2.5.	Graphical descriptions of the state parameter ( $\psi$ ) (Been and Jefferies, 1985), and demonstration of soil initial state ( $e_o$ ) and steady state ( $e_{ss}$ ) in e-p' space for undrained shear. ....	19
Fig. 3.1.	Particle size distribution for average synthetic tailings (AST), fine synthetic tailings (FST) and synthetic waste rock (SWR) developed for this study. Particle size bounds based on a compilation of relevant literature (Fig 2.1). .....	28
Fig. 3.2.	Compaction curves for average synthetic tailings (AST) and fine synthetic tailings (FST). Compaction curves were fitted with a 3rd-order polynomial based on Howell et al. (1997), and the coefficient of determination ( $R^2$ ) represents the fit of the polynomial to the compaction data. ....	29
Fig. 3.3.	Relationship between yield stress and solid content for average synthetic tailings (AST) and fine synthetic tailings (FST) based on modified slump test (Clayton 2003). Fitted curves were logarithmic approximation commonly used for mineral suspensions behave (Boger 2009). Concentrations were chosen to simulate qualitative threshold of paste tailings (Fig. 2.2b).....	30
Fig. 3.4.	Isotropic compression line (ICL) for both synthetic tailings by using height dependent consolidation described on consolidation of ASTM 4767. ....	31
Fig. 3.5.	Calculated values of $R_{opt}$ based on solid content for average synthetic tailings (AST) and fine synthetic tailings (FST). Calculations were based on Eq. 2.3 using following properties: $V_r = 1$ , SWR $\rho_r = 2.7$ , AST $\rho_{slurry} = 2.66$ , FST $\rho_{slurry} = 2.63$ , $e_r = 0.83$ and $w_t$ varying with SC. Schematic shows similarity of curves due to similarity of synthetic tailings. Chosen concentrations for synthetic tailings are shown. ....	32

Fig. 4.1. Relationships of (a) deviator stress and (b) excess pore water pressure versus axial strain for consolidated undrained triaxial compression test on synthetic waste rock. ....	54
Fig. 4.2. Relationships of (a) deviator stress and (b) excess pore water pressure versus axial strain for consolidated undrained triaxial compression test on average synthetic tailings. ....	55
Fig. 4.3. Relationships of (a) deviator stress and (b) excess pore water pressure versus axial strain for consolidated undrained triaxial compression test on fine synthetic tailings. ....	56
Fig. 4.4. Relationships of (a) deviator stress and (b) excess pore water pressure versus axial strain for consolidated undrained triaxial compression test on AST mixtures at $R > R_{opt}$ . ....	57
Fig. 4.5. Relationships of deviator stress and excess pore water pressure versus axial strain for consolidated undrained triaxial compression test on AST mixtures at $R = R_{opt}$ and $R < R_{opt}$ . ....	58
Fig. 4.6. Relationships of (a) principal stress ratio and (b) Skempton A parameter versus axial strain for consolidated undrained triaxial compression test on AST, SWR and AST mixtures at 100 kPa confining stress. ....	59
Fig. 4.7. Relationships of deviator stress and excess pore water pressure versus axial strain for consolidated undrained triaxial compression test on FST mixtures at $R = R_{opt}$ and $R < R_{opt}$ . ....	60
Fig. 4.8. Relationships of (a) principal stress ratio and (b) Skempton A parameter versus axial strain for consolidated undrained triaxial compression test on FST, SWR and FST mixtures at 100 kPa confining stress. ....	61
Fig. 4.9. Stress paths and $K_f$ line at $p'$ - $q$ space for analysis conducted using failure criterion of reaching $K_f$ line for SWR. ....	62
Fig. 4.10. Stress paths and $K_f$ line at $p'$ - $q$ space for analysis conducted using failure criterion of reaching $K_f$ line for AST, (a) a full failure envelope and (b) detail for repeat tests at 100 kPa. ....	62
Fig. 4.11. Stress paths and $K_f$ line at $p'$ - $q$ space for analysis conducted using failure criterion of reaching $K_f$ line for FST. ....	63
Fig. 4.12. Stress paths and $K_f$ line at $p'$ - $q$ space for analysis conducted using failure criterion of reaching $K_f$ line for (a) WR&T mixtures with AST at $R = R_{opt}$ and (b) WR&T mixtures with AST at $R < R_{opt}$ . ....	63
Fig. 4.13. Stress paths and $K_f$ line at $p'$ - $q$ space for analysis conducted using failure criterion of reaching $K_f$ line for WR&T mixtures with AST at $R > R_{opt}$ . ....	64

Fig. 4.14. Summary of $\phi'_t$ accounting for failure envelope and slope of $K_f$ line for AST, SWR and WR&T mixture with AST.....	64
Fig. 4.15. Stress paths and $K_f$ line at $p'$ - $q$ space for analysis conducted using failure criterion of reaching $K_f$ line for (a) WR&T mixtures with FST at $R = 2.5$ and (b) WR&T mixtures with FST at $R = 1.7$ . .....	65
Fig. 4.16. Stress paths at $p'$ - $q$ space for analysis of flow behavior comparing SWR, FST and FST mixtures at $\sigma'_c = 100$ kPa.....	65
Fig. 4.17. Summary of $\phi'_t$ accounting for failure envelope and slope of $K_f$ line for FST, SWR and WR&T-FST mixtures.....	66
Fig. 4.18. Relationships of AST global void ratio with mean effective stress for consolidated undrained triaxial tests. Isotropic consolidation line (ICL) and steady-state line (SSL) are shown as logarithmic regression lines.....	66
Fig. 4.19. Relationships of FST global void ratio with mean effective stress for consolidated undrained triaxial tests. Isotropic consolidation line (ICL) and steady-state line (SSL) are shown as logarithmic regression lines.....	67
Fig. 4.20. Relationships of SWR global void ratio with mean effective stress for consolidated undrained triaxial tests. Steady-state line (SSL) shown as logarithmic regression line. ....	67
Fig. 4.21. Relationships of (a) global void ratio, (b) tailings void ratio, and (c) rock void ratio with mean effective stress for consolidated undrained triaxial tests in WR&T-AST mixtures. ....	68
Fig. 4.22. Relationships of (a) global void ratio and (b) tailings void ratio and with mean effective stress for consolidated undrained triaxial tests in WR&T-FST mixtures. ....	69
Fig. 4.23. Relationships for equivalent fine void ratio and mean effective stress for (a) AST mixtures and (b) FST mixtures sheared undrained. ....	70
Fig. 4.24. Relationships for equivalent coarse void ratio and mean effective stress for AST mixtures sheared undrained. ....	71

## LIST OF SYMBOLS

$A$	Kempton's pore pressure parameter	$k$	hydraulic conductivity
$b$	fraction of fines active in transferring forces	$LL$	liquid limit
$D_{10}$	coarse fraction particle diameter at 10% finer	$M_r$	mass of waste rock
$d_{50}$	fine fraction particle diameter at 50% finer	$M_t$	mass of tailings
$d_{max}$	maximum particle size	$M_w$	mass of water
$e$	void ratio	$p'$	mean effective stress
$e_g$	global void ratio	$R$	mixture ratio
$e_i$	initial void ratio	$R_{opt}$	optimum mixture ratio
$e_{max}$	maximum void ratio	$u_e$	excess pore pressure
$e_{min}$	minimum void ratio	$u_{e,max}$	maximum excess pore pressure
$e_r$	waste rock void ratio	$V_a$	volume of air
$e_{ss}$	steady state void ratio	$V_s$	volume of solids
$e_t$	tailings void ratio	$V_{slurry}$	volume of tailings slurry
$e_r^*$	equivalent rock void ratio	$V_{,r}$	volume of waste rock
$e_t^*$	equivalent tailings void ratio	$V_{,t}$	volume of tailings
$f_c$	fines content	$V_v$	volume of voids
$f_{thres}$	threshold fines content	$V_{v,r}$	volume of voids in waste rock
$G_s$	specific gravity	$V_w$	volume of water
$G_{s,swr}$	specific gravity of synthetic waste rock	$w$	water content
$G_{s,asr}$	specific gravity of average synthetic tailings	$w_t$	tailings water content
$K_f$ line	failure line in $p'$ - $q$ space	$\Delta\sigma_d$ or $q$	deviator stress

$\Delta\sigma_{d,max}$	maximum deviator stress
$\epsilon_a$	axial strain
$\epsilon_{af}$	axial strain at failure
$\rho_{slurry}$	density of tailings slurry
$\rho_w$	density of water
$\sigma'_o$	initial effective stress
$\sigma'_1$	effective major principle stress
$\sigma'_3$	effective minor principle stress
$(\sigma'_1/\sigma'_3)_{max}$	maximum principle stress ratio
$\sigma'_c$	effective confining stress
$\phi'$	effective friction angle
$\phi'_{sc}$	effective secant state friction angle
$\phi'_t$	effective tangent state friction angle
$\psi$	state parameter

## CHAPTER 1: INTRODUCTION

### 1.1 Problem Statement

Waste generated from mining processes has been associated with social and environmental issues, while the volume of waste produced is increasing rapidly due population growth and exploitation of lower grade ore bodies. Geotechnical engineers are responsible for designing and maintaining facilities to manage the two most common types of mine waste: waste rock and tailings (Bussi re 2007; Blight 2010). Waste rock primarily consists of coarse-grained particles (e.g. sand, gravel, cobbles) and is generated via excavation of non-economical rock to access ore. Mine tailings are composed of sand-, silt-, and clay-size particles and are commonly managed as slurry (i.e., high water content) as result from ore processing. Due to differences in generation, handling, and composition of these two materials, mine tailings are managed in tailings storage facilities (TSF) and waste rock is managed in piles. Relevant challenges related to these waste facilities include mechanical stability, environmental contamination, water management, and closure and reclamation (Williams et al. 2003; Leduc et al. 2004; Wickland et al. 2006; Bussi re 2007; Blight 2010).

Co-mixing of waste rock and tailings (WR&T) has been evaluated as an option to improve the following challenges related to mine waste management: (i) reduce watershed disturbance by decreasing the footprint for waste disposal; (ii) improve water management by reducing potential contamination; (iii) increase stability of waste deposits to reduce risk of failure; and (iv) facilitate post closure and reclamation of mine waste facilities (e.g., Williams et al. 2003; Leduc et al. 2004; Wickland et al. 2006; Bussi re 2007). The mixture ratio ( $R$ ) of WR&T is defined as the ratio of dry mass of waste rock to dry mass of tailings. The optimum mixture ratio ( $R_{opt}$ ) represents a mixture where tailings “just fill” all waste rock void space, and this mixture state can serve as a water storage layer for a final cover system that can potentially mitigate exposure of mine waste to oxygen that can lead to acid mine drainage (AMD).

Evaluating shear behavior of a new earthen material via laboratory testing has key role in defining engineering properties for design (Khalili et al. 2005). Monotonic and cyclic triaxial tests on WR&T mixtures prepared at  $R_{opt}$  have improved shear behavior and shear strength when compared to pure tailings (Khalili et al. 2005; Khalili et al. 2010). Jehring and Bareither (2016) evaluated the effect of tailings composition on shear behavior of WR&T and found that mixtures prepared at  $R_{opt}$  with various types of tailings have shear strength comparable to waste rock; however, shear behavior of the mixture was dependent on composition of the tailings and the actual mixture ratio. Large-scale use of WR&T mixtures in mining and earthwork applications can be anticipated to exhibit spatial variability in the  $R$  ratio. Thus, an evaluation of the influence of  $R$  on engineering properties (e.g., shear strength parameters) is needed for design. Limited research has been performed on the geotechnical behavior of WR&T mixtures (Leduc et al. 2004; Wickland et al. 2006), and currently there are no existing studies on the effect of  $R$  on undrained shear behavior and shear strength of WR&T mixtures.

## **1.2 Research Objectives and Tasks**

The objective of this study was to evaluate the effect of  $R$  and tailings composition on the shear behavior and shear strength of WR&T. This study included one type of synthetic waste rock (SWR) and two types of synthetic mine tailings: average synthetic tailings (AST) and fine synthetic tailings (FST). The WR&T mixtures were prepared at various  $R$ , whereby mixtures at  $R < R_{opt}$  were fine-dominated by the tailings fraction and mixtures prepared at  $R > R_{opt}$  were coarse-dominated by the waste rock fraction. This study represents a step towards understanding the shear behavior of different WR&T mixtures such that guidelines and target mixtures can be developed for specific applications.

The following research tasks were completed as a part of this study:

1. Identified optimum mixture ratios ( $R_{opt}$ ) and target mixture ratios ( $R > R_{opt}$  and  $R < R_{opt}$ ) for WR&T mixtures composed of each synthetic tailings;
2. Determined specimen preparation techniques for pure materials and mixtures with different  $R$  that promote repeatability;
3. Evaluated shear strength and behavior of SWR, AST and FST to establish a baseline for comparison with the WR&T mixtures;
4. Evaluated shear behavior and shear strength of WR&T mixtures; and
5. Evaluated steady-state behavior of pure materials and mixtures to assess the uniqueness of a single steady-state line that can be used to represent the undrained shear behavior of mixtures at varying  $R$ .

Consolidated undrained (CU) triaxial compression tests were conducted on pure synthetic tailings, pure SWR, and mixtures of WR&T in accordance with ASTM D 4767 (2011). Large-scale triaxial (LSTX) compression tests were conducted on 150-mm-diameter specimens for synthetic waste rock and WR&T mixtures, and conventional 38-mm-diameter triaxial (TX) tests were conducted synthetic tailings. Different specimen preparation methods were used to better suit material tested. Triaxial compression tests on all materials were conducted at effective confining pressures ( $\sigma'_c$ ) = 10, 50, and 100 kPa to capture a failure envelope for each material.

## CHAPTER 2: BACKGROUND

The Mining, Minerals, and Sustainable Development Project (MMSD) reported in 2002 that approximately 3500 active mine waste facilities exist worldwide (MMSD 2002). Moreover, approximately one major tailings dam failure has been reported each year for the last 70 yr according to the World Information Service on Energy (WISE 2016). Hard rock mining operations, which include ore such as iron, copper, silver, gold, molybdenum, lead, and zinc, generate two predominant waste materials: mine tailings and waste rock. Tailings, residue generated from ore processing, typically are fine-grained with high water content (i.e., slurry), whereas waste rock primarily consists of coarse-grained particles (e.g. sand, gravel, cobbles) generated via excavation of non-economical rock to access ore. Tailings are managed within tailings storage facilities (TSFs) and waste rock typically is deposited in piles. Engineering design of TSFs and waste rock piles require short- and long-term considerations such as mechanical stability, water management, and environmental consideration. Co-mixing mine waste rock and tailings (WR&T) can offer engineering design improvement or solutions to challenges related to mine waste storage capacity, geotechnical stability, environmental contamination, and mine closure (Williams et al. 2003; Leduc et al. 2004; Wickland et al. 2006; Bussi re 2007).

### **2.1 Mine Waste**

#### *2.1.1 Waste Rock*

Waste rock properties generally include low compressibility, high hydraulic conductivity ( $k$ ), and high shear strength, which are typical of coarse-grained materials. Although geotechnical stability of waste rock piles is usually not a major concern, environmental contamination via acid mine drainage (AMD) presents a challenge at many mines.

Acid mine drainage is generated from the oxidation of sulfide minerals. Water and oxygen react with sulfide minerals to generate sulfuric acid, which is exacerbated when intact rock is crushed and exposed to atmospheric air and precipitation. Leachate from AMD contains dissolved metals and low pH, which can contaminate groundwater and streams and lead to long-term ecosystem damage (Jennings et al. 2008). According to MEND (2011), AMD is the largest liability for Canadian mines, with an estimated cost of 2 to 5 billion U.S. dollars to the mining industry each year.

The chemical processes involved in AMD are naturally occurring when sulfide minerals, oxygen, and water interact. However, AMD generated in a mining operation is typically large in volume and high in contaminant concentration. Due to the difficulty of treating AMD, most mitigation solutions have focused on avoiding acid generation. Common mitigation solutions isolate elements of the oxidation process, such as subaqueous disposal of waste rock to minimize oxygen exposure or backfilling in underground mining to minimize exposure to both oxygen and water. Another mitigation solution involved isolating oxygen from the system by mixing mine tailings and waste rock to form a material with limited oxygen diffusion potential (Williams et al. 2003).

### *2.1.2 Mine Tailings*

Mine tailings commonly are composed of sand-, silt-, and clay-size particles. Particle-size distributions (PSDs) representing the average, upper bound, and lower bound from literature on mine tailings are shown in Fig. 2.1. Variation in particle sizes and distribution is attributed to differences in mine operation, which include differences in mineral type and industrial extraction process.

The nature of mine tailings is similar to soils, and therefore, common geotechnical characteristics and properties of soils can be inferred for mine tailings. Tailings are generally classified as silty sands (SM) or non-plastic silts (ML) by the Unified Soil Classification System,

with low to moderate plasticity (Bussi re 2007). The hydraulic conductivity ( $k$ ) of hard rock tailings typically ranges between  $10^{-7}$  to  $10^{-9}$  m/s, which can vary within a TSF based on PSD that varies with depth and location (Bussi re 2007). Strength parameters measured in consolidated undrained (CU) tests, which include the effective stress friction angle ( $\phi'$ ), commonly range from  $30^\circ$  to  $42^\circ$  (Bussi re 2007). Although mine tailings have reasonable drained strength, the nature of the material (i.e., loosely deposited fine-grained material) can be potentially dangerous when subjected to undrained shear, whereby the contractive nature of some tailings can lead to dramatic loss of strength (Davies et al. 2002).

Rheology is the science that deals with flow and deformation of matter, and is used to describe the slurry behavior of mine tailings. Mineral suspensions (i.e., slurry tailings) commonly behave as non-Newtonian fluids that have fundamental properties of viscosity ( $\eta$ ) and yield stress ( $\tau_y$ ). A schematic of the relationship between shear stress ( $\tau$ ) and shear rate ( $\dot{\gamma}$ ) is shown in Fig 2.2(a). Viscosity is defined as the ratio of  $\tau$  to  $\dot{\gamma}$  and is represented by the slope of the  $\tau$ - $\dot{\gamma}$  relationship. Yield stress is a property of non-Newtonian fluids that represents the limit stress that the fluid resists before initiation of flow, and is represented as the  $\tau$ -intercept in Fig. 2.2(a). A common representation for non-Newtonian behavior of concentrated mineral suspensions, such as mine tailings, is a Bingham model, which assumes a linear relationship between  $\tau$  and  $\dot{\gamma}$  for  $\tau > \tau_y$ .

Solids content (SC) is a measure of concentration, defined as the ratio of dry solid mass to total mass, which influences the rheology of a non-Newtonian, Bingham fluid. Yield stress is a property that can describe the difference between slurry, paste, and cake (i.e., filtered) mine tailings. Although fixed numbers for  $\tau_y$  do not exist to determine the transition from slurry to paste to cake tailings, general ranges and empirical thresholds have been reported in literature (e.g., Bussi re 2007). The influence of SC on  $\tau_y$  of slurry tailings is shown in Figure 2.2(b). A logarithmic relationship can be used to describe the increase in  $\tau_y$  as a function SC (Boger

2009). Qualitative thresholds between slurry to cake tailings are shown on the logarithmic curve between  $\tau_y$  and SC, where a slight increase in  $\tau_y$  describes the transition from slurry to paste tailing, and a drastic increase of  $\tau_y$  describes the transition to cake tailings.

## 2.2 Mixture Theory

Mixtures of coarser- and finer-grained soils have been studied in geotechnical engineering to understand behavior and evaluate applicability (e.g., sand-bentonite, silty sands, etc.) (Chapuis 1990; Thevanayagam 1998; Thevanayagam et al. 2002; Gutierrez 2003; Wickland et al. 2010). A schematic with mixtures of varying coarser and finer fractions is shown in Fig 2.3. Mechanical behavior of mixtures with low fines content (i.e., percentage of fine-grained material in the mixture by dry mass) are mainly controlled by the coarse fraction and are referred to as coarse-dominated mixtures. With an increase in fines content, a threshold is reached whereupon the coarse-grained skeleton no longer retains particle-to-particle contacts. At this “threshold fines content”, mechanical behavior transitions to be controlled predominantly by the fine-grained matrix and is referred to as a fine-dominated mixture (Thevanayagam et al. 2002; Zuo 2015).

Various parameters have been used to describe mixtures of coarse and fine particles. Fines content ( $f_c$ ) is defined as ratio of the dry mass of the fine fraction to the total dry mass of the bulk mixture and has been used to describe shear behavior of silt and sand mixtures (Thevanayagam 1998). Waste rock and tailings mixtures have been evaluated as a function of the mixture ratio ( $R$ ):

$$R = \frac{M_r}{M_t} \quad (2.1)$$

where  $M_r$  is the mass of waste rock and  $M_t$  is the mass of tailings. The correlation between  $f_c$  and  $R$  is shown in Eq. 2.2.

$$R = \frac{1 - f_c}{f_c} \quad (2.2)$$

Wickland et al. (2006) introduced the concept of an optimum mixture ratio ( $R_{opt}$ ), which represents a mixture whereby the tailings matrix completely fills void space between the waste rock particles without compromising particle-to-particle contacts throughout the waste rock skeleton (Fig. 2.3). The  $R_{opt}$  represents the threshold mixture between coarse- and fine-dominated structures. An  $R_{opt}$  can be calculated based on mass-volume relationships with the following assumptions (Wickland et. al. 2006; Jehring and Bareither 2016): (i) rock, tailings, and water are incompressible; (ii) mass of air is negligible; (iii) waste rock void spaces are larger than the average tailings particles diameter, and (iv) waste rock volume ( $V_r$ ) = 1 unit volume. The formula for  $R_{opt}$  is as follows,

$$R_{opt} = \frac{M_r}{M_t} = \frac{\rho_r V_r}{\frac{\rho_{slurry} V_{slurry}}{1 + w_t}} = \frac{\rho_r V_r}{\frac{\rho_{slurry} e_r}{1 + w_t}} \quad (2.3)$$

where  $\rho_r$  is density of rock,  $V_r$  is volume of rock,  $\rho_{slurry}$  is density of slurry,  $V_{slurry}$  is volume of slurry, and  $w_t$  is water content of tailings.

### 2.2.1 Mixture Void Ratios

Thevanayagam (1998) investigated the effect of silt content on the undrained shear strength of silty sands and implied that the silty sand mixture can be described with three relevant void ratios: (i) global or bulk void ratio of the composite mixture,  $e_g$ , (ii) void ratio of the fine fraction,  $e_t$ , and (iii) void ratio of the coarser fraction,  $e_r$ . Thevanayagam (1998) presented the following two equations for  $e_r$  and  $e_t$  as a function of  $f_c$  for mixture with single specific gravity ( $G_s$ ):

$$e_r = \frac{e_g + f_c}{1 - f_c} \quad (2.4)$$

$$e_t = \frac{e_g}{f_c} \quad (2.5)$$

whereby  $e_r$  represents the void ratio of the coarse fraction and translate the active coarse frictional contact, and  $e_t$  represents the fine fraction void ratio, which safely ignores the coarse fraction once the volume of coarse does not affect the force transfer of fine grains. Thus, Thevanayagam (1998) reported three relevant void ratios ( $e_g$ ,  $e_r$ , and  $e_t$ ) can be used to describe a given mixture containing a distinct coarser and a finer fraction to more effectively evaluate shear behavior.

Thevanayagam (2007) considered coarse-fraction dominated mixtures (Fig. 2d) and fine-fraction dominated mixtures (Fig. 2.2b) separately to analyze the influence of imperfect mixing. For each mixture category, an equivalent void ratio was introduced to more effectively describe a fraction-specific void ratio (i.e.,  $e_r$  or  $e_t$ ). Subsequent studies have shown that these equivalent void ratios are effective parameters to compare mixture shear strength and behavior to the predominant fraction (Thevanayagam et al. 2002; Ni et al. 2004; Rahman et al. 2008; Bobei et al. 2009).

The coarse-fraction equivalent void ratio ( $e_r^*$ ) is:

$$e_r^* = \frac{e_g + (1-b) \cdot f_c}{1 - (1-b) \cdot f_c} \quad (2.6)$$

where  $b$  is a parameter that ranges from 0 and 1 and represents the influence of the finer-fraction on the transfer of stress during shear (Rahman et al. 2008). For  $b = 0$  there is no influence of the fine fraction on stress transfer throughout the mixture and Eq. 2.6 reduces to the equation for  $e_r$  in the mixture (Eq. 2.4). For  $b = 1$ , Eq. 2.6 reduces to  $e_r^* = e_g$ , which implies that

the global void ratio is more representative of the mixture as a whole. The fine-fraction equivalent void ratio ( $e_t^*$ ) for fine-fraction controlled mixtures is computed as:

$$e_t^* = \frac{e_g}{f_c + \frac{1-f_c}{d_R^m}} \quad (2.7)$$

where  $d_R$  is the particle size disparity (i.e.,  $D_{10}$  coarser fraction /  $D_{50}$  finer fraction) and  $m$  is a coefficient ranging between 0 and 1 that depends on particle characteristics and packing of the finer fraction. Thus, the  $b$  parameter in Eq. 2.6 and  $m$  parameter in Eq. 2.7 are empirical fitting parameters. In general,  $b$  and  $m$  decrease with an increase in  $d_r$  (Thevanayagam et al. 2007; Rahman et al. 2008).

Eq. 2.6 was derived assuming  $G_s$  of both coarse and fine fraction are the same (Thevanayagam et al. 2007). For materials with different  $G_s$  Eq. 2.8 will be used as adaptation. No necessary adaptation is needed for Eq. 2.7.

$$e_r^* = \frac{e_g \cdot G_{s,r} + [f_c(1-b)](G_{s,t} + e_g \cdot G_{s,t} - e_g \cdot G_{s,r})}{G_{s,r} [1 - f_c(1-b)]} \quad (2.8)$$

### 2.2.2 Previous Studies on Co-Mixed WR&T

Waste rock and tailings mixtures have been studied to evaluate the potential to reduce land requirements for waste disposal, protect acid generating rock from oxygen exposure, and as a low hydraulic conductivity material or water storage layer for final cover systems. These geotechnical engineering applications make co-managing WR&T an economical, long-term solution that can provide the following benefits: (i) reduce watershed disturbance by decreasing the footprint for waste disposal; (ii) improve water management by reducing potential contamination; (iii) increase stability of waste deposits to reduce risk of failure; and (iv) facilitate post closure and reclamation of mine waste facilities via improving final cover systems (Wickland et al. 2006).

Methods for mixing and managing WR&T include (i) co-mixing, (ii) co-layering, and (iii) co-disposal (Bussi re 2007). Co-layering consists of depositing waste rock and tailings in sequential layers, whereas co-disposal consists usually of using waste rock as a drainage layer at the bottom of tailings impoundment (Khalili et al. 2005). Co-layering and co-disposal primarily relate to disposal techniques whereby generation of AMD decreases, but homogeneity and proportions of the mixture are not critically important. In contrast, co-mixing implies creation of a controlled, homogeneous mixture with predictable engineering properties that can be incorporated into engineering design. Thus, in addition to mitigating AMD generation, co-mixed WR&T can be factored into engineering design (e.g., storage layer for final cover system earthen construction material) based on understanding the geotechnical properties of mixtures (e.g., compressibility, shear strength, hydraulic conductivity).

Experimental studies have been conducted on co-mixed WR&T to assess geotechnical behavior for mixtures (Leduc et al. 2004; Khalili et al. 2005; Wickland et al. 2006; Jehring and Bareither 2016). In general, mixed WR&T at  $R_{opt}$  has shear strength and compression behavior governed by the waste rock portion and  $k$  controlled by the tailings matrix. Monotonic and cyclic triaxial test results suggest that shear strength of a fine-dominated structure is comparable to pure tailings only with slight improvement, whereas coarse-dominated structures show behavior similar to pure waste rock. However, there are no studies with controlled coarse- and finer-fraction materials that have evaluated shear behavior and shear strength of WR&T mixtures for varying mixture ratio to confirm these general observations.

### **2.3 Undrained Shear Behavior**

The potential for undrained shear failure in co-mixed WR&T may develop due to concentrated loading of the tailings fraction in a fine dominated mixture. Evaluating the potential for undrained shear is important when considering application of a new material, and laboratory analysis has a key role in defining necessary undrained shear characteristics (Khalili et al.

2005). Generation of excess pore water pressure during undrained shear, either positive or negative, directly affects shear resistance. Positive excess pore pressure is generated from a tendency to contract (i.e. decrease volume) and can lead to strain-softening behavior. Negative excess pore pressure is generated from a tendency to dilate (i.e. increase volume) and can lead to strain-hardening behavior.

Schematics of possible undrained shear behavior for deviator stress ( $\Delta\sigma$ ) and excess pore water pressure ( $u_e$ ) versus axial strain ( $\epsilon_a$ ) and effective stress paths for undrained failure are shown in Fig. 2.4. The effective stress paths are shown in a  $p'$ - $q$  space, where  $p' = (\sigma_1' + \sigma_3')/2$ ,  $q = (\sigma_1' - \sigma_3')/2$ , and  $\sigma_1'$  and  $\sigma_3'$  are the major and minor principal effective stresses, respectively. The three different undrained shear behaviors are shown in Fig. 2.4 and include flow, limited-flow, and no-flow. The concept of flow is based on a material that will lose strength during undrained shear due to an increase in  $u_e$  such that the material “flows” as a liquid. This flow behavior represents a worst case scenario for undrained failure. No-flow behavior is representative of a dilative, strain-hardening material, whereby an increase in axial strain ( $\epsilon_a$ ) during undrained shear results in an increase in shear strength. Limited-flow behavior is characterized with a moderate loss of strength followed by an increase in strength, which is an intermediate behavior stage between flow and no-flow conditions. Shear behavior is affected by the initial state of the soil before undrained shear initiates, where state refers to the stress and physical condition of the soil and can be described by void ratio ( $e$ ) and mean effective stress ( $p'$ ).

A schematic of a relationship between void ratio and  $p'$  is shown in Fig. 2.5 that includes graphical descriptions of the state parameter ( $\psi$ ). Been & Jefferson (1991) defined  $\psi$  as the difference in void ratio between initial void ratio ( $e_i$ ) and void ratio that falls on the steady-state line (SSL) for the same  $p'$ . A given soil that is sheared undrained achieves a condition called steady state (SS), during which the soil shears at constant excess pore water pressure ( $u_e$ ) and

constant deviator stress ( $\Delta\sigma$ ) with increasing axial strain ( $\epsilon_a$ ). Soil particles within the shear plane at SS have been sufficiently re-orientated such that no additional increase in shear stress is needed to continue deformation. The SSL represents a series of SS points in  $e$ - $p'$  space, and is a unique line independent of initial stress state or stress history of soil (Casagrande 1975; Been and Jefferies 1985). The SSL is unique to a material, the same way as isotropic consolidation line (ICL), that represents the normally consolidated state of a soil in a  $e$ - $p'$  space.

The state parameter shown in Fig. 2.5 is helpful to quantify contractive or dilative behavior of a soil during undrained shear, which can be translated to the potential for flow behavior. Flow behavior is associated with positive  $\psi$ , or an initial state point that is located above the SSL in a  $p'$ - $e$  space. Limited-flow is associated with an initial point located near the SSL, and no-flow behavior is associated with negative  $\psi$ , or an initial state point below the SSL (Bobei et al. 2009). Limited-flow behavior is an intermediate flow behavior characterized by a change from an initially strain softening behavior to a strain hardening behavior. This behavior does not show constant  $u_e$  and  $\Delta\sigma$  for achievable  $\epsilon_a$  in laboratory experiments. Therefore, a given state ( $p'$ - $e$ ) of a soil exhibiting intermediate flow behavior can be referred to as quasi-steady-state (QSS) (Zhang and Garga 1997; Thevanayagam et al. 2002). Studies show that points for SS and QSS in  $p'$ - $e$  space fall essentially on the same SSL (Finno et al. 1996; Zhang and Garga 1997).

The possibility of flow behavior for a WR&T mixture is important for understanding the applicability of the material at different mixture ratios for geotechnical engineering projects. A combination of mixture theory with steady state behavior can provide an assessment and prediction of flow behavior of mixtures. Thevanayagam (2007) analyzed  $e_g$ ,  $e_t$ ,  $e_r$ ,  $e_t^*$ , and  $e_r^*$  in a SS  $p'$ - $e$  space using silty sand mixtures in the attempt to define a single SSL that was independent of mixture ratio. Definition of a single SSL for mixtures at different  $R$  allows a prediction of a mixture flow behavior based on initial state of the mixture. The use of  $e_g$  was not effective, as the SSL for each mixture changed slope as  $R$  varied. Fraction void ratios (i.e.,  $e_r$

and  $e_r$ ) were more effective descriptors of shear behavior of the mixtures for any  $R$ , once fraction void ratios were more representative of the host material; however, a single SSL was not possible to define.

Thevanayagram (2007) concluded that a single SSL, independent of  $R$ , can represent a mixture by using equivalent void ratios (i.e.,  $e_t^*$  and  $e_r^*$ ) that more effectively represent the coarser- or finer-dominated structure. Studies on flow behavior of silty sand mixtures indicate that a single SSL for any  $R$  can be determined using equivalent void ratios, considering that mixture will behave similar to the predominant host material at a comparable void ratio (Thevanayagram 2007; Rahman et al. 2008; Bobei et al. 2009). However, an investigation steady-state undrained shear behavior and flow behavior in WR&T mixtures has not been conducted. Previous work by Jehring and Bareither (2016) suggests that tailings composition in the finer fraction and  $R$  for  $R < R_{opt}$  are important factors that can lead to differences in flow behavior during undrained shear. This study was focused on an assessment of undrained shear behavior of synthetic mine residues to evaluate the effects of tailings composition and  $R$ , as well as evaluate the uniqueness of a single SSL for mixtures based on equivalent void ratios.

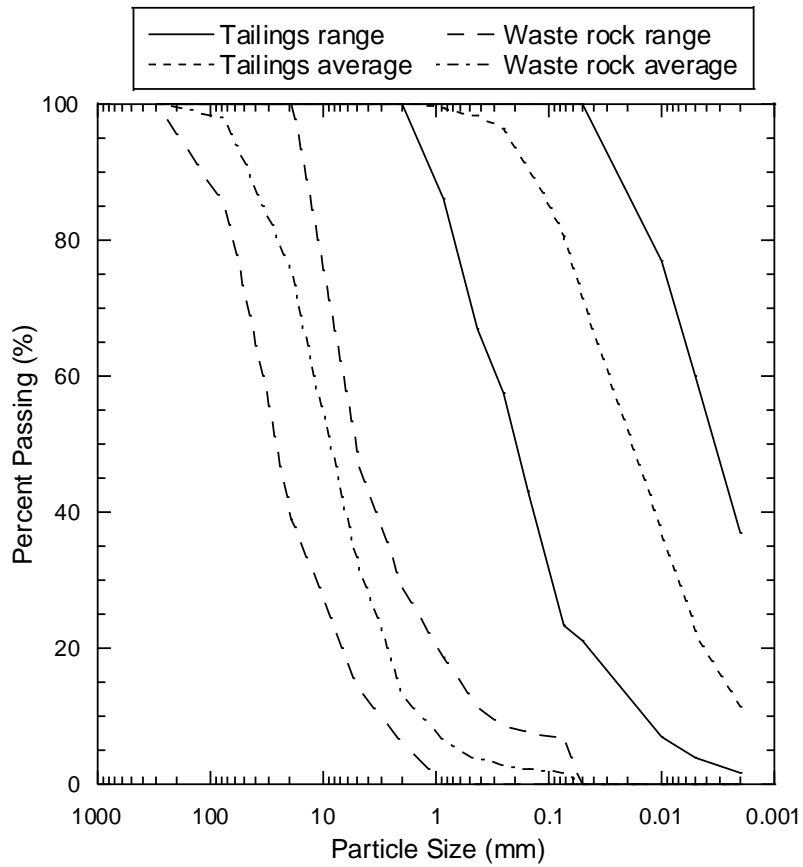


**Fig. 2.1.** Range and average particle-size distributions for mine tailings and waste rock compiled from Qiu and Segó (2001), Morris and Williams (2005), Khalili et al. (2005), Wickland and Wilson (2005), Wickland et al. (2006) Bussière (2007), Khalili et al. (2010), and Wickland et al. (2010).

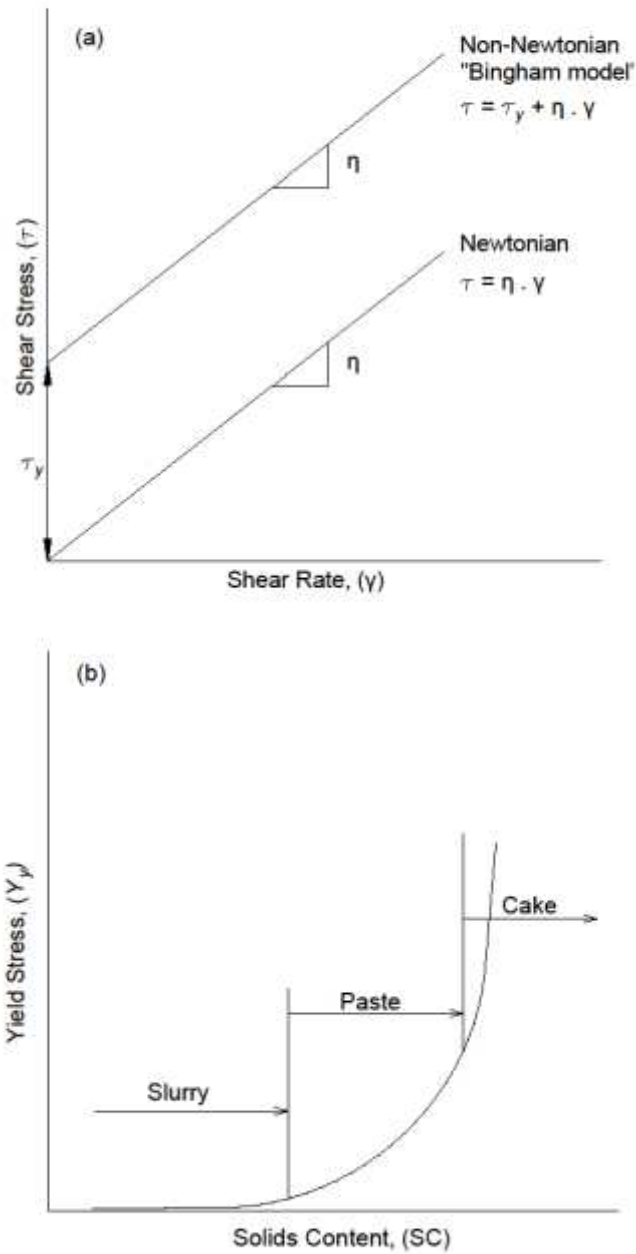


**Fig. 2.2.** Typical curve for rheology measurement of a non-Newtonian fluid in Bingham regime. Curve shows increase of strength with increase on concentration. For this study, concentration was chosen targeting initial strength gain, or paste tailings.

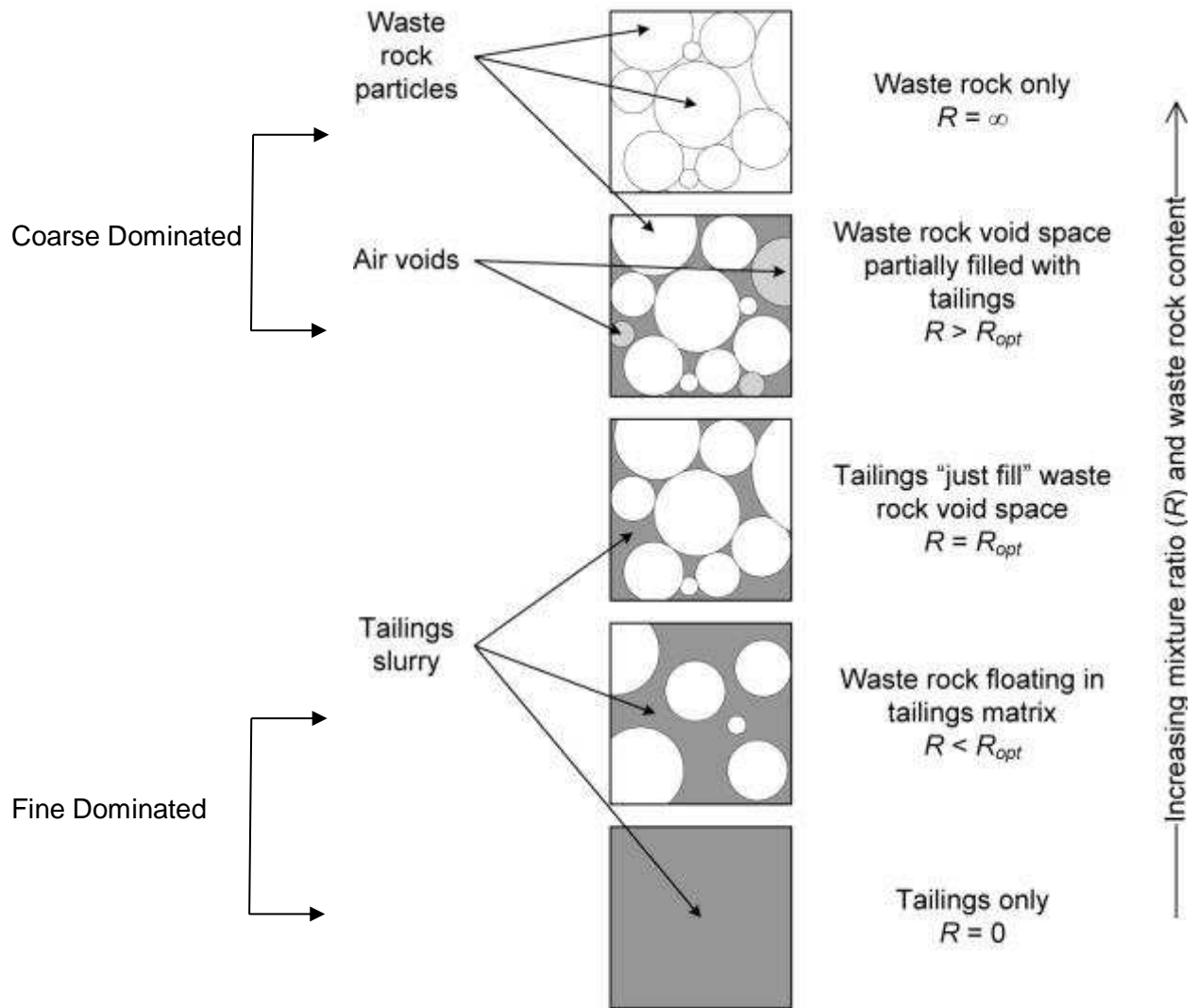


**Fig. 2.3.** Particle structure of co-mixed waste rock and tailings for different mixture ratios,  $R$ . Adapted from Wickland et al. (2006).

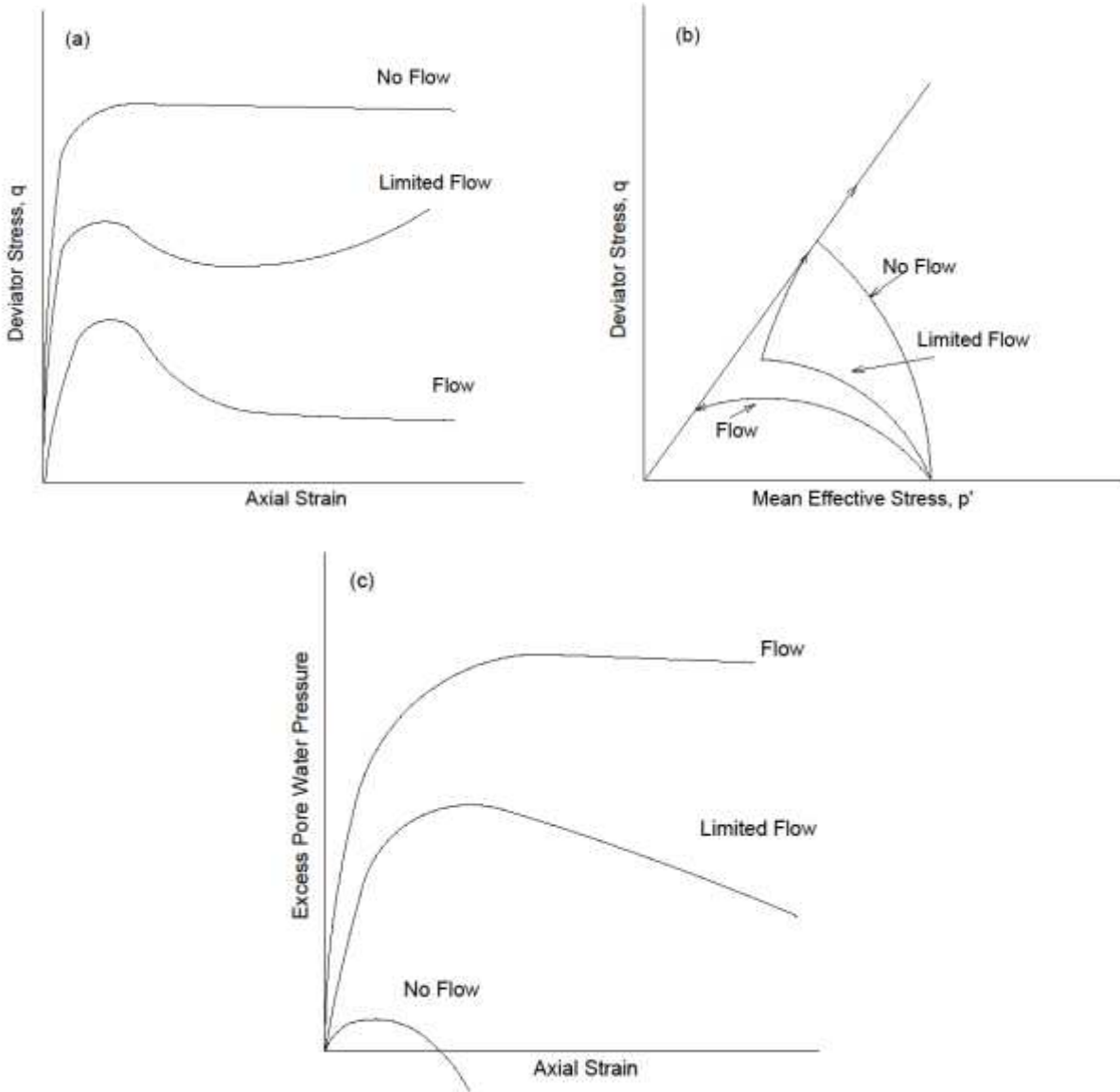


**Fig. 2.4.** Schematics of three possible undrained shear flow behaviors for (a) deviator stress ( $\Delta\sigma$ ) versus axial strain ( $\epsilon_a$ ), (b) effective stress paths, and (c) excess pore water pressure ( $u_e$ ) versus axial strain ( $\epsilon_a$ ). Modified from Bobei et al. (2009).

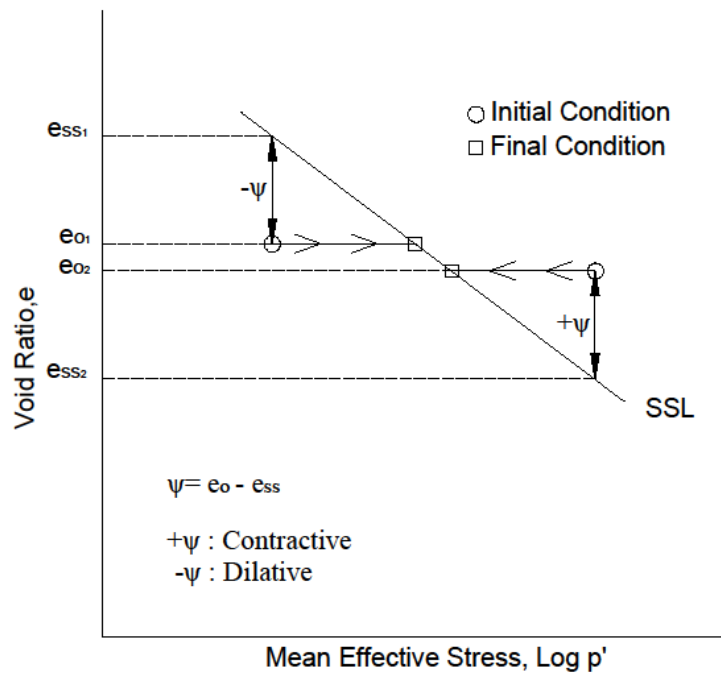


**Fig. 2.5.** Graphical descriptions of the state parameter ( $\psi$ ) (Been and Jefferies, 1985), and demonstration of soil initial state ( $e_o$ ) and steady state ( $e_{ss}$ ) in  $e$ - $p'$  space for undrained shear.

## CHAPTER 3: MATERIALS AND METHODS

This study included two types of synthetic mine tailings, average synthetic tailings (AST) and fine synthetic tailings (FST), and one type of synthetic waste rock (SWR). Synthetic mine wastes were created from commercially-available materials to control material variability and waste characteristics (e.g., pore water chemistry, PSD, water content). Synthetic mine tailings were created from mixing kaolin clay, composed mostly of clay size kaolinite (Thiele Kaolin Company, U.S.A.), silica powder, primarily containing mostly silt size silica (U.S Silica, Maryland, U.S.A.), and crushed sand that passed a No. 10 sieve (< 2 mm particle diameter). Synthetic waste rock was created from crushed granite obtained from a local quarry (Wyoming, USA).

### 3.1 Synthetic Waste Rock

The particle size distribution (PSD) for SWR is shown in Fig. 3.1 and geotechnical characteristics for the SWR are in Table 3.1. Synthetic waste rock was angular and primarily composed of granite. The SWR was classified as poorly-graded gravel according to the USCS (ASTM 2487). The target PSD for SWR was based on a compilation of waste rock PSDs from literature (Fig 2.1). Parallel particle gradation was applied to the average PSD compiled from literature to create SWR with a maximum particle diameter of 24.5 mm to adhere to particle constraints in laboratory testing (Marachi et al. 1972; Frossard et al. 2012; Jehring & Bareither 2016).

Maximum void ratio ( $e_{max}$ ) of SWR was determined according to Methods A and B in ASTM D 4254: Method A incorporated placing material in a 14,200-cm<sup>3</sup> mold via a hand scoop, and Method B incorporated removing a soil-filled tube from the mold such that material can flow out into the mold. Minimum void ratio ( $e_{min}$ ) was measured according ASTM D 4253-Method 2A, whereby a specimen is vibrated at a frequency of 60 Hz for 8 min with an 80-kg surcharge on

top of the specimen. Results of  $e_{max}$  from Method A was 0.83 and from Method B was 0.88; the  $e_{min}$  was 0.65. Specific gravity ( $G_s$ ) was measured using the buoyant weight method described in ASTM C 127. The  $G_s$  of 2.7 refers to an oven-dried specific gravity.

### 3.2 Mine Tailings

The particle size distribution (PSD) curves and geotechnical characteristics for synthetic tailings are in Fig 3.1 and Table 3.1, respectively. Synthetic tailings were created based on a PSD compilation for actual mine tailings (Fig 2.1) and the PSDs were measured using mechanical sieve and hydrometer testing (ASTM D422). Average synthetic tailings were composed of 20% crushed sand and 80% silica powder, by dry mass. Fine synthetic tailings were composed of 40% silica powder and 60% kaolin clay, by dry mass. Average synthetic tailings targeted the average PSD and FST targeted the lower bound PSD compiled from literature (Fig. 3.1). Close replication of the compiled PSDs from literature was achieved for both the AST and FST.

A compilation of geotechnical characteristics for AST and FST are in Table 3.1. Atterberg limits were evaluated following ASTM D4318; FST yielded a liquid limit ( $LL$ ) of 37% and plastic index ( $PI$ ) of 15%, where AST was non-plastic. Average synthetic tailings classified as low-plasticity silt (ML), and FST classified as low-plasticity clay (CL) according to the USCS. Compaction tests were executed following ASTM D 698 and the compaction curves for AST and FST are shown in Fig. 3.2. Optimum water content ( $w_{opt}$ ) for AST was estimated 17.6% representing a dry density ( $\gamma_d$ ) of 16.45 kN/m<sup>3</sup>, and for FST  $w_{opt} = 23\%$  corresponding to a  $\gamma_d = 14.9$  kN/m<sup>3</sup>. The water pycnometer method outlined in ASTM D 854 was used to determine a specific gravity ( $G_s$ ) of each commercially available material and for synthetic tailings. The  $G_s$  for AST was 2.66 and for FST 2.63.

### 3.3 Triaxial Compression Testing

Consolidated undrained (CU) triaxial compression tests were conducted on pure synthetic tailings, pure SWR, and mixtures of WR&T in accordance with ASTM D 4767. Triaxial tests were conducted at target effective confining stresses ( $\sigma'_c$ ) of 10, 50, and 100 kPa, which represent a range of effective stress that can be anticipated in final cover applications and shallow co-mixed WR&T deposits. All specimens were sheared to an axial strain of at least 20%. Saturation of the all specimens was confirmed via B-check, and  $B > 0.95$  was achieved for all tests. Specimens were consolidated via isotropic consolidation for 24 h after for each consolidation step after saturation. Changes in specimen height and volume were measured during consolidation to compute density and void ratio of the specimen prior to shearing.

Large-scale triaxial (LSTX) compression tests were conducted on 150-mm-diameter specimens for synthetic waste rock and WR&T mixtures. The maximum particle diameter ( $d_{max}$ ) was 25 mm to adhere with stipulations in ASTM D 4767. A linear variable displacement transducer (LVDT) was used to measure vertical displacement (Macro Sensors Model PR 750 2000,  $100 \pm 0.07$  mm) and a load cell was used to measure axial load (Tovey Engineering, Inc. Model SW20-25K-B00,  $110 \pm 0.29$  kN). Pressure transducers were used to measure cell and pore pressures (Omega Engineering, Inc. Model SR-PR-OM-1000,  $1000 \pm 0.1$  kPa) and collected by a data acquisition system (CATS Triaxial Mode 1.85, GCTS)

Conventional-scale 38-mm-diameter triaxial (TX) tests were conducted on synthetic tailings since all materials had  $d_{max} \leq 2$  mm. Axial load was measured using a load cell (Artech Industries, Inc.,  $8900 \pm 0.4$  N) and axial displacement was measured with an LVDT (Novotechnik,  $50 \pm 0.003$  mm). Cell and pore pressure were monitored with pressure transducers (GeoTac,  $1378 \pm 0.07$  kPa; ELE International, Ltd.,  $700 \pm 0.07$  kPa) and collected by a data acquisition system (CU Triaxial Mode, GeoTac)

Tailings specimens were isotopically consolidated within the triaxial cell prior to shearing. During consolidation, the change in specimen volume was measured using an outflow burette

and change in specimen height was measured via an LVDT. Specimen dimensions before shearing were performed following Method A in ASTM D 4767. Shear rate calculations were based on the time required to reach 50% primary consolidation as described in ASTM D 4767. Consolidated undrained tests containing AST were sheared at an axial strain rate of 5 %/h and tests on FST were sheared at 1 %/h. Pure waste rock specimens were sheared at axial strain rate of 20%/h.

### *3.3.1 Tailings Specimen Preparation*

Tailings specimens were prepared to target final dimensions of 38-mm diameter and 75-mm tall. A version of the slurry deposition method described in Wang et. al. (2011) was used to create triaxial specimens from tailings slurries. Slurry was poured into a 38-mm-diameter by 101-mm tall split mold lined with a 0.31-mm thick latex membrane. A 0.05-mm thick paper mold was placed on the outside of the latex membrane to keep the low strength slurry specimen intact after removing the split mold and assembling the triaxial cell. Once water was added to the triaxial cell, the paper lost strength and fell apart prior to shearing.

Tailings slurries were prepared at water contents intended to simulate the rheology of paste tailings based on  $\tau_y$ -SC relationships, whereby the transition from slurry to paste tailings corresponds to the SC at which a given tailing develops  $\tau_y$  (Fig. 2.2b). The  $\tau_y$  of AST and FST was measured via modified slump tests described in Clayton et al. (2003). Modified slump tests incorporated a 113.5-mm tall by 101.6-mm diameter PVC mold filled with tailings. Slump was measured as the vertical deformation of the specimen following removal of the PVC mold. Slump tests were performed on AST at SC = 72, 75, and 80% and on FST at SCs = 50, 60, 70 and 80%. Relationship between  $\tau_y$  and SC for AST and FST are shown in Fig 3.3. Logarithmic trend lines were added to the data sets based on recommendations in Boger (2009) for

representing rheological behavior of slurries. A SC = 72% ( $w = 40\%$ ) was selected for AST and SC = 60 ( $w = 66\%$ ) was selected for FST for all experiments in this study.

### 3.3.2 Specimen Preparation for Waste Rock and Waste Mixtures

Synthetic waste rock and WR&T specimens were prepared in a 300-mm tall by 150-mm diameter split mold lined with a 5-mm-thick rubber membrane. The membrane thickness was necessary for LSTX testing to avoid membrane puncture from the angular rock particles and to support the specimen during large axial deformations (i.e., up to 60 mm). Membrane correction calculations presented in by La Rochelle et al. (1998) were applied to LSTX test data to account for additional strength contributed by the membrane.

Specimen preparation for both pure SWR and WR&T at  $R_{opt}$  were intended to achieve a loose waste rock skeleton representative of  $e_{max}$ . The WR&T mixture at  $R_{opt}$  was prepared following the slurry displacement method in Khalili and Wijewickreme (2008). This method consists of depositing WR&T mixture into slurry tailings such that all void space, to the extent possible, is filled with tailings slurry. Mixture specimens were prepared in six layers, with each layer lightly tamped to achieve a level surface. A similar method to slurry displacement was used to prepare the pure SWR specimens. Clean waste rock particles were deposited in deionized and de-aired water in six layers, with each layer lightly taped to achieve a level surface.

An  $R_{opt}$  was computed for WR&T mixtures prepared with each synthetic tailings based on the following assumptions: (i) waste rock void ratio was equal to  $e_{max}$  and (ii) SC of the tailings were representative of paste tailings identified in Fig 3.3. A relationship between  $R_{opt}$  of these materials and tailings solid content is shown in Fig 3.5. The equation for  $R_{opt}$  (Eq. 2.3) has only two parameters ( $w_t$  and  $\rho_{slurry}$ ) that differ between AST and FST mixtures. As  $\rho_{slurry}$  for AST and FST are similar, the only parameter that influences resultant  $R_{opt}$  is  $w_t$ . The relationships between  $R_{opt}$  and SC for AST and FST in Fig. 3.5 are very similar, and the computed  $R_{opt}$  for

both mixture varies similarly, as a function of SC or  $w_t$ . Target  $R_{opt}$  for AST was 2.5 and for FST 3.4 (Fig. 3.5). The higher  $R_{opt}$  for FST was due to a lower SC (higher  $w_t$ ) for the FST, which reduced the mass of the tailings particles within the mixture relative to the AST mixtures.

In addition to the  $R_{opt}$  mixtures, WR&T mixtures containing AST and FST were created to represent fine-dominated ( $R < R_{opt}$ ) and coarse-dominated ( $R > R_{opt}$ ) structures. Different specimen preparation methods were required for these WR&T mixtures since the slurry displacement method was developed to create mixtures as  $R_{opt}$ . Specimen preparation procedures for these mixtures included thoroughly mixing tailings and waste rock fractions at in targeted  $w$  in a container to achieve the desired  $R$  and subsequently deposit the mixture into the mold in six even layers. Each layer was lightly tamped to achieve a level surface. The actual  $R$  of each triaxial specimen was measured following triaxial testing: samples were exhumed from the top, middle, and bottom of a given specimen to compute the actual  $R$  of each test specimen.

### 3.3.3 Isotropic Consolidation

Isotropic consolidation tests were performed on AST and FST to determine an isotropic consolidated line (ICL) to support the analysis of undrained shear behavior. These isotropic consolidation tests were conducted to simulate the consolidation stage described in ASTM D 4767. Specimens that were 71-mm diameter by 127-mm tall were prepared in a triaxial cell at the target initial water content of tailings slurries (40% for AST and 66% for FST). Change in height was manually recorded by rod on top of specimen and change in volume was measured with an outflow burette. The confining stress ( $\sigma_c$ ) was increased from 3.5 kPa to 110 kPa with a load increment ratio of 1 (i.e., stress increase / current stress = 1). Specimens were allowed to consolidate for 24 hr following each increase in  $\sigma_c$ , and volume change measurements were recorded on doubling-time interval (e.g., 1 min, 2 min, 4 min, 8 min, etc.).

Isotropic consolidation lines plotted in of  $p'$ - $e$  space for AST and FST are shown in Fig. 3.4. Logarithmic trendlines representing the ICLs for both synthetic tailings yielded coefficients

of determination ( $R^2$ ) greater than 0.98. As expected, FST yielded a steeper ICL compared to AST, which was attributed to the clay content of FST (Table 3.1) that yielded a more compressible material. Comparison with anisotropically consolidated AST and FST in odometers show normally consolidation lines in the similar magnitude and slope as ICL presented in this work (Gorakhki and Bareither, 2016)

**Table 3.1.** Summary of waste rock and tailings physical characteristics and classification.

Material	Fine Synthetic Tailings (FST)	Average Synthetic Tailings (AST)	Synthetic Waste Rock (SWR)
<i>LL</i> (%)	37	NA	NA
<i>PI</i> (%)	15	NA	NA
USCS	CL	ML	GP
$G_s$	2.63	2.66	2.7
$d_{max}$ (mm)	0.05	2	24.5
Gravel Content (%)	0	0	98
Sand Content (%)	0	14.2	2
Fines Content (%)	100	85.8	0
Clay Content (%)	42	13	0
$e_{min}$	NA	NA	0.65
$e_{max}$	NA	NA	0.83, 0.88
$w_{opt}$ (%)	23	17.6	0
$\gamma_{dmax}$ (kN/m <sup>3</sup> )	14.9	16.45	16.37

Note: *LL* = liquid limit; *PI* = plasticity index (ASTM D4318); USCS = Unified Soil Classification System (ASTM D2487);  $d_{max}$  = maximum particle size (ASTM D422);  $G_s$  = specific gravity (ASTM D854);  $w_{opt}$  = optimum water content and  $\gamma_{dmax}$  = maximum dry unit weight (ASTM D698);  $e_{min}$  &  $e_{max}$  (ASTM D 4253 & 4254); NA = not applicable.

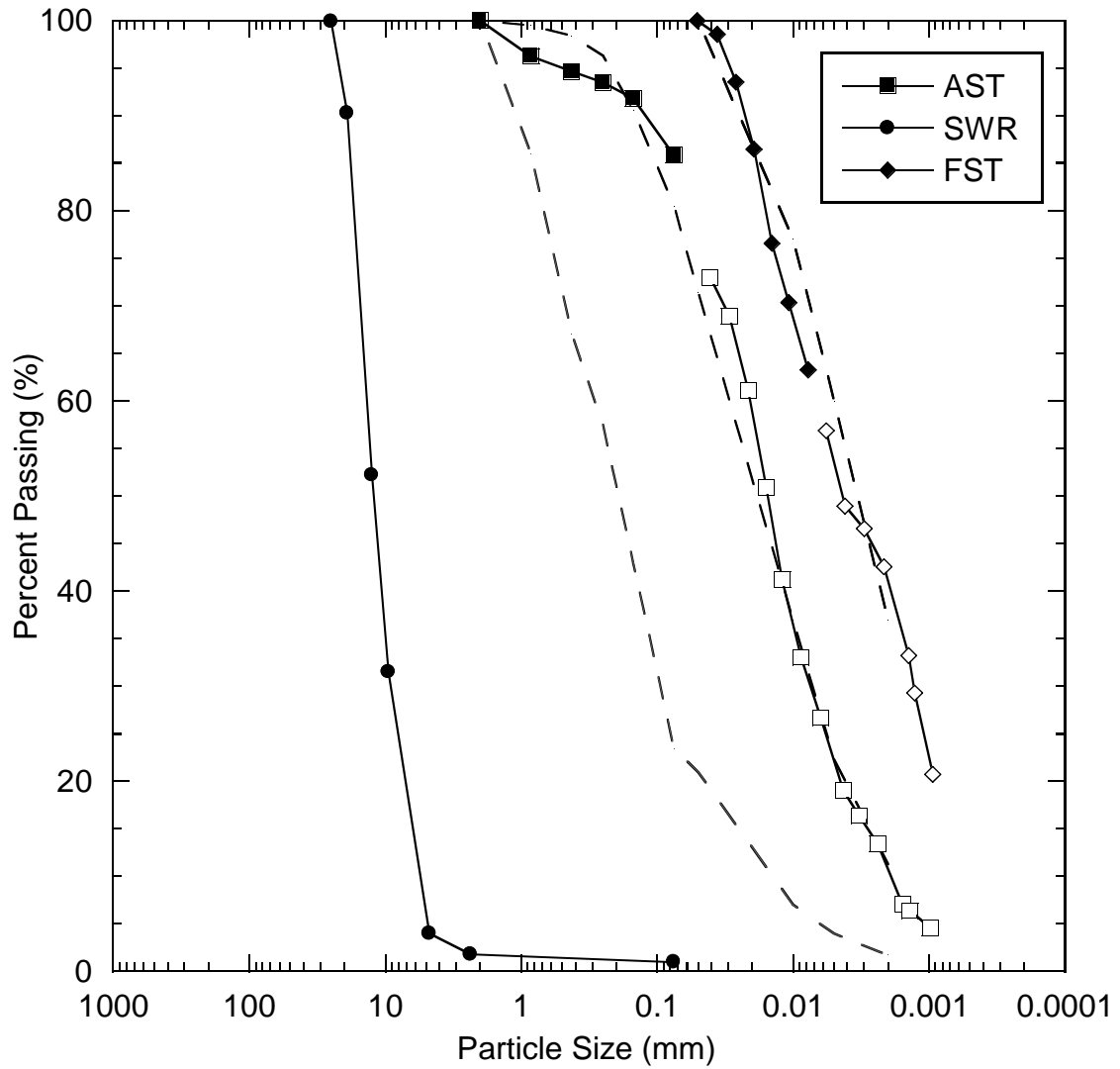


**Fig. 3.1.** Particle size distribution for average synthetic tailings (AST), fine synthetic tailings (FST) and synthetic waste rock (SWR) developed for this study. Particle size bounds based on a compilation of relevant literature (Fig. 2.1).

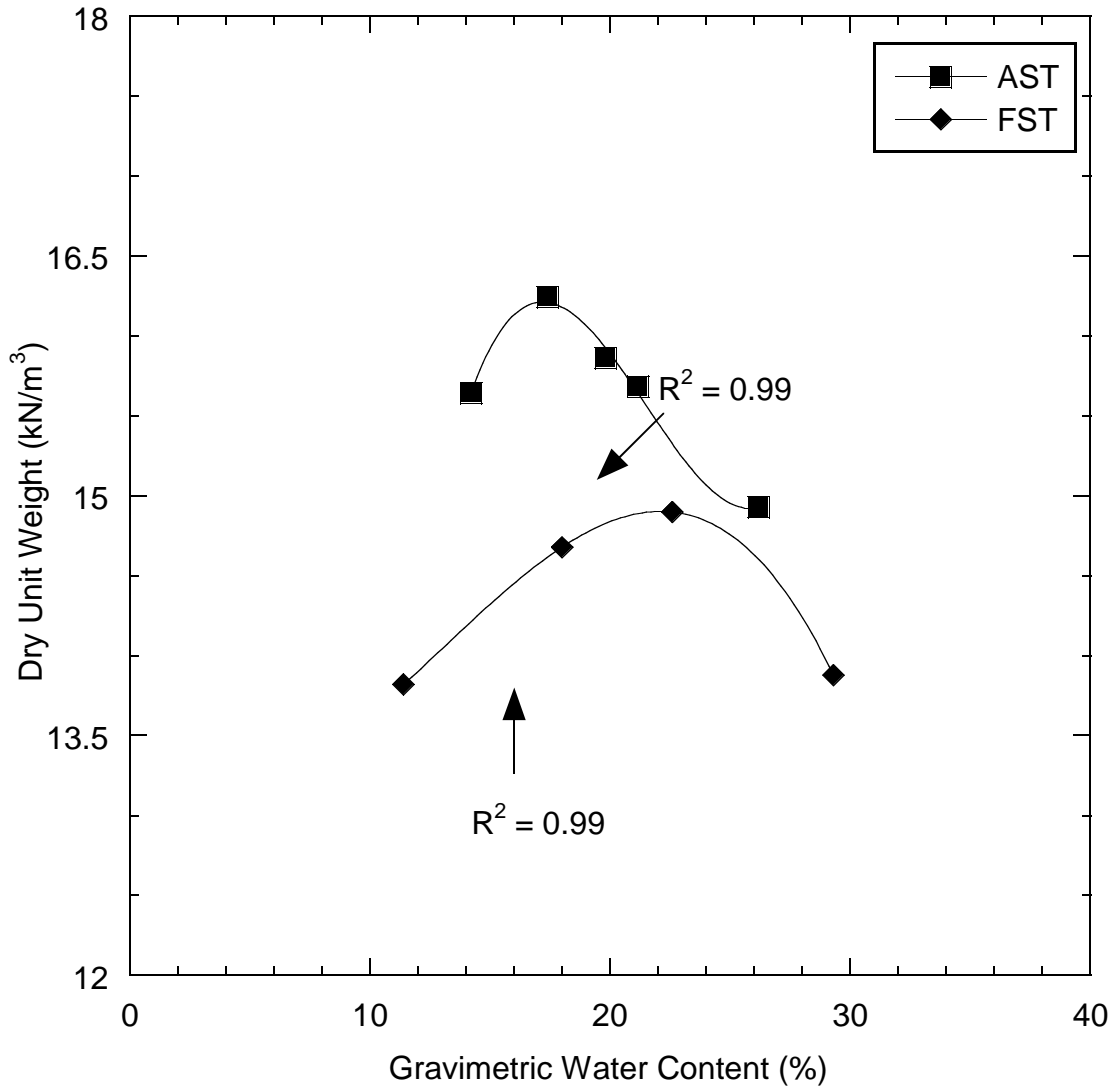


**Fig. 3.2.** Compaction curves for average synthetic tailings (AST) and fine synthetic tailings (FST). Compaction curves were fitted with a third-order polynomial based on Howell et al. (1997), and the coefficient of determination ( $R^2$ ) represents the fit of the polynomial to the compaction data.

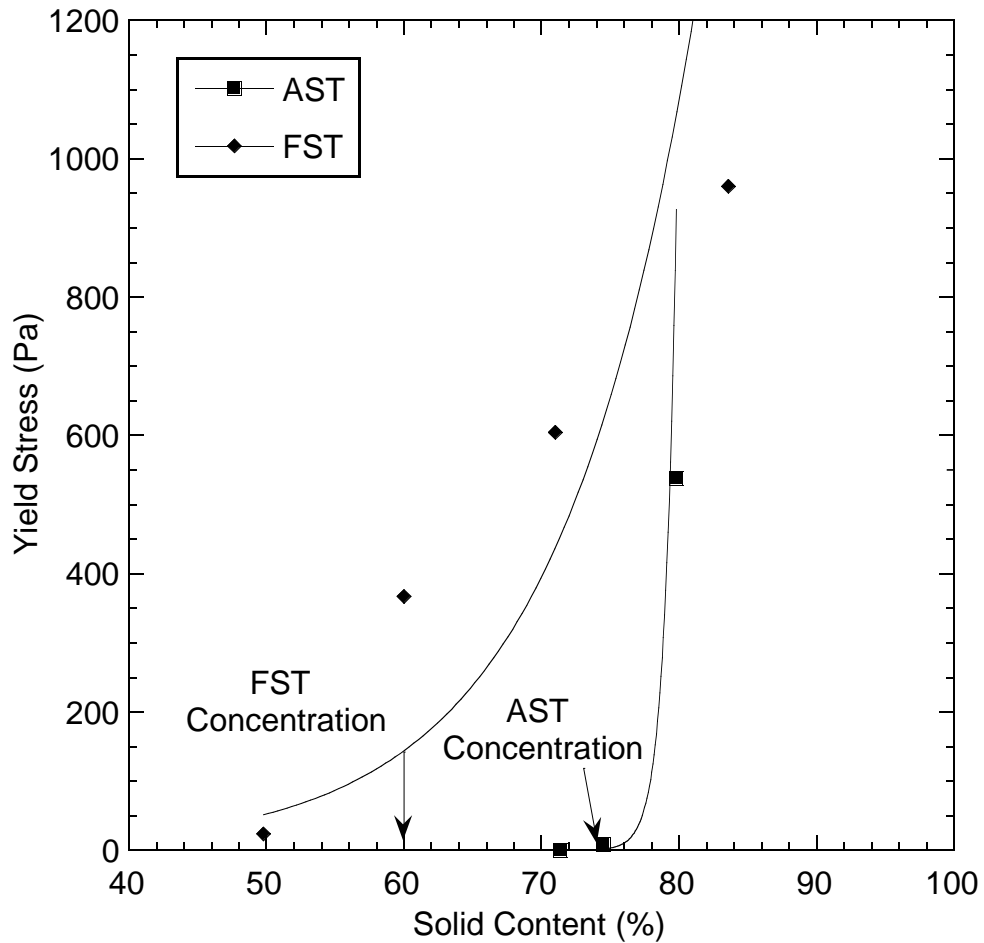


**Fig. 3.3.** Relationship between yield stress and solid content for average synthetic tailings (AST) and fine synthetic tailings (FST) based on modified slump test (Clayton 2003). Fitted curves were logarithmic approximation commonly used for mineral suspensions behave (Boger 2009). Concentrations were chosen to simulate qualitative threshold of paste tailings (Fig. 2.2b).

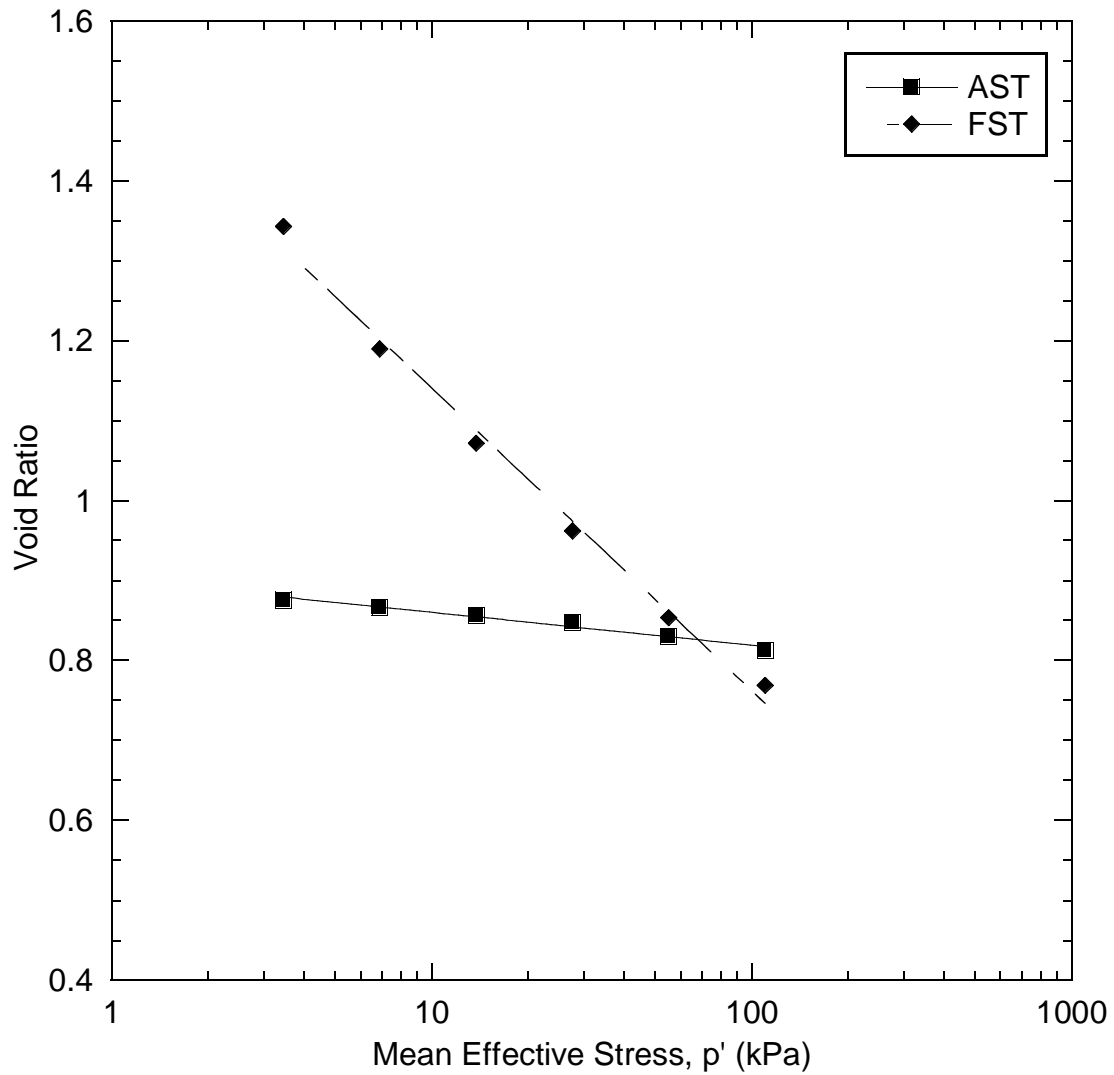


**Fig. 3.4.** Isotropic compression line (ICL) for both synthetic tailings by using height dependent consolidation described on consolidation of ASTM 4767.

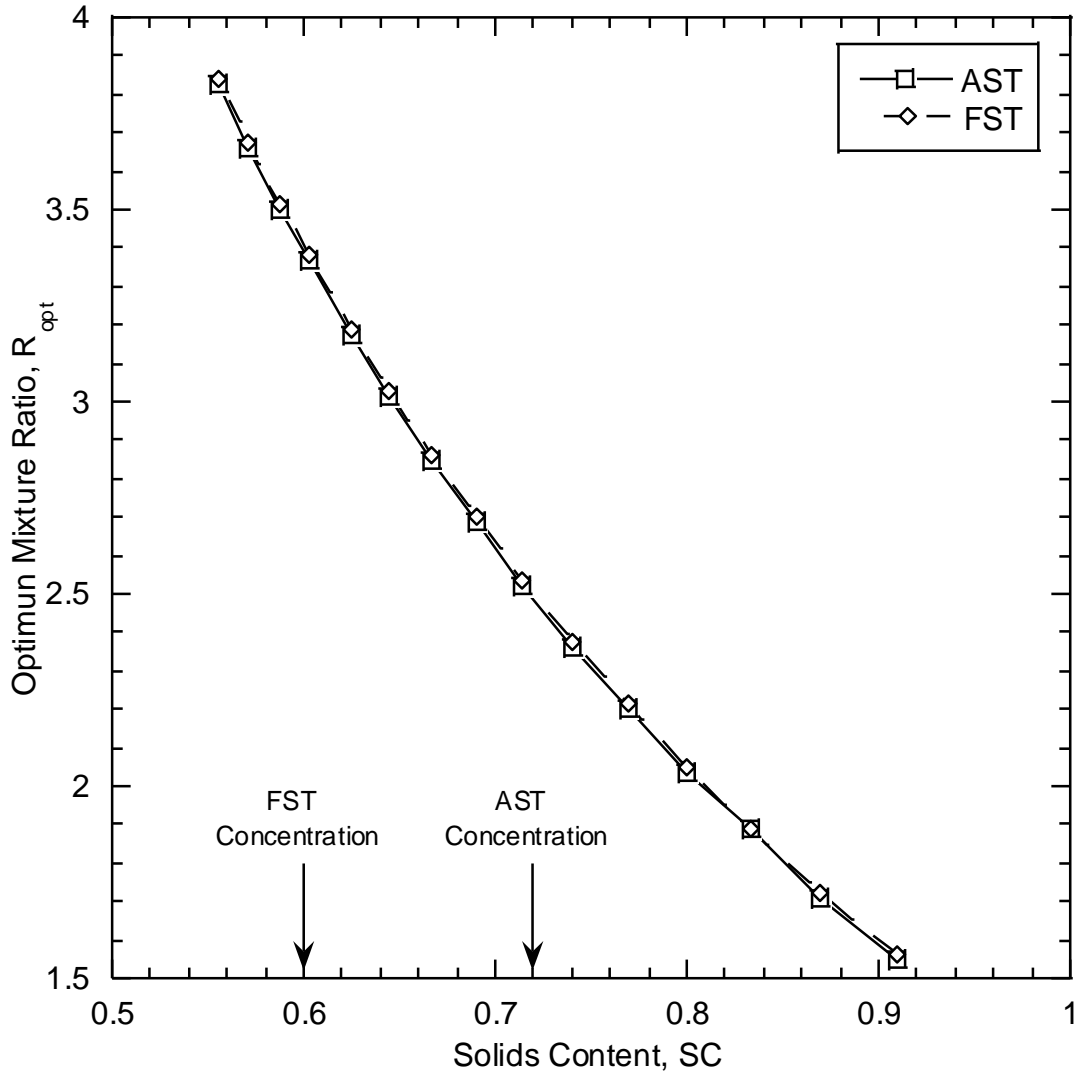


**Fig. 3.5.** Calculated values of  $R_{opt}$  based on solid content for average synthetic tailings (AST) and fine synthetic tailings (FST). Calculations were based on Eq. 2.3 using following properties:  $V_r = 1$ , SWR  $\rho_r = 2.7$ , AST  $\rho_{slurry} = 2.66$ , FST  $\rho_{slurry} = 2.63$ ,  $e_r = 0.83$  and  $w_t$  varying with SC. Schematic shows similarity of curves due to similarity of synthetic tailings. Chosen concentrations for synthetic tailings are shown.

## CHAPTER 4: RESULTS & DISCUSSION

A summary of the consolidated undrained (CU) triaxial tests performed for this study is in Tables 4.1 and 4.2. The data compilation in Tables 4.1 and 4.2 include the following:  $\sigma'_c$ , axial strain at failure ( $\epsilon_{a,f}$ ), deviator stress at failure ( $\Delta\sigma_f$ ), effective major principle stress at failure ( $\sigma'_{1f}$ ), effective minor principle stress at failure ( $\sigma'_{3f}$ ),  $p'$  and  $q$  at failure, Skempton's A pore water pressure parameter at failure ( $A_f$ ), excess pore water pressure at failure ( $u_{e,f}$ ), secant friction angle ( $\phi'_{sc}$ ), axial strain at failure ( $\epsilon_{a,f}$ ), B-value ( $B$ ), and tangent friction angle ( $\phi'_t$ ). In addition, the void ratio ( $e$ ) of the pure synthetic tailings and pure synthetic waste rock is included in Table 4.1 and the mixture ratio ( $R$ ) achieved for a given waste mixture is included in Table 4.2. Mixtures of WR&T were created with AST and FST, and ranged from fine-dominated structures (i.e.,  $R < R_{opt}$ ) to coarse-dominated structures (i.e.,  $R > R_{opt}$ ). The coarse-dominated structure was only evaluated using two experiments to confirm anticipated behavior (described subsequently). Three confining stresses were targeted for each material (10, 50, 100 kPa) to construct a failure envelope and determine relevant shear strength properties. Select tests were repeated to check results and assess repeatability (Table 4.1).

### 4.1 Shear Behavior

#### 4.1.1 Pure Materials

##### 4.1.1.1 Synthetic Waste Rock

Relationships of deviator stress ( $\Delta\sigma$ ) and excess pore water pressure ( $u_e$ ) versus axial strain ( $\epsilon_a$ ) for SWR are shown in Fig. 4.1. Triaxial tests on SWR were performed to an axial strain ( $\epsilon_a$ ) of 25%, which was near the physical limit of the LSTX apparatus. The SWR exhibited a tendency to contract ( $+u_e$ ) on initial loading followed by a tendency to dilate ( $-u_e$ ) with continued axial deformation. The SWR exhibited strain-hardening behavior with an increase in  $\Delta\sigma$  until approximately 20% axial strain. The  $\Delta\sigma$  and  $u_e$  were approximately constant for the  $\epsilon_a >$

20%, which were taken to represent steady state (SS) behavior. The undrained shear behavior of SWR agrees with that of loosely-prepared coarse-grained material (Lambe and Whitman 1969).

#### 4.1.1.2 Average Synthetic Tailings

Relationships of  $\Delta\sigma$  and  $u_e$  versus  $\epsilon_a$  for AST are shown in Fig. 4.2. Triaxial tests on AST conducted until  $\epsilon_a = 30\%$ , with the intent of reaching steady state. The AST specimen tested at  $\sigma'_c = 10$  kPa exhibited negligible tendency for volume change and achieved a low  $\Delta\sigma$ , which were attributed to the slurry-like consistency of the material. An increase in  $\sigma'_c$  to 50 and 100 kPa (Test 1) consolidated the AST, which led to a strain-hardening response characterized by continued increase in  $\Delta\sigma$  with axial displacement. This shear behavior for a normally consolidated silty material is consistent with behavior of non-plastic silts described in Brandon et al. (2006). Quasi-steady state (QSS) conditions of AST at  $\sigma'_c = 50$  and 100 kPa (Test 1) were adopted for the end of the experiment. These QSS points were used to generate a SSL considering that points for QSS and SS are located essentially along the same line in  $e-p'$  space (Finno et al. 1996; Zhang and Garga 1997).

Repeat tests for AST at  $\sigma'_c = 100$  kPa [100 kPa (Test 2) and 100 kPa (Test 3)] yielded slightly looser specimens with higher void ratios before shear when compared to Test 1 at 100 kPa (Table 4.1). This was considered within normal variability of specimen preparation. The two looser specimens exhibited contractive tendencies and strain-softening behavior common for loose, low plasticity silty sands. The comparison between the three tests on AST at  $\sigma'_c = 100$  kPa highlights the importance of the initial soil state on undrained shear behavior, whereby small changes in void ratio can influence contractive versus dilative tendencies (Casagrande 1975; Been and Jefferies 1985; Thevanayagam 2007; Rahman et al. 2008). A true SS was inferred from the two tests on AST at  $\sigma'_c = 100$  kPa that exhibited contractive tendencies (Test 2 and Test 3) due to achieving a constant pore pressure and shear stress for continuous axial

deformation (Fig. 4.2). An evaluation of undrained failure for AST relative to steady state conditions (described subsequently) supports the observed contractive and dilative tendencies for three tests at  $\sigma'_c = 100$  kPa.

Analysis of  $\Delta\sigma$  versus  $\varepsilon_a$  relationships to define type of flow behavior based in Fig. 2.4 inferred a flow behavior for test 100 kPa (test 3), characterized by a post-peak drop in  $\Delta\sigma$ , and limited-flow behavior for tests 100 kPa (test 2), characterized by a post-peak drop followed by modest increase in  $\Delta\sigma$ . Described behavior was attributed to the higher void ratio encountered for repeat tests. Section 4.2 discusses the type of flow behavior based on different spaces to confirm this analysis. Other tests of AST presented no flow behavior.

#### 4.1.1.3 Fine Synthetic Tailings

Relationships of  $\Delta\sigma$  and  $u_e$  versus  $\varepsilon_a$  for FST are shown in Fig. 4.3. Maximum axial strain for CU tests on FST was  $> 20\%$  to attempt assessment of SS conditions. The test on FST at  $\sigma'_c = 10$  kPa exhibited negligible volume change ( $u_e = 0$ ) and essentially no change in  $\Delta\sigma$  with increasing axial strain. An increase in  $\sigma'_c$  corresponded to more contractive, strain-softening behavior for both tests conducted at  $\sigma'_c = 50$  kPa (Test 1 and Test 2) and for the single test at 100 kPa (Fig. 4.3).

Flow behavior analysis of  $\Delta\sigma$  versus  $\varepsilon_a$  supports the development of flow behavior for Test 1 at 50 kPa and the single test at 100 kPa, whereby  $\Delta\sigma$  decreases following peak strength (Fig. 4.3a). Materials that present flow behavior experience a pronounced loss of strength due to generation of  $u_e$  in undrained shear. Test 2 at  $\sigma'_c = 50$  kPa resulted in a limited-flow behavior characterized by a moderate loss of strength after peak strength at  $\varepsilon_a \approx 1\%$  followed by an increase in  $\Delta\sigma$ . The difference in shear behavior between the two tests at  $\sigma'_c = 50$  kPa further documents the effects of a small variability in soil state prior to shear. Test 2 at  $\sigma'_c = 50$  kPa had a larger void ratio relative to Test 1 at  $\sigma'_c = 50$  kPa, which contributed to the observed difference

in flow versus limited-flow behavior. Finally, the test at  $\sigma'_c = 10$  kPa yielded nearly constant values of  $\Delta\sigma$  and  $u_e$  for the majority of the experiment, which is characteristic of SS behavior.

#### 4.1.2 Waste Rock and Tailings Mixtures

A summary of test parameters and results for the CU tests on WR&T mixtures is in Table 4.2. The  $R$  for WR&T specimens in Table 4.2 are based on measured masses at the end of each experiment. A compilation of the three possible void ratios for each mixture ( $e_g$ ,  $e_r$ , and  $e_t$ ) is in Table 4.3. The  $e_g$  were calculated from measured masses of solids and water at end of consolidation under a given  $\sigma'_c$ . The  $e_r$  were computed assuming all volume not occupied by solid rock particles is void space. This assumption leads to  $e_r > e_{max}$  of the SWR, which implies that rock particles are floating within a fine-dominated structure (Fig 2.3). The  $e_t$  were computed as the void ratio of tailings only, disregarding volume of rock, assuming that behavior is controlled by fine fraction as described in Section 2.2.

As previously mentioned in Chapter 3, coarse-dominated structures for AST yielded hypothesized results of shear behavior that was controlled by the waste rock (i.e., coarse fraction). Relationships of  $\Delta\sigma$  and  $u_e$  versus  $\epsilon_a$  for two AST mixtures at  $R > R_{opt}$  are shown in Fig. 4.4. These mixtures at  $R > R_{opt}$  yielded  $R = 3.8$  and  $5.8$  (Table 4.2) and exhibited shear behavior similar to pure SWR. Similar magnitudes of  $\Delta\sigma$  and  $u_e$  were observed for both the pure SWR (Fig 4.1) and coarse-dominated mixtures (Fig 4.4). Both tests at  $R > R_{opt}$  exhibited segregation between the waste rock and tailings fractions was observed throughout the specimens with considerably large air voids. These coarse-dominated mixtures with large air voids do not meet the intended applications of WR&T for use as a water storage layer in a final water balance cover or as co-disposed waste to mitigate against AMD. Thus, considering that impracticalness of WR&T mixtures at  $R > R_{opt}$  functioning in the intended applications and the support of coarse-fraction controlled shear behavior being similar to SWR, no additional CU experiments were conducted on coarse-dominated WR&T mixtures.

The analysis of WR&T shear behavior in this section is focused on mixtures prepared to target conditions of  $R_{opt}$  and  $R < R_{opt}$ . Average synthetic tailings mixtures prepared to target  $R_{opt}$  yielded  $R$  close to the target  $R$ , whereas mixtures for FST yielded an  $R$  lower than  $R_{opt}$ . The lower  $R$  for FST was due to difficulty in using the slurry displacement method (Khalili and Wijewickreme 2008) with the consistency of the FST slurry, which inhibited free settling of SWR particles within the slurry to create a rock skeleton. The denser nature of the FST slurry supported SWR particles within the slurry to create a fine-dominated WR&T matrix that included SWR particles “floating” in the mixture (Fig. 2.3). This issue was also observed by Jehring and Bareither (2016), in that WR&T mixtures prepared with low plasticity clay tailings to target  $R_{opt}$  yielded  $R < R_{opt}$ . Thus, results and discussions on AST and FST WR&T mixtures focus on fine-dominated structures.

#### 4.1.2.1 Mixtures with AST

Relationships of  $\Delta\sigma$  and  $u_e$  versus  $\varepsilon_a$  for AST mixtures targeting  $R = R_{opt}$  and  $R < R_{opt}$  are shown Fig. 4.5. Mixtures prepared to target  $R_{opt} = 2.5$  yielded  $R = 2.2$  to  $2.7$ , whereas mixtures prepared to target  $R < R_{opt}$  yielded  $R = 1.3$  to  $1.4$  (Table 4.2) In general, AST WR&T mixtures prepared at a higher  $R$  yielded considerably larger  $\Delta\sigma$  and more negative  $u_e$  for a given  $\sigma'_c$ . For example, mixtures targeting  $R_{opt}$  resulted in  $\Delta\sigma_f \approx 500$  kPa for  $\sigma'_c = 100$  kPa, whereas the AST mixture prepared at  $R < R_{opt}$  yielded  $\Delta\sigma_f \approx 100$  kPa for the same  $\sigma'_c$  (Table 4.2). An increase in shear resistance during shear was observed for both mixtures, and is evidence of strain-hardening, no-flow behavior. All tests for AST mixtures yielded an initial tendency to contract at low  $\varepsilon_a$  ( $+u_e$ ) followed by a tendency to dilate with continued shear (decrease in  $u_e$  and transition to  $-u_e$ ). The magnitude of dilative behavior for all specimens prepared for  $R_{opt}$  conditions was more pronounced than  $R < R_{opt}$ .

Undrained shear behavior of WR&T mixtures prepared to target  $R_{opt}$  yielded a pronounced increase in shear resistance and strain-hardening behavior that agrees with

previous studies. Jehring and Bareither (2016) conducted CU triaxial compression on mixtures of on low plasticity, silty, mine tailings and crushed gravel, and reported enhanced shear behavior for mixtures prepared to target  $R_{opt}$  compared to pure materials. Kahlili et al. (2010) conducted monotonic and cyclic CU triaxial tests on mixtures of waste rock with carbon in pulp tailings and reported that mixtures prepared at  $R_{opt}$  exhibited shear behavior comparable to waste rock. These findings all support that the addition of waste rock to tailings that targets  $R_{opt}$  will enhance shear resistance of tailings. This behavior can be attributed to tailings filling the void space between waste rock particles, which provides resistance against rearrangement of waste rock particles and results in increased shear resistance.

The presence of waste rock in AST WR&T mixtures at  $R < R_{opt}$  supports an overall increase in  $\Delta\sigma$  (Fig. 4.5) when compared to pure AST (Fig. 4.2). The experiments on pure AST at  $\sigma'_c = 100$  kPa exhibited shear behavior ranging strain hardening and  $\Delta\sigma_f \approx 180$  kPa (Test 1) to strain softening and  $\Delta\sigma_f \approx 40$  kPa (Test 3). Mixtures prepared at  $R < R_{opt}$  resulted in  $\Delta\sigma_f \approx 100$  kPa for same confining stress. However, the WR&T mixture prepared at  $R = R_{opt}$ , exhibited a considerable increase in strength relative to all other tests conducted for this mixture (Fig. 4.5) and pure materials (Fig. 4.2 and Fig. 4.3), yielding a  $\Delta\sigma_f \approx 500$  kPa, which was larger than all pure AST, the WR&T mixture at  $R < R_{opt}$ , and the SWR ( $\Delta\sigma_f \approx 230$  kPa).

Relationships of the principal stress ratio ( $\sigma_1'/\sigma_3'$ ) versus  $\epsilon_a$  and Skempton's A parameter ( $u_e/\Delta\sigma$ ) versus  $\epsilon_a$  for tests conducted at  $\sigma'_c = 100$  kPa on pure AST, pure SWR, and both WR&T mixtures are shown in Fig 4.6. These normalized relationships illustrate the influence of  $R$  on undrained shear behavior. The largest  $\sigma_1'/\sigma_3'$  were attained for both WR&T mixtures, and these trends indicate improved shear strength compared to pure materials. The decrease in  $\sigma_1'/\sigma_3'$  as  $\epsilon_a$  increases for  $R = R_{opt}$  indicates that a true steady-state for this mixture was not attained, whereas the approximately constant  $\sigma_1'/\sigma_3'$  with increasing  $\epsilon_a$  for the other three materials in Fig. 4.6 imply steady-state conditions. The A parameter for pure AST implies strongly contractive tendencies and the potential for flow behavior. The addition of SWR to the tailings matrix to

create a fine-dominated mixture ( $R < R_{opt}$ ) mitigated this undrained shear behavior and transitioned shear behavior to a more dilative and stronger material.

#### 4.1.2.2 Mixtures with FST

Relationships of  $\Delta\sigma$  and  $u_e$  versus  $\epsilon_a$  for FST mixtures targeting  $R = R_{opt}$  and  $R < R_{opt}$  are shown in Fig. 4.7. Mixtures prepared to target  $R_{opt} = 3.5$  yielded  $R = 2.2$  to  $2.5$ , whereas mixtures prepared to target  $R < R_{opt}$  yielded  $R = 1.8$  to  $1.9$ . Although values of  $R_{opt}$  were not reached, comparison between  $\Delta\sigma$  versus  $\epsilon_a$  at the two  $R_s$  achieved for FST mixtures indicate an increase in  $\Delta\sigma$  with increase in  $R$ . Considering the two specimens tested at  $\sigma'_c = 100$  kPa, the specimen with  $R = 2.2$  yielded  $\Delta\sigma_f \approx 50$  kPa, whereas the specimen with  $R = 1.8$  yielded  $\Delta\sigma_f \approx 45$  kPa. Generation of  $u_e$  for both mixtures was similar and indicative of contractive tendencies. All FST WR&T specimens can be considered fine-dominated structures, and volume change tendencies during shear were more representative of the tailings matrix. Thus, the contractive behavior of the mixtures compares favorably to the contractive behavior of the pure FST specimens (Fig. 4.3). The presence of contractive clay tailings particles between waste rock particles that results in a contractive mixture agrees with Jehring and Bareither (2016).

One exception was observed for the specimen prepared to target  $R_{opt}$  and tested at  $\sigma'_c = 50$  kPa. This specimen exhibited strain-hardening and dilative tendencies, characterized by negative  $u_e$  at the end of the test and pronounced increase in  $\Delta\sigma$  compared to all other FST WR&T specimens. The highest  $R = 2.5$  was attained for this specimen (FST,  $R = R_{opt}$ ,  $\sigma'_c = 50$  kPa in Table 4.2), which implies a larger volume of waste rock was present throughout the mixture relative to the other FST mixtures. Undrained shear behavior for this specimen was more influenced by rock particles compared to the other FST mixtures, suggesting that small changes in  $R$  of a given mixture affect shear behavior as the mixture approaches  $R_{opt}$ .

The WR&T FST mixtures show improved strength when compared to pure materials that exhibited flow behavior. For example, the pure FST specimen at  $\sigma'_c = 50$  kPa yielded flow

behavior and  $\Delta\sigma_f \approx 40$  kPa, whereas the WR&T FST mixture with  $R = 2.5$  at  $\sigma'_c = 50$  kPa resulted in no-flow behavior and  $\Delta\sigma_f \approx 80$  kPa. The WR&T mixtures with  $R = 1.7$  to  $1.8$  did not display improved shear resistance compared to pure FST. This suggests that insufficient waste rock was present within these fine-dominated mixtures to improve shear resistance.

Relationships of  $\sigma_1'/\sigma_3'$  versus  $\epsilon_a$  and Skempton's  $A$  parameter versus  $\epsilon_a$  for tests conducted at  $\sigma'_c = 100$  kPa on pure FST, pure SWR, and both WR&T mixtures are shown in Fig 4.8. The  $\sigma_1'/\sigma_3'$  ratio was comparable for both WR&T mixtures and was less than the  $\sigma_1'/\sigma_3'$  ratio for both pure materials. However, the  $A$  parameter for the WR&T mixtures exhibits a more pronounced tendency to dilate and shifts the undrained pore pressure response away from the contractive tendency of the pure FST and towards the dilative tendency of the pure SWR (Fig. 4.8). The higher initial  $A$  and lower  $\sigma_1'/\sigma_3'$  of the WR&T mixtures relative to the pure FST was attributed to higher  $e_t$  in the mixtures ( $e_t \approx 1.2$ ) relative to the pure tailings ( $e_t \approx 0.74$ ). Thus, a lower strength of the fine-dominated WR&T mixtures prepared with the FST would be anticipated relative to the pure FST. The modest strain-hardening and dilative tendencies of the FST WR&T mixtures suggests that the presence of SWR has potential to enhance shear behavior, but the overall SWR fraction was not sufficient in these mixtures to substantially enhance shear resistance.

## 4.2 Shear Strength

### 4.2.1 Evaluation and Definition of Failure

A definition of failure during laboratory triaxial testing is needed to determine shear strength parameters that can best represent a given engineering scenario. Brandon et al. (2006) evaluated the shear behavior and shear strength of silty soils and identified six possible failure criteria: (1) maximum deviator stress,  $\Delta\sigma_{d,max}$ ; (2) maximum principle stress ratio,  $(\sigma_1'/\sigma_3')_{max}$ ; (3) maximum excess pore pressure,  $u_{e,max}$ ; (4) Skempton's pore pressure parameter  $A$  equal to zero; (5) stress path reaches the failure line in  $p'$ - $q$  space ( $K_f$  line); and (6) limiting axial strain

(e.g.,  $\epsilon_a = 5$  or  $10\%$ ). These failure criteria have been evaluated by Wang and Luna (2012) and Jehring and Bareither (2016); the latter study considered all possible interpretations of failure for actual mine tailings and co-mixed WR&T. Jehring and Bareither (2016) identified three methods that were broadly applicable and yielded the smallest bias (i.e.  $\Delta\sigma_{d,max}$ ,  $K_f$  line, and  $\epsilon_a = 15\%$ ). In this study, the point at which a stress path for a given CU test specimen reached the  $K_f$  line was used to define failure.

Effective stress paths in  $p'$ - $q$  space reach the  $K_f$  line at failure and theoretically maintain a constant  $q/p'$  ratio for the remainder of axial deformation in a CU triaxial test. In this study, all tailings, waste rock, and mixture specimens were assumed to be normally consolidated materials such that the  $K_f$  line was assumed to pass through the origin (i.e.,  $p' = 0$  and  $q = 0$ ). Thus, for a set of  $p'$ - $q$  data from a given CU test specimen, all data points that yielded approximately the same  $q/p'$  ratio were included in a least-squares linear regression to determine a  $K_f$  line. Secant friction angles ( $\phi'_{sc}$ ) were determined from linear regression of  $q/p'$  data sets from individual tests. A friction angle was computed for a given material based on regression through all  $q/p'$  data from CU tests at multiple  $\sigma'_c$ . These friction angles determined to represent the composite  $K_f$  line for a given material are referred to as tangent friction angles ( $\phi'_t$ ). All  $\phi'_{sc}$  from individual tests and  $\phi'_t$  for each material are in Tables 4.1 and 4.2.

#### 4.2.2 Shear Strength of Pure Waste Materials

Effective stress paths in  $p'$ - $q$  space for SWR are shown in Fig. 4.9. The  $K_f$  line shown in Fig. 4.9, and in subsequent stress path plots, was regressed through all  $p'$ - $q$  points that defined a common  $K_f$  line. The initial  $p'$ - $q$  point that fell on the  $K_f$  line was characterized qualitatively as the start of a relatively constant  $q/p'$  ratio, and all subsequent  $p'$ - $q$  points were assumed to represent failure conditions. The slope of the  $K_f$  line ( $\alpha$ ) for SWR was 0.656, which yielded  $\phi'_t = 41^\circ$ . This  $\phi'_t$  agrees with previously reported  $\phi'_t$  for gravel and waste rock (Bussi re 2007; Jehring and Bareither 2016).

Effective stress paths in  $p'$ - $q$  space for AST are shown in Fig. 4.10. The entire stress paths are shown in Fig 4.10a, whereas a zoomed-in plot is shown in Fig 4.10b to more effectively show undrained shear behavior of the different stress paths. Regardless of the variance in the initial state conditions for repeated tests at  $\sigma'_c = 100$  kPa, all tests terminate on approximately the same  $K_f$  line (Fig 4.10 a), which supports that selected failure criterion. Test 2 and Test 3 at  $\sigma'_c = 100$  kPa showed contractive behavior, whereas Test 2 presented limited-flow behavior and Test 3 a flow behavior, confirming analysis of stress strain (Fig 4.2). Test 1 at  $\sigma'_c = 100$  kPa exhibited dilated behavior, and lead to a similar failure line. The  $K_f$  line for AST has a slope of  $\alpha = 0.623$  ( $\phi'_t = 38^\circ$ ), which agrees with the range of  $\phi'$  for silty tailings in Matyas et al. (1984) and Qiu and Sego (2001).

Effective stress paths in  $p'$ - $q$  space for FST are shown in Fig. 4.11. Stress paths are consistent with undrained shear behavior shown in Fig. 4.3: Test 2 at  $\sigma'_c = 50$  kPa exhibited limited-flow behavior, whereas Test 1 at  $\sigma'_c = 50$  kPa the test at  $\sigma'_c = 100$  kPa exhibited flow behavior. All individual stress paths for FST yielded consistent  $\phi'_{sc}$  ranging from 36 to 40°, and the average  $K_f$  line for FST had a slope of  $\alpha = 0.63$  that yielded  $\phi'_t = 39^\circ$ . The high friction angle for a silty-clayey material is comparable to friction angles reported by Jehring and Bareither (2016) for actual mine tailings. Although the  $\phi'_t$  of FST is comparable to AST, the development of flow behavior in FST during undrained shear is a concern, in that the loss of strength during undrained shear can potentially lead to static liquefaction.

#### 4.2.3 Average Synthetic Tailings Mixture

Effective stress path in  $p'$ - $q$  space for AST mixtures targeting  $R = R_{opt}$  are shown in Fig. 4.12a and for AST mixtures targeting  $R < R_{opt}$  are shown in Fig. 4.12b. All mixtures prepared to target  $R = R_{opt}$  exhibited a dilative strain-hardening response, which yielded no-flow behavior as shown by the effective stress paths in Fig. 4.12a. An increase in the tailings fraction for  $R < R_{opt}$  mixtures of AST changed undrained shear behavior to a more contractive and modestly dilatant

material. The limited-flow effective stress paths for AST at  $R < R_{opt}$  support this behavior (Fig. 4.12b). The  $K_f$  line for AST at  $R = R_{opt}$  yielded  $\phi'_t = 48^\circ$ , whereas the  $K_f$  line for AST at  $R < R_{opt}$  yielded  $\phi'_t = 44^\circ$ . The largest  $\phi'$  was determined for the AST WR&T mixture prepared to target  $R = R_{opt}$ , which was attributed to the stiff, dilatant response of the material (Fig. 4.5). Although  $\phi'_t$  decreased with an increase in tailings for the  $R < R_{opt}$  condition, the addition of waste rock increased strength relative to pure tailings. This finding is important for documenting the range of  $R$  that can be achieved via co-mixing waste rock and tailings to obtain an increase in strength for a fine-dominated mixture. Overall, the increase in  $\phi'_t$  for mine tailings with addition of waste rock agrees with previous research on co-mixed WR&T (e.g., Wickland et al. 2010; Jehring and Bareither 2016).

Effective stress paths of AST mixtures prepared at  $R > R_{opt}$  are shown in Fig. 4.13. These two mixtures contained coarse-dominated structures at considerably different  $R$  (Table 4.2). The effective stress paths are similar for both mixtures and yielded  $\phi'_t = 41^\circ$ . The similarity between the stress paths and  $\phi'_t$  of the mixtures to pure SWR indicates that waste rock controls shear behavior and shear strength for these coarse-dominated mixtures even with varying  $R$ .

A compilation of the linear failure envelopes and  $\phi'_t$  for pure AST, pure SWR, and all AST mixtures prepared to target the three mixture conditions (i.e.,  $R < R_{opt}$ ,  $R = R_{opt}$ , and  $R > R_{opt}$ ) are shown in Fig 4.14. The  $\phi'_t$  determined for AST ( $38^\circ$ ) was the lowest of all materials, which was anticipated based on the loose, slurry-like nature of the pure tailings. The slope of the  $K_f$  line and  $\phi'_t$  increased from  $R > R_{opt}$  to  $R < R_{opt}$  to  $R = R_{opt}$ , which was attributed to the interaction between the coarse waste rock particles and tailings fraction. The optimum mixture ratio defines a mixture in which tailings completely fill void space between the waste rock particles. In this condition, the propensity for the loose waste rock skeleton to contract transfers load to the tailings fraction, which resulted in a stiff, dilatant material.

#### 4.2.4 Fine Synthetic Tailings Mixture

Effective stress paths in  $p'$ - $q$  space for FST mixtures prepared at  $R = 2.5$  are shown in Fig. 4.15a and for FST mixtures prepared at  $R = 1.7$  are shown in Fig. 4.15b. The  $K_f$  line for FST mixtures at  $R = 2.5$  yielded  $\phi'_t = 38^\circ$ , whereas FST mixtures at  $R = 1.7$  yielded  $\phi'_t = 32^\circ$ . Fine synthetic tailings mixtures at  $R = 2.2$  for  $\sigma'_c = 10$  kPa and 100 kPa (Fig. 4.15a) exhibit limited-flow behavior, which was a slight improvement for undrained shear behavior of the pure FST that exhibited flow behavior (Fig. 4.11). The experiment at  $\sigma'_c = 50$  kPa yielded no-flow behavior, which was attributed to higher  $R$  ( $R = 2.5$ ). The comparison of  $K_f$  lines and  $\phi'_t$  between the two different FST WR&T mixtures (Fig. 4.15) implies that the addition of more waste rock to increase  $R$  results in an increase in strength and  $\phi'_t$ .

To illustrate the effect of mixing on flow behavior, stress paths for SWR, FST, and WR&T FST mixtures tested at  $\sigma'_c = 100$  kPa are shown in Fig. 4.16. Flow behavior was observed for FST, whereas no-flow behavior was observed for SWR. The WR&T FST mixtures at  $R = 1.8$  and  $R = 2.2$  show limited-flow behavior. This comparison further supports the finding that the addition of waste rock particles to tailings to create a fine-dominated structure can mitigate the development of flow behavior. Similarity in the effective stress paths for  $R = 1.8$  and  $R = 2.2$  shown in Fig. 4.16 suggests that the material within the shear plane for these materials is behaving similarly during undrained shear. This observation alludes to the existence of a threshold waste rock content that is required to shift undrained shear behavior to be more influenced by the waste rock particles. Additional research is required to evaluate this observation and assess the existence of a threshold waste rock content.

A compilation of the failure envelopes and  $\phi'_t$  for pure FST, pure SWR, and FST mixtures prepared to target  $R < R_{opt}$  and  $R = R_{opt}$  are shown in Fig 4.17. Friction angles for FST, SWR, and the mixtures prepared at an actual  $R = 2.2$  to 2.5 yielded similar friction angles ranging from  $38^\circ$  to  $41^\circ$ . The WR&T mixture prepared at  $R = 1.7$  yielded  $\phi'_t = 32^\circ$ . This low friction angle may be attributed to larger  $e_t$  of mixtures in comparison to pure FST (Table 4.3). A

fine dominated structure such as FST mixtures has shear strength controlled by fine fraction, whereupon a looser tailings matrix resulted in lower shear strength.

### 4.3 Steady State Analysis

The steady state of a soil relates to a specific state during shear defined by void ratio and effective stress that can be represented by a steady-state line (SSL). The SSL is a material property, similar to the isotropic consolidation line, which is independent of initial conditions or stress history of a soil (Casagrande 1975). The SSL is an effective property of a given soil to assess the potential for contractive or dilative behavior during undrained shear (Been and Jefferies 1985). The position of an initial state point in  $e$ - $p'$  space relative to the SSL can aid in determining flow behavior, whereby  $e$ - $p'$  points below a SSL tend towards no-flow behavior,  $e$ - $p'$  points above a SSL tend towards limited-flow and flow behavior depending on proximity to the SSL. An assessment was conducted to evaluate the uniqueness of SSLs for pure materials and mixtures. The objectives of this analysis were to assess if (i) undrained shear behavior of mixtures can be related to  $e_g$ ,  $e_r$ , or  $e_t$  of the mixture and (ii) if a single SSL can be development via equivalent void ratios to represent undrained behavior of mixtures at varying  $R$ . This analysis builds on past research of undrained shear behavior and steady state analysis of mixtures (Thevanayagam 2007; Rahman et al. 2008) via assessment of WR&T mixtures.

#### 4.3.1 Pure Materials

A summary of key parameters incorporated in the steady-state analysis for each material is in Table 4.3. The initial mean effective principal stress ( $p'$ ), steady state mean effective principal stress ( $p'_{ss}$ ), and  $e_r$  or  $e_t$  are included in Table 4.3 for pure materials. The  $e_g$  in Table 4.3 for the pure materials is equal to  $e_r$  for SWR and  $e_t$  for tailings. All void ratios are representative of specimens after consolidation and before shear. These void ratios are also representative of final conditions since no volume change was allowed during undrained shear.

Steady-state lines for the pure materials were defined by regression of the SS and QSS  $e-p'$  points. The SS, QSS, and initial state points for AST, FST and SWR are shown in Fig. 4.18, 4.19, and 4.20 respectively. Arrows included in the  $e-p'$  plots show the direction of stress change during undrained shear, where a dilative material will shift to the right as  $-u_e$  increases  $\sigma'$  and a contractive material will shift to the left as  $+u_e$  decreases  $\sigma'$ . Regression of the SS and QSS points for both synthetic tailings and the SWR yielded a unique SSL for each material. All SSLs are statistically significant with coefficients of determination ( $R^2$ ) = 0.9 for the regression lines. The  $e-p'$  plots for AST (Fig. 4.18) and FST (Fig. 4.19) include ICLs determined for independent specimens for comparison.

The ICL and SSL for AST are shown in Fig. 4.18. The similarity in slopes of the ICL and SSL, location of the ICL above the SSL in  $e-p'$  space, and location of initial  $e-p'$  points for the CU test specimens below the ICL agrees with steady state theory (Been and Jefferies 1985; Olson and Stark 2003). The two tests conducted at  $\sigma'_c = 100$  kPa with initial  $e-p'$  points above the SSL (Test 2 and Test 3) exhibited contractive behavior, whereas the three other CU tests on AST had initial  $e-p'$  points below the SSL and all exhibited dilatant behavior. Thus, all five AST specimens tested in CU had different initial  $e-p'$  points and all five moved towards a single SSL.

The ICL and SSL for FST are shown in Fig. 4.19. Similar to the observations made for AST, the ICL for FST plots above the SSL, all initial  $e-p'$  points of the CU test specimens plot below ICL, and the ICL and SSL have comparable slopes. The initial  $e-p'$  points for all tests on pure FST, except 10 kPa, plot above the SSL. The two initial  $e-p'$  points that plot closest to the ICL are Test 1 for  $\sigma'_c = 50$  kPa and the test at 100 kPa. These two CU tests exhibited flow behavior (Fig. 4.11) and the stress paths in  $e-p'$  space show a pronounced decrease in  $\sigma'$ . Test 2 for  $\sigma'_c = 50$  kPa is represented by an initial  $e-p'$  point that plots above SSL, but in closer proximity; this experiment exhibited limited-flow behavior.

The initial and final  $e-p'$  points and the SSL for SWR are shown in Fig. 4.20. Undrained shear behavior of the SWR was dilative for all four CU tests (Fig. 4.1), which corresponds to

initial  $e$ - $p'$  points plotting to the left (i.e., below) the SSL. The strong dilative, strain hardening, and no-flow behavior response of SWR sheared undrained supports the pronounced increase in  $\sigma'$  and shift to higher  $p'$  for the steady-state  $e$ - $p'$  points.

#### 4.3.2 Waste Rock and Tailings Mixtures

A summary of relevant parameters for the steady-state analysis conducted on WR&T mixtures is in Table 4.3. The  $p'_i$  and  $p'_{ss}$  for the mixtures are analogous to the stress state parameters computed for the pure tailings and SWR. The three void ratios of the mixtures,  $e_g$ ,  $e_r$ , and  $e_t$ , were computed in accordance with Eqs. 2.4 and 2.5, such that the  $e_r$  represents the waste rock void ratio and  $e_t$  represents the tailings void ratio. Additional parameters for the WR&T mixtures in Table 4.3 include the following: normalized  $R$  ratio ( $R/R_{opt}$ ), coarse fraction (i.e., waste rock) equivalent void ratio ( $e^*_r$ ), fine fraction (i.e., tailings) equivalent void ratio ( $e^*_t$ ), as well as the  $b$  parameter,  $m$  parameter, and  $d_r$  used to compute the equivalent void ratios (Eqs. 2.7 and 2.8). Mixtures were analyzed as fine-dominated structures or coarse-dominated structures based on  $R/R_{opt}$ , whereby  $R/R_{opt} > 1$  represents a coarse-dominated structure and  $R/R_{opt} < 1$  represents a fine-dominated structure. Thus, equivalent void ratios were only computed for the relevant structure type (i.e.,  $e^*_t$  for fine-dominated structures and  $e^*_r$  for coarse-dominated structure). Empirical parameters  $b$  and  $m$  (Eqs. 2.7 and 2.8) were chosen following theoretical definitions and ranges presented in literature (Thevanayagam 2007; Rahman et al. 2008). An example calculation of for fraction-specific void ratios of a WR&T mixture ( $e_g$ ,  $e_r$ ,  $e_t$ ) and equivalent void ratios is in Appendix A.

The steady-state analysis for mixtures considered the efficacy of  $e_g$  or fraction specific void ratios of the mixture ( $e_r$  and  $e_t$ ) to represent undrained shear behavior relative to steady-state conditions of the predominant fraction controlling behavior. In other words, can the SSL of mixtures determined using fraction void ratios (e.g.  $e_r$  and  $e_t$ ) represent anticipated undrained shear behavior of a mixture? Subsequently, effective void ratios ( $e^*_r$  and  $e^*_t$ ) for coarse- and

fine-dominated mixtures were evaluated to assess if these void ratios provide an improved steady state analysis of undrained behavior of mixtures relative to the predominant fraction in the WR&T mixture. The statistical significance of a single SSL to represent a material was proposed by Yang et al. (2006) to have root square mean deviation (RMSD) < 0.043 for linear or power function trend lines regressed through steady-state  $e-p'$  points. This assessment of statistical significance and implications of the uniqueness of a single SSL to represent a WR&T mixture was conducted for equivalent void ratios plots.

A compilation of  $e-p'$  plots for AST is shown in Fig. 4.21 and a compilation of  $e-p'$  plots for FST is shown in Fig. 4.22 for different void ratio considerations of the WR&T mixtures. Steady state  $e-p'$  points and SSLs for the pure tailings and pure SWR are shown in Figs. 4.21a and 4.22a along with  $e_g$  of the WR&T mixtures. The  $e_g$  of both the AST mixtures (Fig. 4.21a) and FST mixtures (Fig. 4.22a) are less than all pure material  $e_g$  and the final steady state points of the mixtures plot considerably below the SSLs for both the tailings and SWR. The SS points of pure materials have higher  $e_g$  than mixtures, as the mixing process fill waste rock void space and increases specimen density. Thus, the  $e_g$  of the WR&T mixtures is not an effective parameter to assess undrained shear behavior relative to steady-state conditions of the pure materials constituting the mixture.

Steady state  $e-p'$  points for the pure tailings are shown in Figs. 4.21b and 4.22b along with  $e_t$  of the WR&T mixtures. The  $e_t$  of the AST and the  $e_t$  of the FST in the WR&T mixtures were all larger than the  $e_t$  of the pure tailings. The larger  $e_t$  of the mixtures was attributed to the presence of waste rock particles that decreased compression of the tailings fraction. Thus, all  $e_t$  used to define the  $e-p'$  points of the WR&T mixtures plot considerably above the SSL for the pure tailings and are not effective in representing the state of the mixture to assess undrained behavior relative to the pure tailings.

Steady state  $e-p'$  points for the pure SWR are shown in Fig. 4.21c along with  $e_r$  of the WR&T mixtures. A coarse dominated structure is defined by a waste rock force structure with

tailings within the void, and  $e_r$  consider tailings volume as voids volume. For this reason, the analysis using  $e_r$  of mixtures compares better with pure SWR than  $e_t$  does for pure tailings (Figs. 4.21b and 4.22b). Nevertheless, similar to  $e_r$  in Fig. 4.21b, the fraction void ratio does not represent a statistically significant regression to represent a SSL.

The steady state  $e-p'$  points and initial  $e-p'$  points using  $e_t^*$  for fine dominated structures and are shown in Fig. 4.23a for AST and Fig. 4.23b for FST. The equivalent void ratio SS points of the mixtures and pure material combine to form a better representation of a single SSL. The initial  $e-p'$  points of the mixtures plotted as  $e_t^*-p'$  move towards pure tailings, which supports the effectiveness of the  $e_t^*$  in representing steady-state behavior of fine-dominated mixtures. The one outlier for the AST is for the test conducted at  $\sigma'_c = 10$  kPa for the  $R = R_{opt}$  mixture (i.e., largest  $e_t^*$  in Fig. 4.23a). The previous discussion on undrained shear behavior and flow analysis of AST WR&T mixtures revealed that all AST mixtures exhibited some tendencies to dilate during shear. All of the initial  $e_t^*$  for the WR&T mixtures plot below the SSL in Fig 4.23a, which is further evidence of dilative behavior and the effectiveness of the single SSL to represent undrained shear behavior of the mixtures as a function of  $e_t^*$ . Regression analysis of all steady-state  $e_t^*-p'$  points in Fig. 4.23a and Fig. 4.23b meets the statistically significant conditions of  $RMDS < 0.043$ .

A similar conclusion regarding the effectiveness of  $e_t^*-p'$  points to represent the undrained shear behavior of WR&T mixtures can be made for FST. The  $e_t^*-p'$  points for FST mixtures that had fine-dominated structures are shown in Fig. 4.23b. All steady state  $e_t^*-p'$  points coalesce to a single SSL. The initial  $e_t^*-p'$  points are all near the SSL, which supports the limited-flow behavior observed for the FST mixtures. The one exception is for the test on the mixture at  $R = 2.5$  and  $\sigma'_c = 50$  kPa, which exhibited no-flow behavior. The initial  $e_t^*-p'$  condition for this specimens plots below the SSL (i.e., lowest data point from the SSL in 4.23b) and supports the no-flow behavior observed in the CU test.

Analysis of the coarse dominated structure of AST mixtures using  $e^*_r$  are shown in Fig. 4.24. Steady state points in  $e^*_r-p'$  space for coarse dominated structure mixtures and pure SWR coalesce to a single SSL. Use of  $e^*_r$  resulted in regression of SS points the statistically significant (RMDS < 0.043) to represent a SSL for coarse dominated structure of AST mixtures. All initial state points show dilative behavior (i.e. bellow SSL) and move toward SSL, which supports no-flow behavior observed on CU tests for AST mixtures.

**Table 4.1.** Summary of test parameters and results for pure materials. Failure criterion of reaching  $K_f$  line was used to determine the effective friction angle and test parameters at failure.

	Test #	$\sigma'_c$	$\epsilon_{a,f}$	$\Delta\sigma_f$ (kPa)	$\sigma'_{3f}$ (kPa)	$\sigma'_{1f}$ (kPa)	$p'$ (kPa)	$q$ (kPa)	$A_f$	$u_{e,f}$ (kPa)	$\Phi'_{sc}$	B	e	$\phi'_t$
AST	10 kPa	6.8	8%	7.6	6.7	14.3	10.5	3.8	0.0	-0.1	21.1	0.97	0.68	38°
	50 kPa	49.5	2%	40.0	34.7	74.7	54.7	20.0	0.4	14.8	28.3	0.95	0.64	
	100 kPa (Test 1)	100.3	4%	186.3	49.7	236.0	142.8	93.1	0.3	50.6	40.6	0.95	0.61	
	100 kPa (Test 2)	89.9	6%	56.6	25.2	81.9	53.5	28.3	1.1	64.6	32.9	0.95	0.67	
	100 kPa (Test 3)	102.0	8%	38.8	22.9	61.6	42.3	19.4	2.0	79.2	27.3	0.95	0.68	
FST	10 kPa	4.9	22%	12.8	3.6	16.4	10.0	6.4	0.0	0.5	37.8	0.95	0.85	39°
	50 kPa (Test 1)	48.8	17%	40.1	13.0	53.1	33.0	20.0	0.9	35.8	36.8	0.95	0.72	
	50 kPa (Test 2)	49.8	8%	34.9	10.3	45.2	27.8	17.5	1.1	39.2	38.2	0.95	0.82	
	100 kPa	101.3	3%	81.0	23.9	104.9	64.4	40.5	1.0	77.4	40.2	0.96	0.74	
SWR	10 kPa	9.9	1%	26.1	9.2	35.3	22.2	13.1	0.2	4.4	42.3	0.96	0.78	41°
	50 kPa	50.1	3%	141.9	37.9	179.8	108.8	71.0	0.1	18.4	40.4	1.00	0.74	
	100 kPa (Test 1)	100.0	3%	211.5	59.6	271.0	165.3	105.7	0.2	45.9	40.7	0.96	0.66	
	100 kPa (Test 2)	100.0	2%	233.2	68.1	301.3	184.7	116.6	0.2	36.6	41.0	0.98	0.68	

Note:  $\sigma'_c$  = effective confining stress;  $\epsilon_{a,f}$  = axial strain at failure;  $\Delta\sigma_f$  = deviator stress at failure;  $\sigma'_{3f}$  = minor effective principle stress at failure;  $\sigma'_{1f}$  = major effective principle stress at failure;  $p'$  = mean effective stress at failure;  $q$  = mean shear stress at failure;  $A_f$  = Skempton's pore pressure parameter;  $u_{e,f}$  = excess pore pressure at failure;  $\Phi'_{sc}$  = secant friction angle; B = b-check for saturation;  $e_g$  = global void ratio before shear;  $\phi'_t$  = tangent friction angle.

**Table 4.2.** Summary of test parameters and results for mixtures. Failure criterion of reaching  $K_f$  line was used to determine the effective friction angle and test parameters at failure.

	Test #	$\sigma'_c$	$\epsilon_{a,f}$	$\Delta\sigma_f$ (kPa)	$\sigma'_{3f}$ (kPa)	$\sigma'_{1f}$ (kPa)	$p'$ (kPa)	$q$ (kPa)	$A_f$	$u_{e,f}$ (kPa)	$\Phi'_{sc}$	B	R	$\phi'_t$
WR&T AST $R < R_{opt}^a$	10 kPa	9.7	1.8%	9.1	4.9	14.1	9.5	4.57	1.0	9.4	38.6	0.98	1.35	44°
	50 kPa	48.8	1.2%	11.2	10.7	21.9	16.3	5.60	3.7	41.9	39.4	0.95	1.34	
	100 kPa	99.4	1.0%	102.1	32.0	134.1	83.0	51.06	0.7	71.2	44.9	1.00	1.31	
WR&T AST $R = R_{opt}^a$	10 kPa	9.5	1.2%	22.2	6.7	28.9	17.8	11.10	0.3	6.5	43.4	0.98	2.44	48°
	50 kPa (Test 1)	50.0	0.9%	75.2	28.1	103.3	65.7	37.58	0.3	25.2	44.9	0.99	2.7	
	50 kPa (Test 2)	50.0	1.0%	97.1	28.3	125.4	76.8	48.56	0.3	25.4	46.5	0.98	2.4	
	100 kPa	100.3	0.4%	495.6	78.9	574.5	326.7	247.81	0.0	23.8	49.5	0.96	2.22	
WR&T AST $R > R_{opt}^a$	50 kPa (Test 1)	50.0	1.7%	152.2	39.9	192.1	116.0	76.10	0.1	14.5	41.2	0.98	5.8	41°
	50 kPa (Test 2)	50.0	1.2%	144.5	43.9	188.4	72.3	72.25	0.1	9.7	40.5	0.95	3.8	
WR&T FST $R < R_{opt}^b$	10 kPa	9.6	0.9%	7.4	7.2	14.6	10.9	3.7	0.8	5.7	27.3	0.96	1.9	32°
	50 kPa	49.7	2.9%	23.5	17.0	40.5	28.7	11.8	1.6	38.6	30.5	0.96	1.83	
	100 kPa	99.7	2.5%	46.4	25.5	72.0	48.8	23.2	1.7	80.0	34.3	0.96	1.88	
WR&T FST $R = R_{opt}^b$	10 kPa	9.9	1.2%	7.6	7.4	15.0	11.2	3.8	0.8	6.2	30.8	0.95	2.21	38°
	50 kPa	49.2	4.9%	79.0	25.0	104.0	64.5	39.5	0.4	31.8	33.8	1.00	2.47	
	100 kPa	99.9	4.9%	49.5	24.8	74.3	49.6	24.8	1.7	82.8	39.0	0.95	2.24	

Note:  $\sigma'_c$  = effective confining stress;  $\epsilon_{a,f}$  = axial strain at failure;  $\Delta\sigma_f$  = deviator stress at failure;  $\sigma'_{3f}$  = minor effective principle stress at failure;  $\sigma'_{1f}$  = major effective principle stress at failure;  $p'$  = mean effective stress at failure;  $q$  = mean shear stress at failure;  $A_f$  = Skempton's pore pressure parameter;  $u_{e,f}$  = excess pore pressure at failure;  $\Phi'_{sc}$  = secant friction angle; B = b-check for saturation; R = Mixture Ratio;  $\phi'_t$  = tangent friction angle.

<sup>a</sup> Optimum mixture ratio ( $R_{opt}$ ) = 2.5

<sup>b</sup> Optimum mixture ratio ( $R_{opt}$ ) = 3.4

**Table 4.3.** Void ratio at initial conditions and at steady state with equivalent void ratios and parameters used in calculation.

	b	m	dr	Test #	R/R <sub>opt</sub>	p' <sub>i</sub> (kPa)	p' <sub>ss</sub> (kPa)	e <sub>g</sub>	e <sub>r</sub>	e <sub>t</sub>	e* <sub>r</sub>	e* <sub>t</sub>
AST	-	-	-	10 kPa	-	6.82	13.3	0.68	-	0.68	-	-
				50 kPa	-	49.5	193.1	0.64	-	0.64	-	-
				100 kPa (Test 1)	-	100.3	474.2	0.61	-	0.61	-	-
FST	-	-	-	10 kPa	-	4.86	4.86	0.85	-	0.85	-	-
				50 kPa (Test 2)	-	49.8	49.8	0.72	-	0.72	-	-
				100 kPa	-	101.4	101.4	0.74	-	0.74	-	-
GWR	-	-	-	10 kPa	-	9.90	9.90	0.78	0.78	-	-	-
				50 kPa	-	50.1	50.1	0.74	0.74	-	-	-
				100 kPa (Test 1)	-	100.0	100.0	0.66	0.66	-	-	-
WR&T AST <i>R &lt; R<sub>opt</sub></i>	0.2	0.28	400	10 kPa	0.54	9.70	62.7	0.32	1.31	0.74	-	0.60
				50 kPa	0.54	48.8	156.3	0.32	1.32	0.74	-	0.60
				100 kPa	0.52	99.4	373.7	0.30	1.31	0.69	-	0.56
WR&T AST <i>R = R<sub>opt</sub></i>				10 kPa	0.99	9.50	359.3	0.29	0.83	0.98	-	0.68
				50 kPa (Test 1)	1.1	50.0	676.7	0.29	0.78	1.06	0.65	-
				50 kPa (Test 2)	0.96	50.0	726.2	0.25	0.78	0.85	-	0.59
WR&T AST <i>R &gt; R<sub>opt</sub></i>				100 kPa	0.89	100.3	1341	0.23	0.79	0.72	-	0.51
				50 kPa (Test 1)	2.3	50.0	301.7	0.48	0.74	3.23	0.68	-
WR&T FST <i>R &lt; R<sub>opt</sub></i>				-	0.13	1364	10 kPa	0.56	9.60	29.5	0.50	1.31
	50 kPa	0.54	49.7				27.9	0.44	1.25	1.24	-	0.73
	100 kPa	0.55	99.7				48.6	0.42	1.19	1.18	-	0.69
WR&T FST <i>R = R<sub>opt</sub></i>	10 kPa	0.65	9.90				35.9	0.47	1.15	1.47	-	0.80
	50 kPa	0.73	49.2				206.3	0.36	0.93	1.24	-	0.64
	100 kPa	0.66	99.9				45.4	0.39	1.02	1.24	-	0.67

Note: *b* = calculation parameter for rock equivalent void ratio; *m* = calculation parameter for tailings equivalent void ratio; *R/R<sub>opt</sub>* = Ratio of mixture ratio to optimum; *p'<sub>i</sub>* = initial mean effective stress; *p'<sub>ss</sub>* = steady state mean effective stress; *e<sub>g</sub>* = global void ratio; *e<sub>r</sub>* = rock void ratio; *e<sub>t</sub>* = tailings void ratio; *e\*<sub>r</sub>* = rock equivalent void ratio; *e\*<sub>t</sub>* = tailings equivalent void ratio.

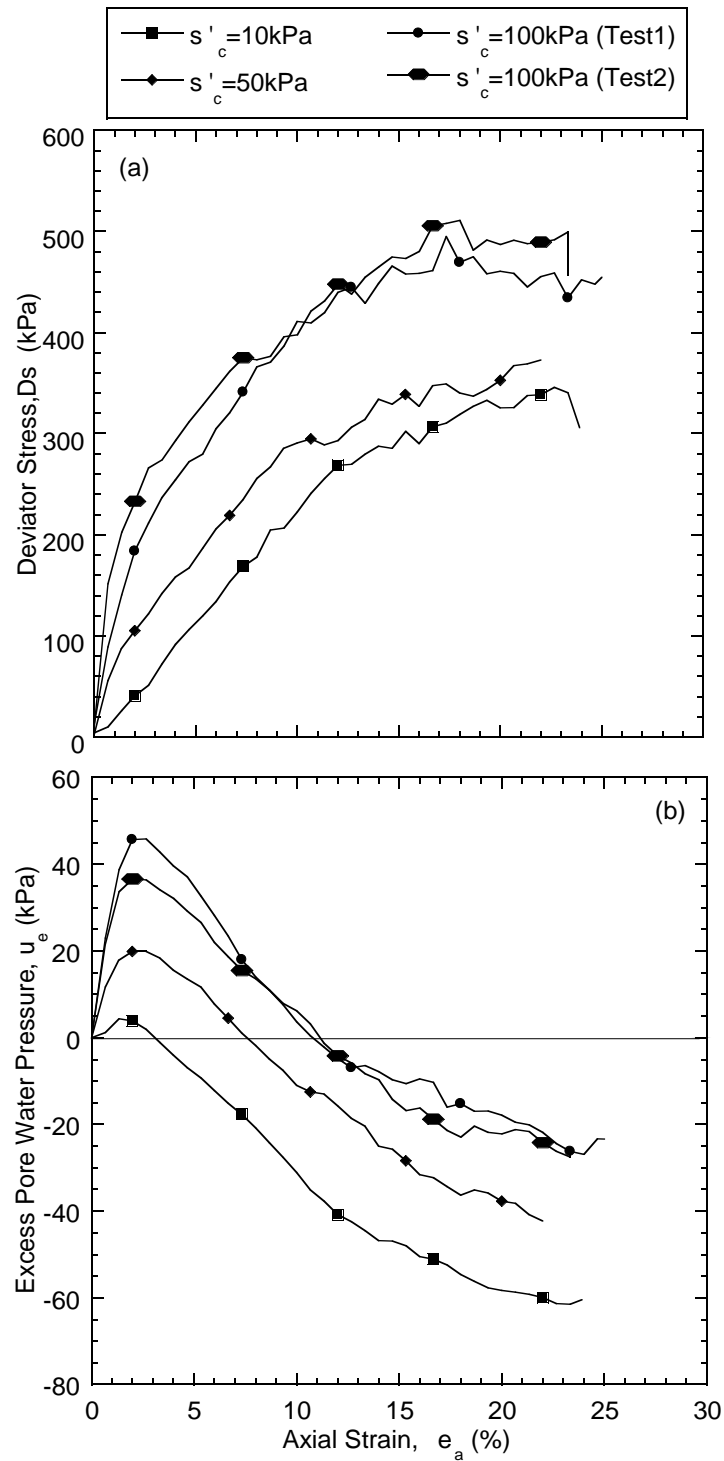


**Fig. 4.1.** Relationships of (a) deviator stress and (b) excess pore water pressure versus axial strain for consolidated undrained triaxial compression test on synthetic waste rock.

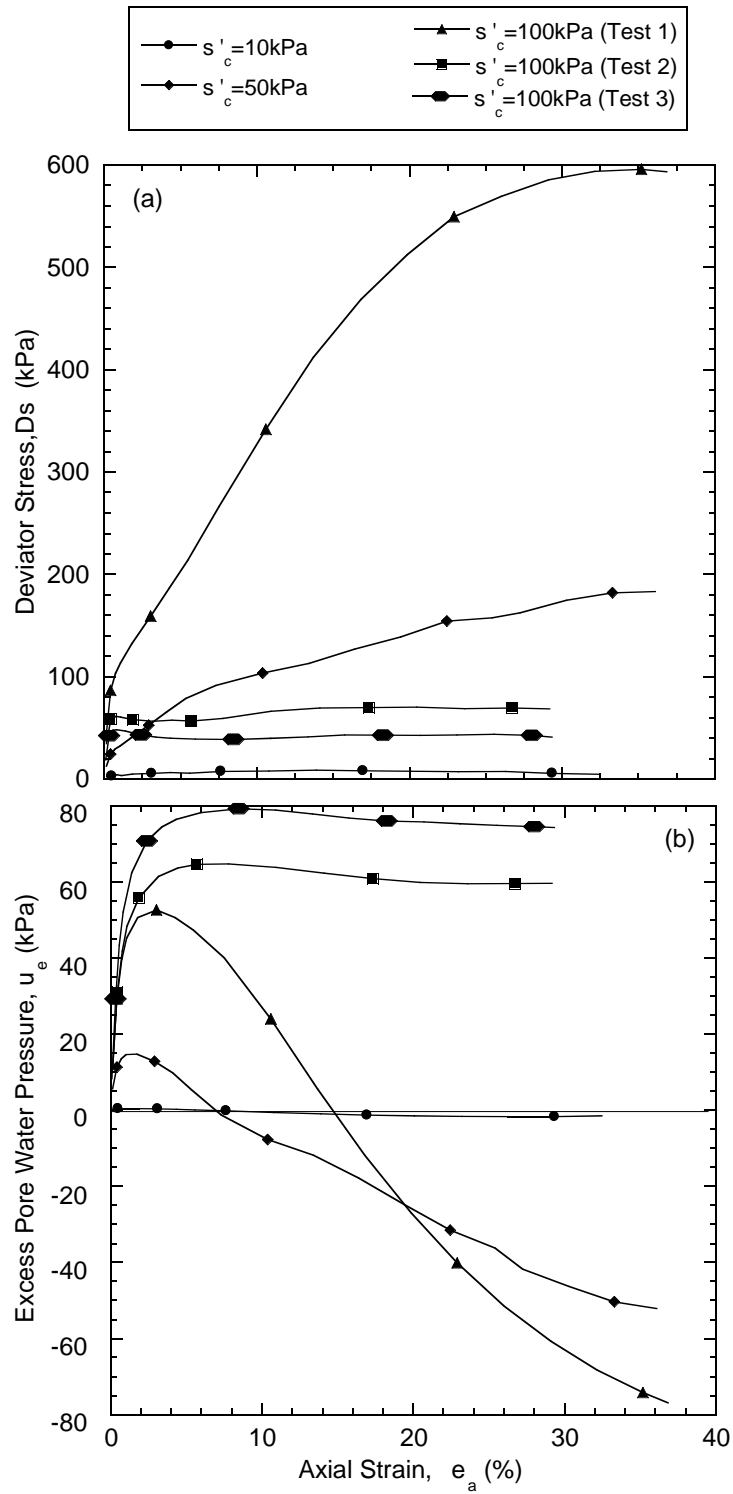


**Fig. 4.2.** Relationships of (a) deviator stress and (b) excess pore water pressure versus axial strain for consolidated undrained triaxial compression test on average synthetic tailings.

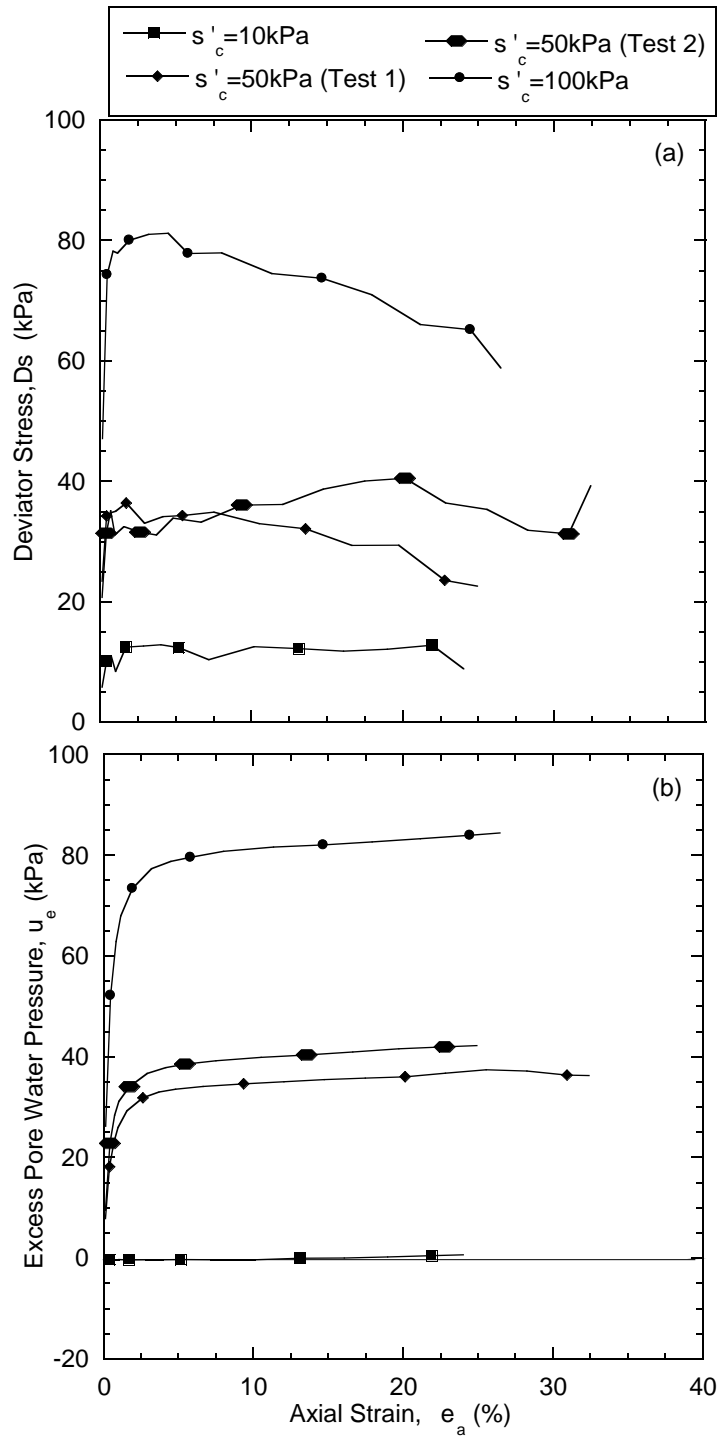


**Fig. 4.3.** Relationships of (a) deviator stress and (b) excess pore water pressure versus axial strain for consolidated undrained triaxial compression test on fine synthetic tailings.

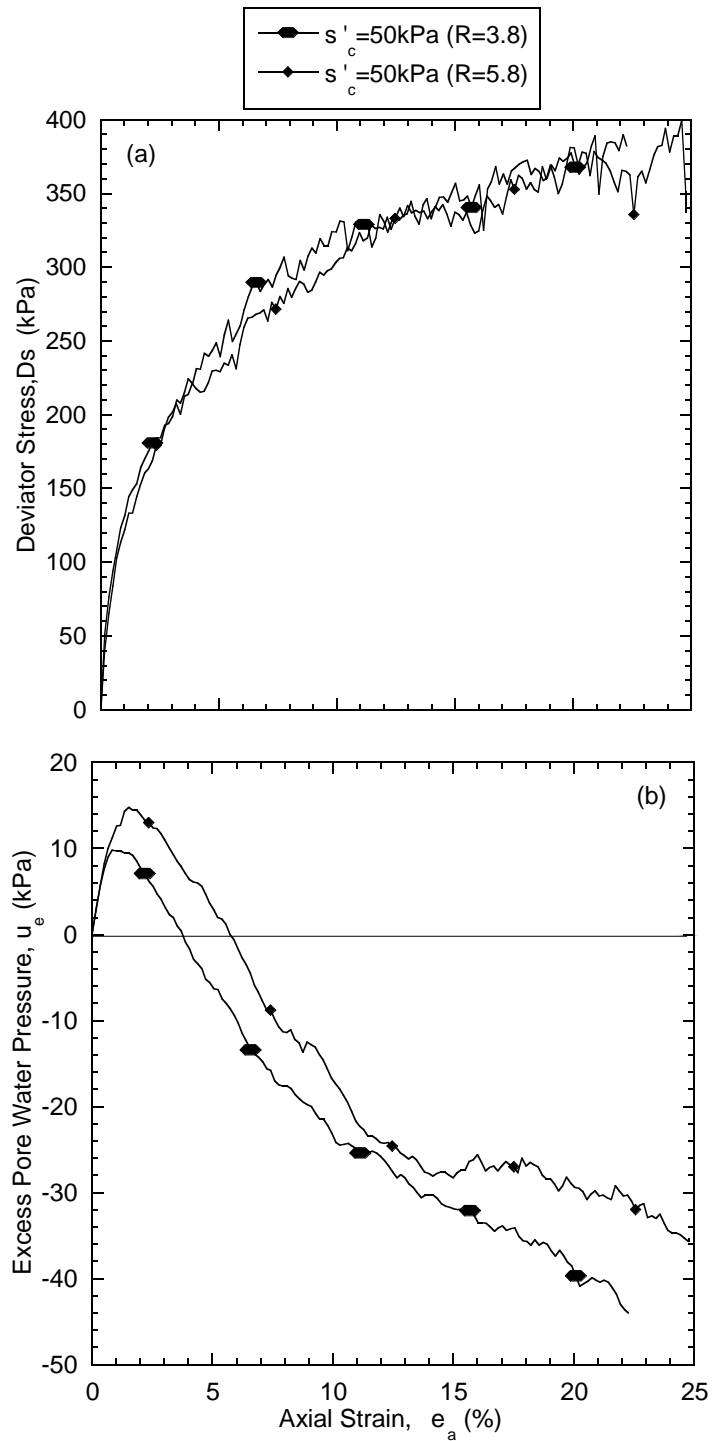


**Fig. 4.4.** Relationships of (a) deviator stress and (b) excess pore water pressure versus axial strain for consolidated undrained triaxial compression test on AST mixtures at  $R > R_{opt}$ .

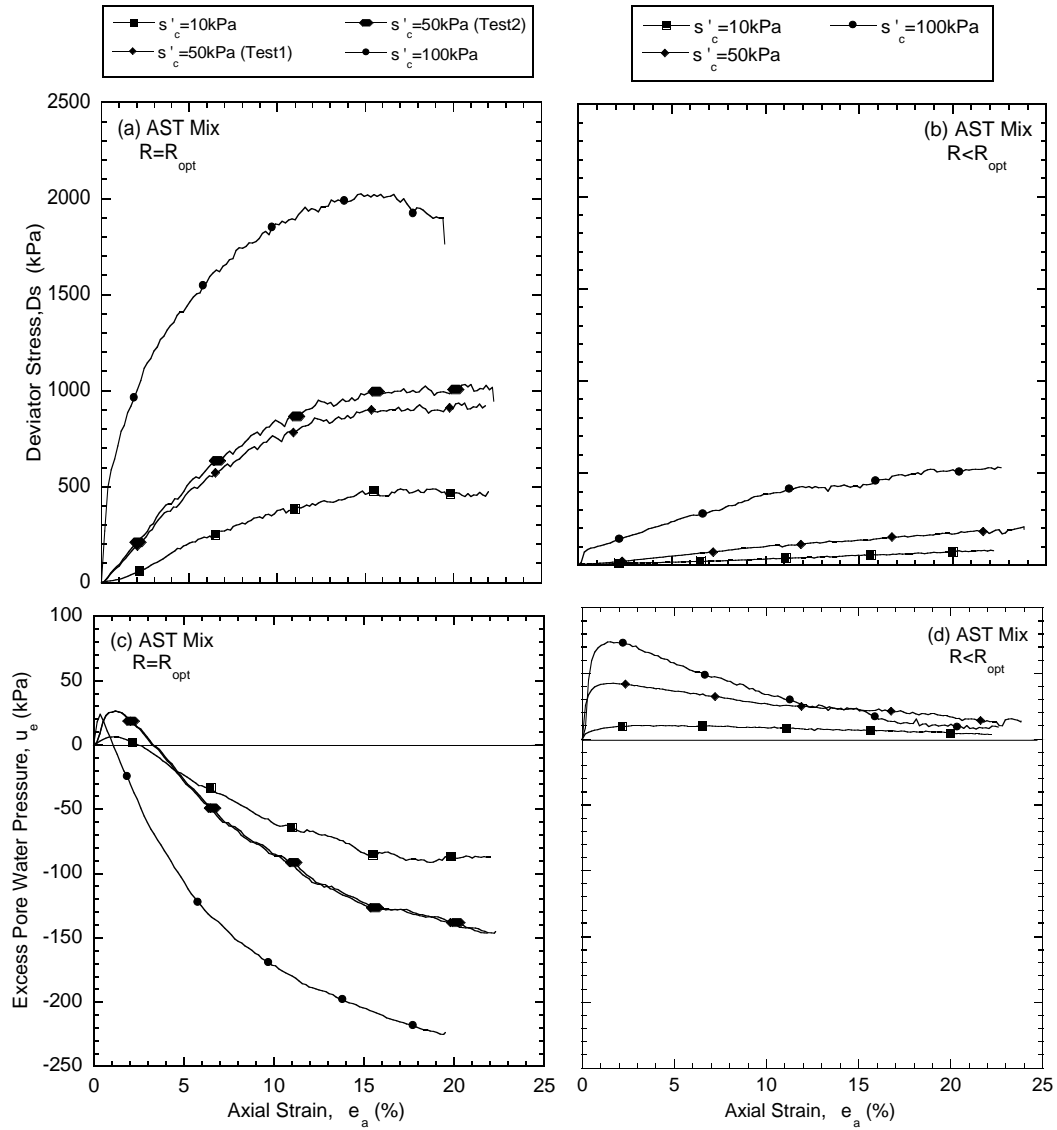


**Fig. 4.5.** Relationships of deviator stress and excess pore water pressure versus axial strain for consolidated undrained triaxial compression test on AST mixtures at  $R = R_{opt}$  and  $R < R_{opt}$ .

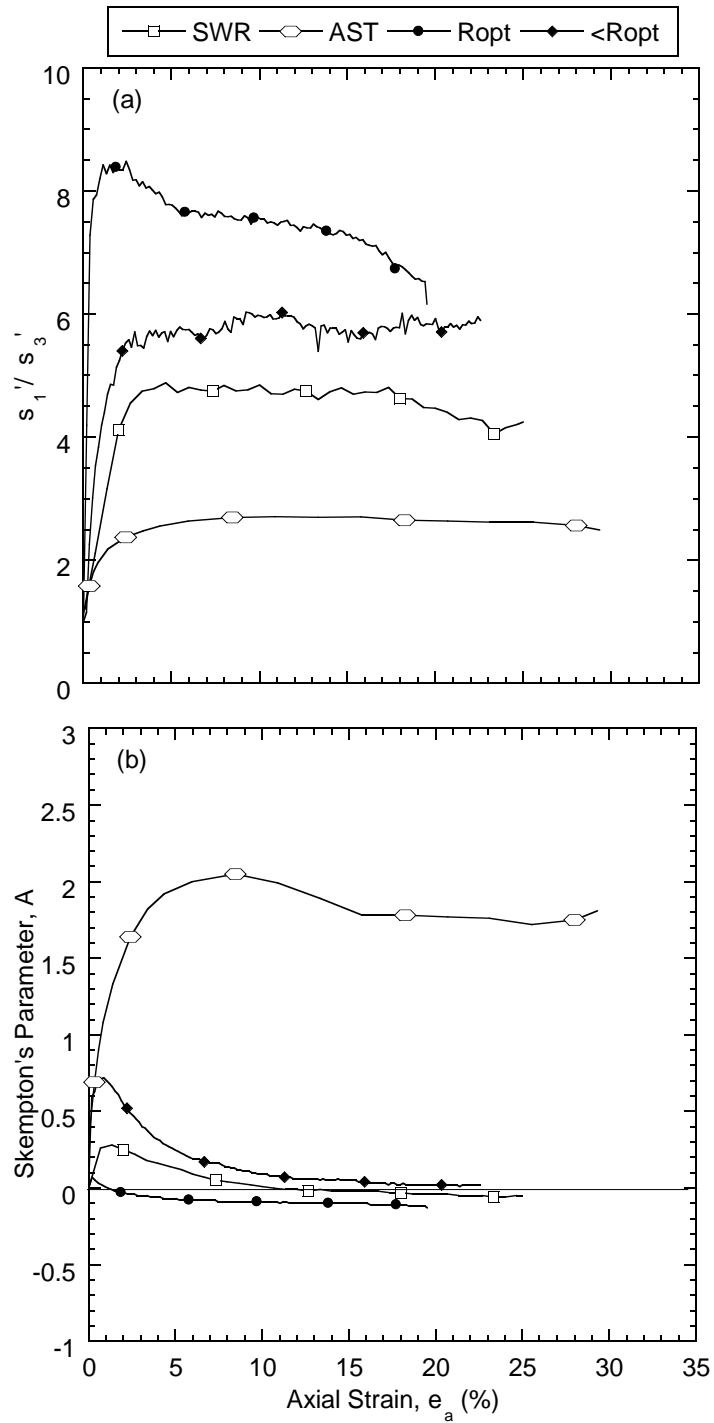


**Fig. 4.6.** Relationships of (a) principal stress ratio and (b) Skempton's A parameter versus axial strain for consolidated undrained triaxial compression test on AST, SWR and AST mixtures at 100 kPa confining stress.

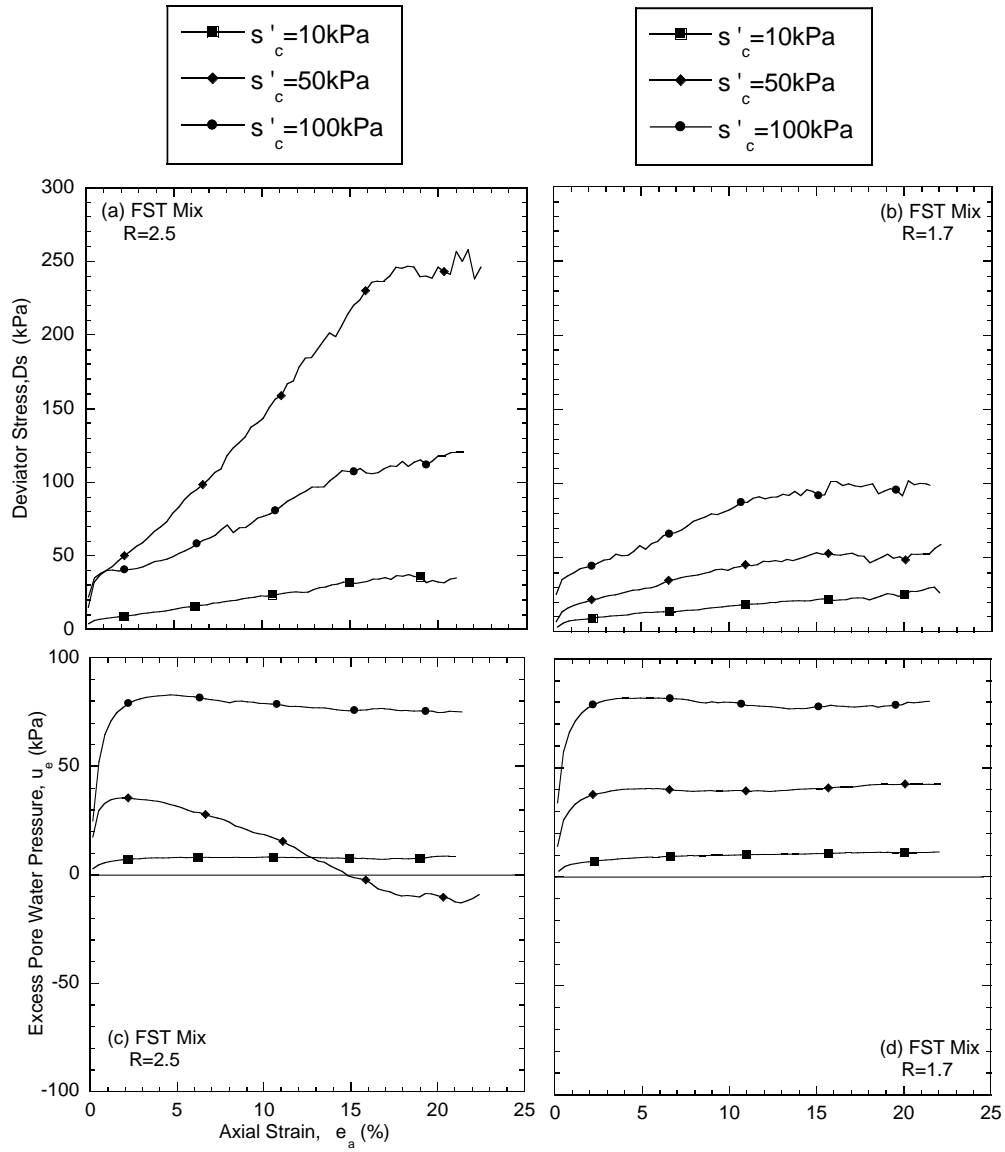


**Fig. 4.7.** Relationships of deviator stress and excess pore water pressure versus axial strain for consolidated undrained triaxial compression test on FST mixtures at  $R = R_{opt}$  and  $R < R_{opt}$ .

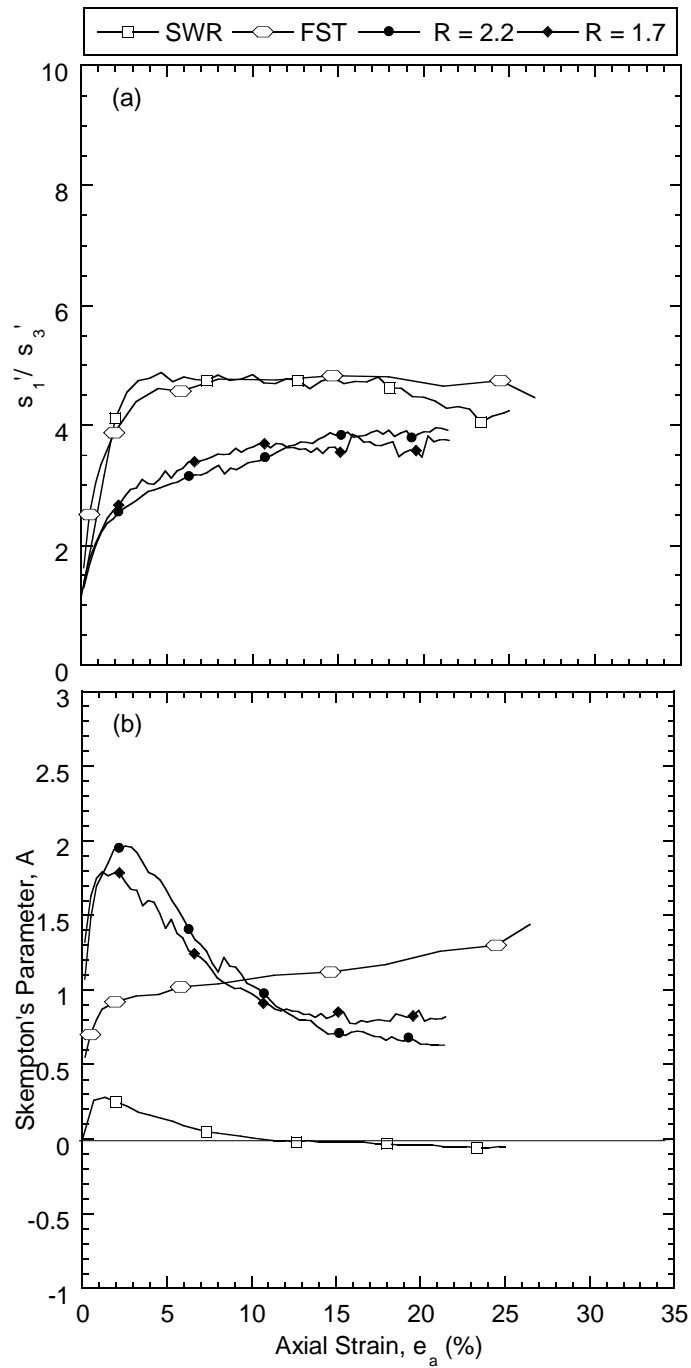


**Fig. 4.8.** Relationships of (a) principal stress ratio and (b) Skempton's A parameter versus axial strain for consolidated undrained triaxial compression test on FST, SWR and FST mixtures at 100 kPa confining stress.

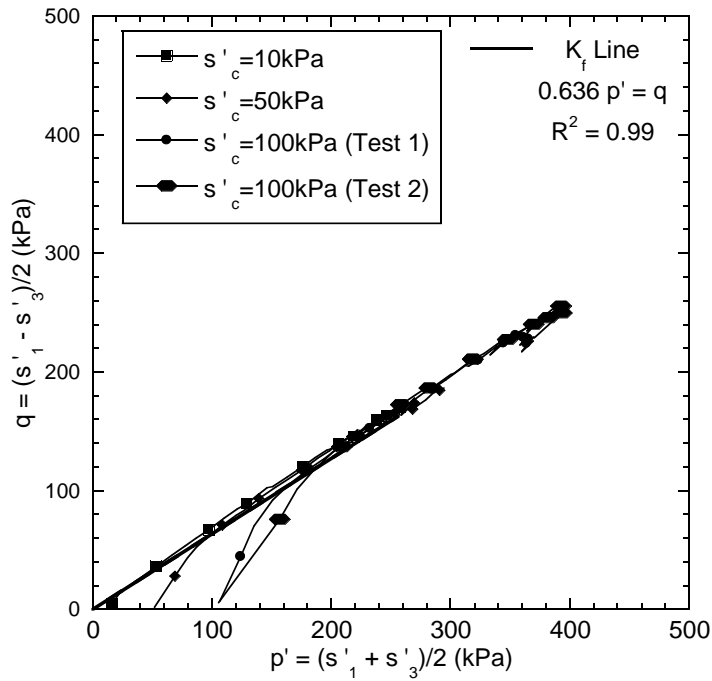


**Fig. 4.9.** Stress paths and  $K_f$  line at  $p'$ - $q$  space for analysis conducted using failure criterion of reaching  $K_f$  line for SWR.

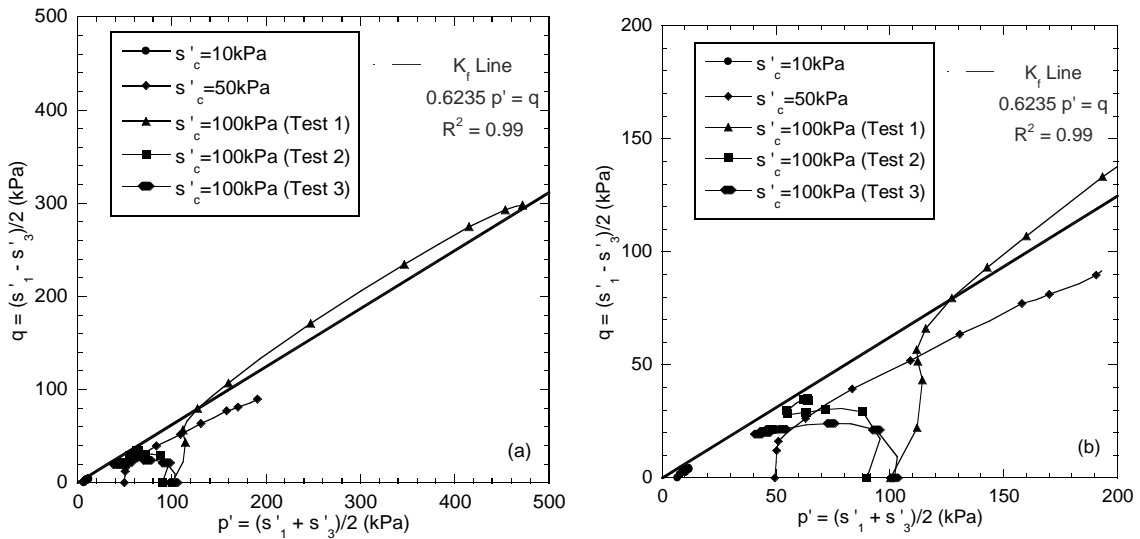


**Fig. 4.10.** Stress paths and  $K_f$  line at  $p'$ - $q$  space for analysis conducted using failure criterion of reaching  $K_f$  line for AST, (a) a full failure envelope and (b) detail for repeat tests at 100 kPa.

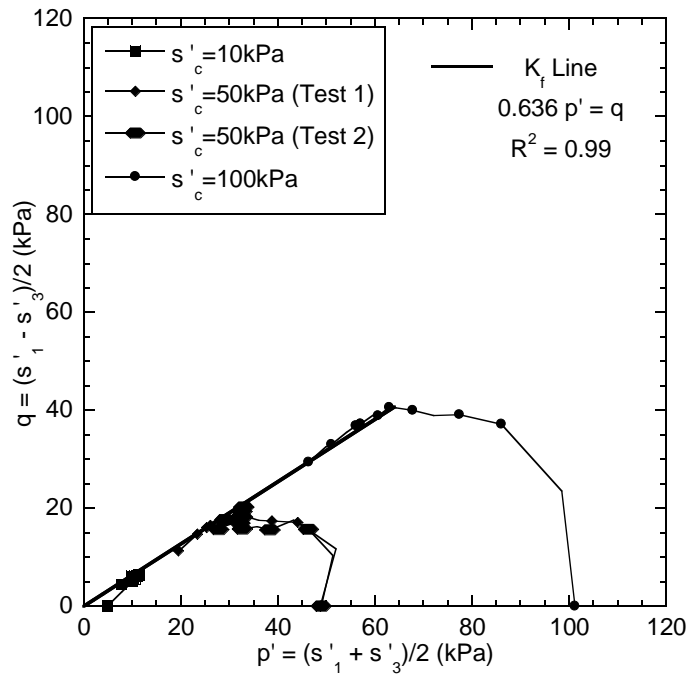


**Fig. 4.11.** Stress paths and  $K_f$  line at  $p'$ - $q$  space for analysis conducted using failure criterion of reaching  $K_f$  line for FST.

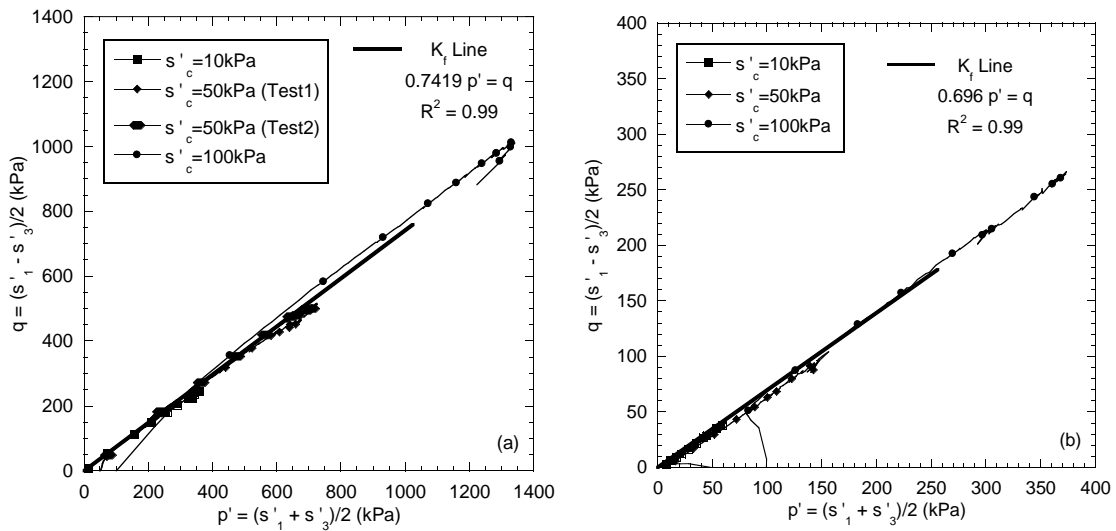


**Fig. 4.12.** Stress paths and  $K_f$  line at  $p'$ - $q$  space for analysis conducted using failure criterion of reaching  $K_f$  line for (a) WR&T mixtures with AST at  $R = R_{opt}$  and (b) WR&T mixtures with AST at  $R < R_{opt}$ .

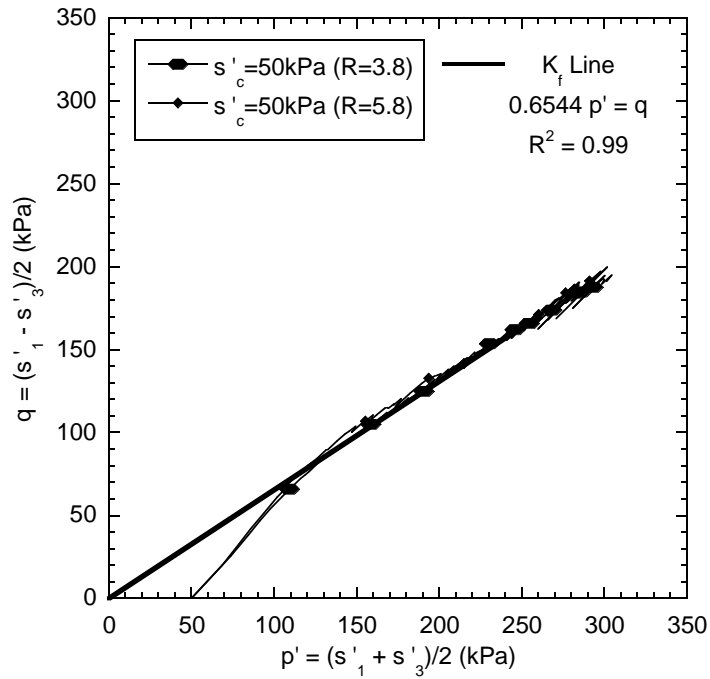


**Fig. 4.13.** Stress paths and  $K_f$  line at  $p'$ - $q$  space for analysis conducted using failure criterion of reaching  $K_f$  line for WR&T mixtures with AST at  $R > R_{opt}$ .

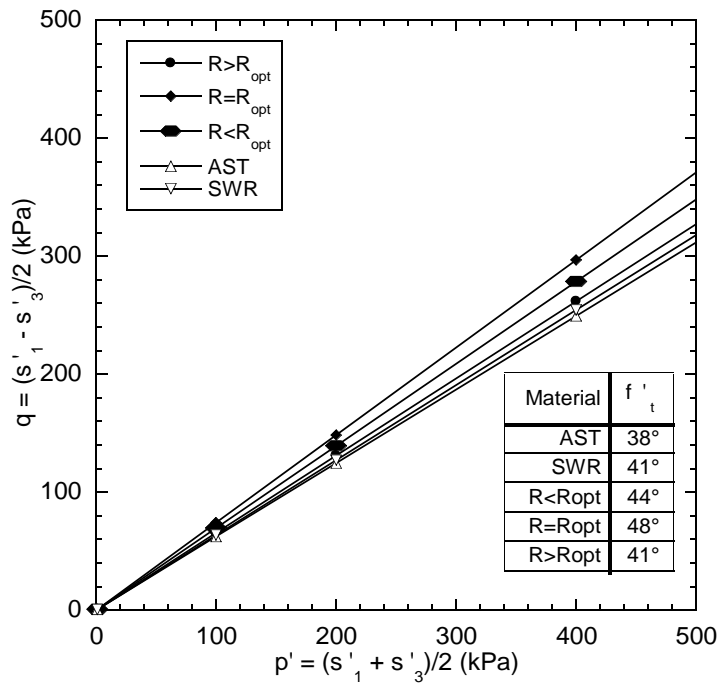


**Fig. 4.14.** Summary of  $\phi'_t$  accounting for failure envelope and slope of  $K_f$  line for AST, SWR and WR&T mixture with AST.

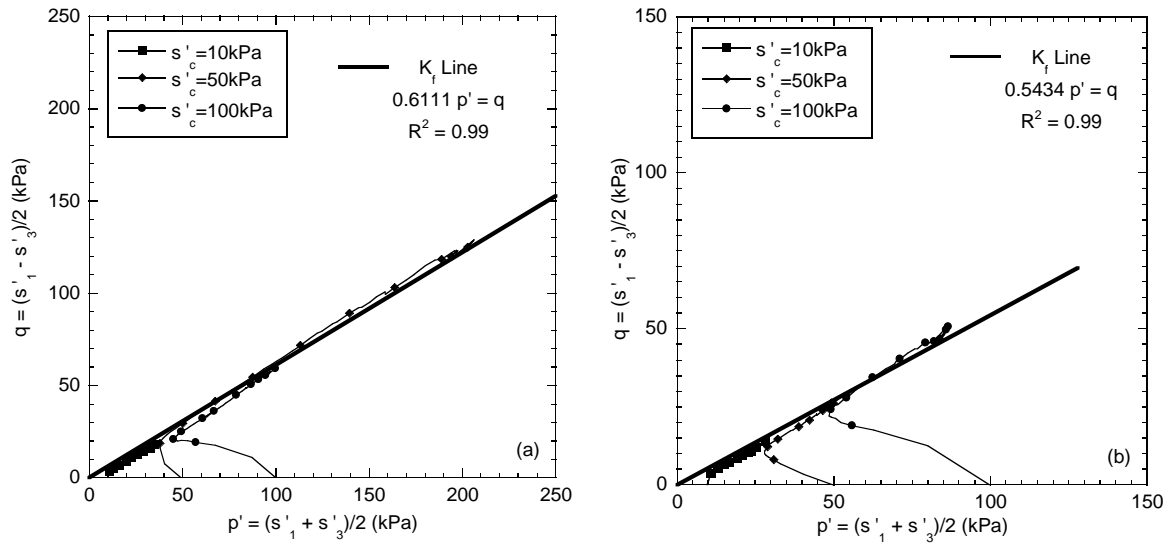


**Fig. 4.15.** Stress paths and  $K_f$  line at  $p'$ - $q$  space for analysis conducted using failure criterion of reaching  $K_f$  line for (a) WR&T mixtures with FST at  $R = 2.5$  and (b) WR&T mixtures with FST at  $R = 1.7$ .

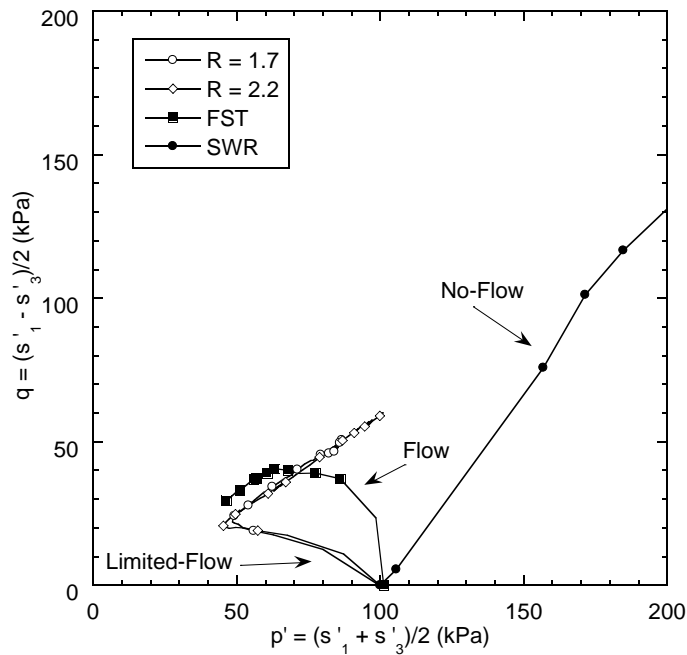


**Fig. 4.16.** Stress paths at  $p'$ - $q$  space for analysis of flow behavior comparing SWR, FST and FST mixtures at  $\sigma'_c = 100$  kPa.

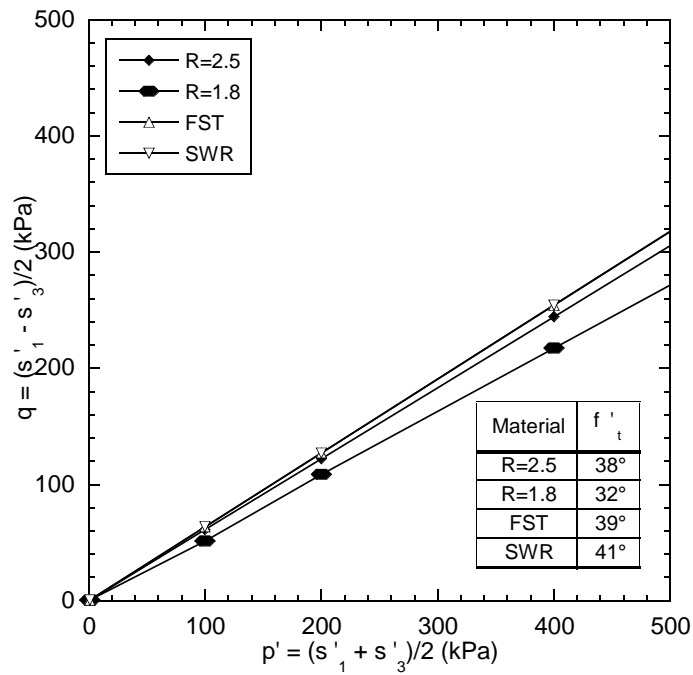


**Fig. 4.17.** Summary of  $\phi'_t$  accounting for failure envelope and slope of  $K_f$  line for FST, SWR and WR&T-FST mixtures.

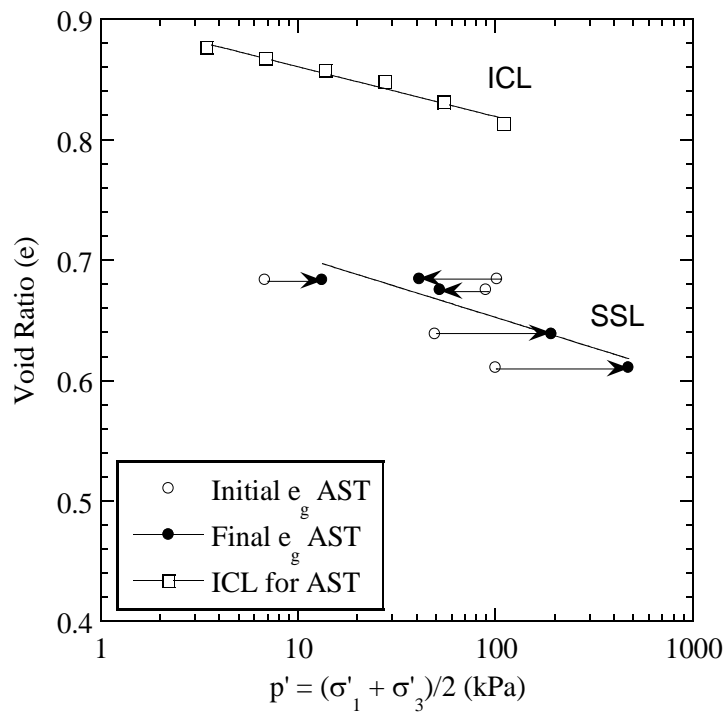


**Fig. 4.18.** Relationships of AST global void ratio with mean effective stress for consolidated undrained triaxial tests. Isotropic consolidation line (ICL) and steady-state line (SSL) are shown as logarithmic regression lines.

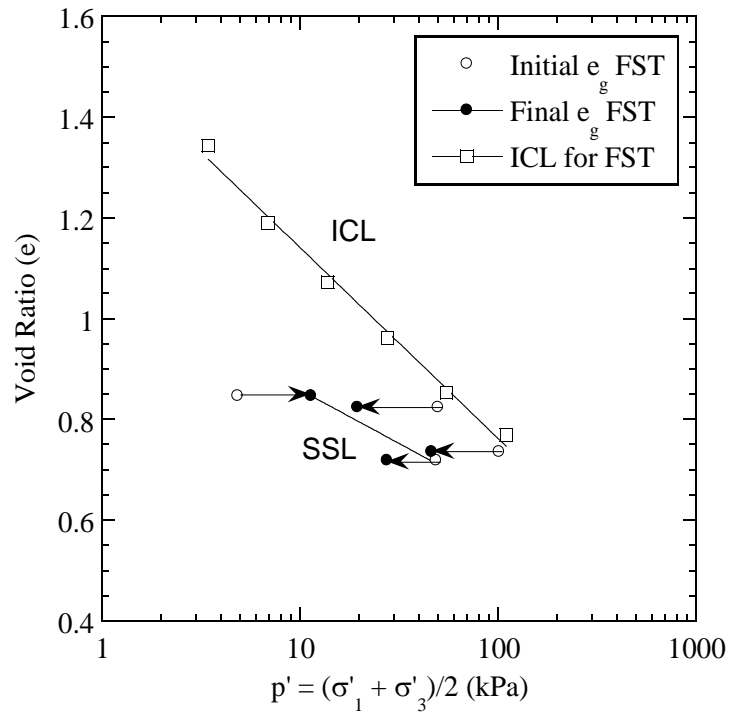


**Fig. 4.19.** Relationships of FST global void ratio with mean effective stress for consolidated undrained triaxial tests. Isotropic consolidation line (ICL) and steady-state line (SSL) are shown as logarithmic regression lines.

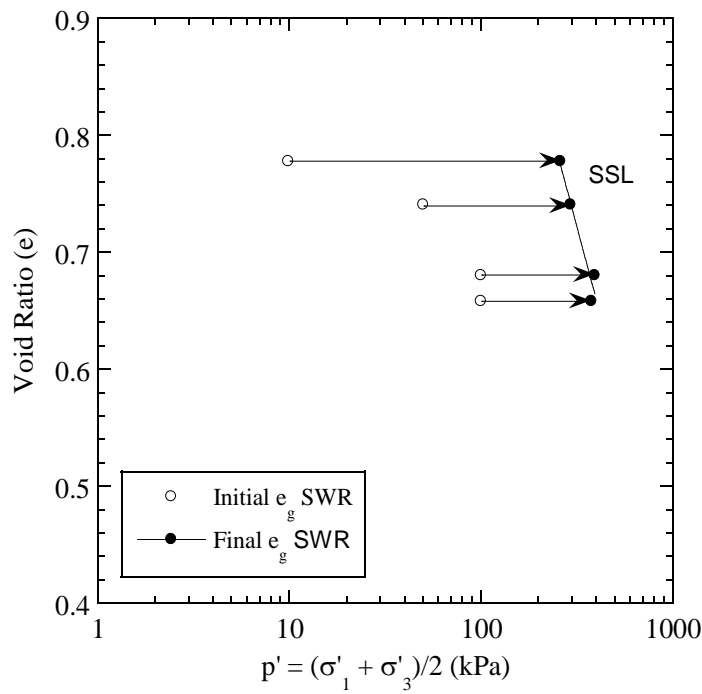


**Fig. 4.20.** Relationships of SWR global void ratio with mean effective stress for consolidated undrained triaxial tests. Steady-state line (SSL) shown as logarithmic regression line.

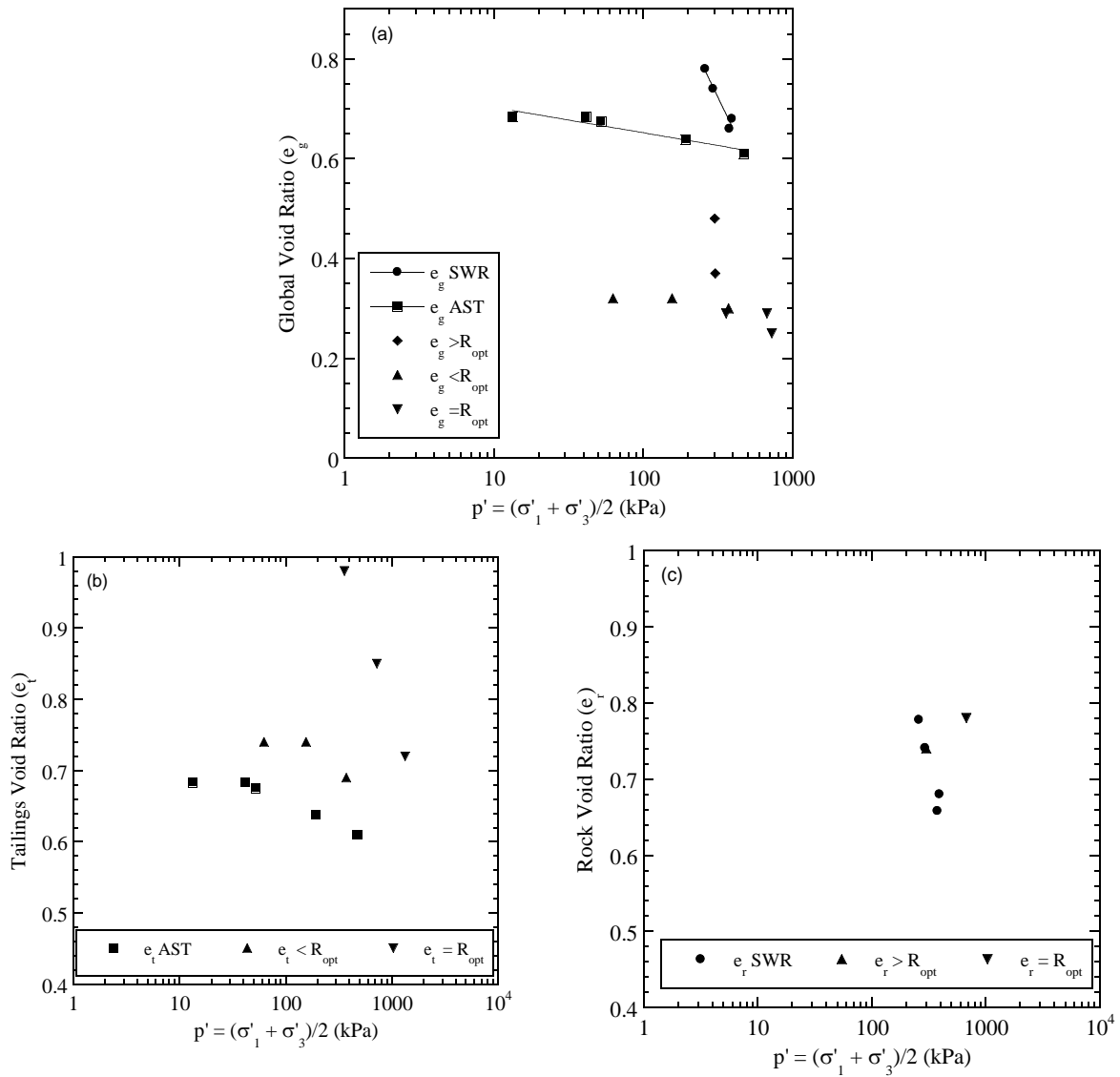


**Fig. 4.21.** Relationships of (a) global void ratio, (b) tailings void ratio, and (c) rock void ratio with mean effective stress for consolidated undrained triaxial tests in WR&T-AST mixtures.

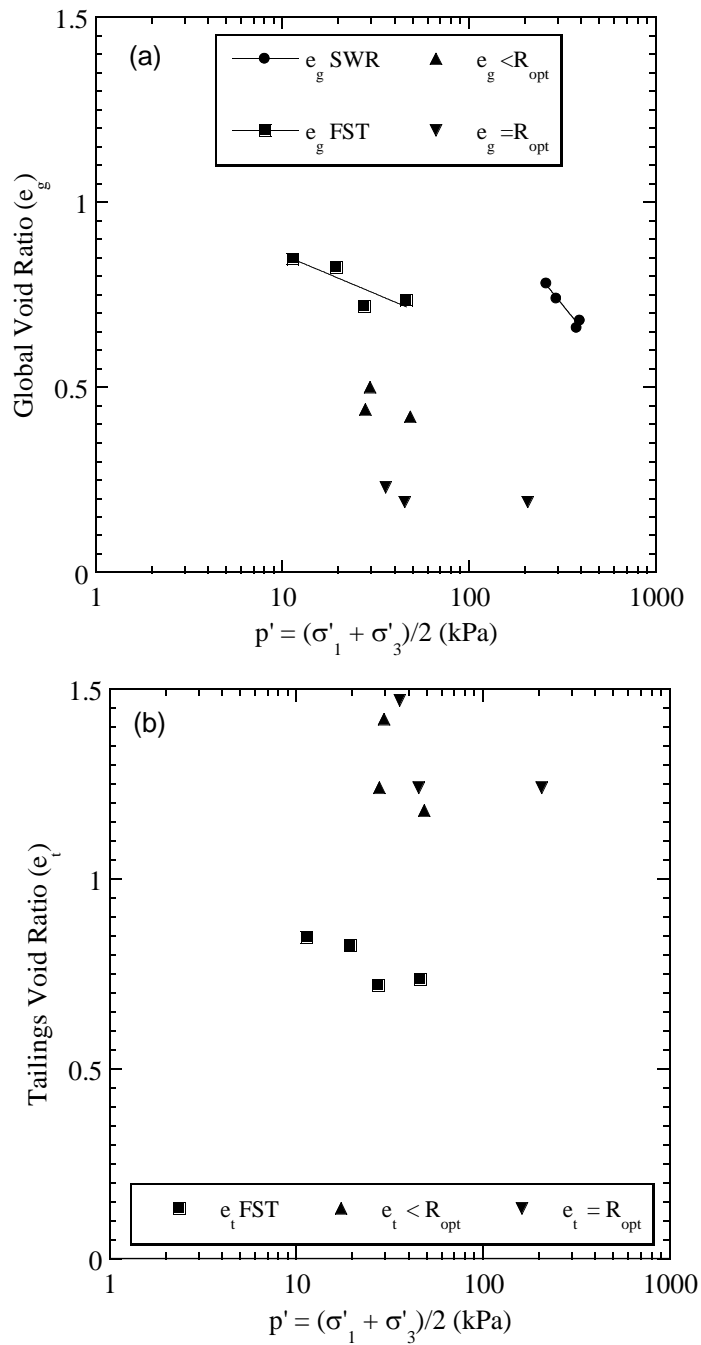


**Fig. 4.22.** Relationships of (a) global void ratio and (b) tailings void ratio and with mean effective stress for consolidated undrained triaxial tests in WR&T-FST mixtures.

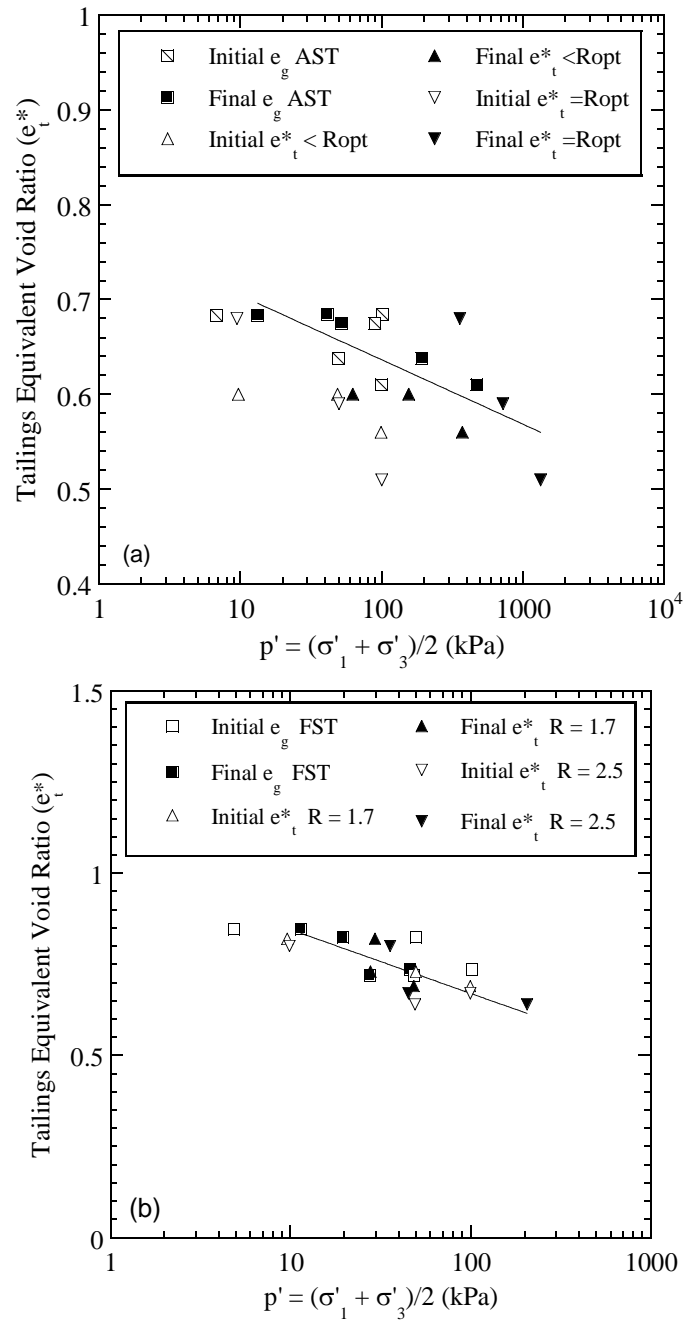


**Fig. 4.23.** Relationships for equivalent fine void ratio and mean effective stress for (a) AST mixtures and (b) FST mixtures sheared undrained.



## 5.1 Summary and Conclusion

In this study, the effects of tailings composition and mixture ratio ( $R$ ) on undrained shear behavior were evaluated. Crushed granite was used as a synthetic waste rock (SWR), and mixtures of sand, silt, and clay were used to create two synthetic mine tailings: average synthetic tailings (AST) and fine synthetic tailings (FST). Consolidated undrained (CU) triaxial compression tests were conducted on pure SWR, AST, and FST to determine baselines for comparison with mixtures of waste rock and tailings (WR&T). Mixtures of WR&T were prepared at different  $R$  and evaluated in CU triaxial compression. The following conclusions were drawn from this study.

- Pure SWR yielded no-flow, dilative, strain-hardening behavior and a tangent friction angle ( $\phi'_t$ ) = 41°. Pure AST yielded no-flow, strain-hardening behavior as well as limited-flow and flow behavior; the differences in undrained shear behavior were attributed to differences in initial specimen void ratio ( $e_o$ ). Pure FST yielded predominantly limited-flow and flow behavior. Synthetic tailings tangent friction angles were  $\phi'_t = 38^\circ$  for AST and  $\phi'_t = 39^\circ$  for FST.
- Coarse-dominated WR&T structures (i.e.,  $R > R_{opt}$ ) exhibited similar shear behavior to pure SWR (i.e., similar magnitudes of  $\Delta\sigma$  and  $u_e$  for a given  $\sigma'_c$  and similar  $\phi'_t$ ). Comparable undrained shear behavior was attributed to the presence of large air voids throughout the WR&T specimens that yielded a similar structure to pure SWR.
- Fine-dominated WR&T structures (i.e.,  $R < R_{opt}$ ) for both AST and FST yielded shear behavior that was more comparable to the behavior of the tailings. As  $R$  increased from  $R < R_{opt}$  to  $R \approx R_{opt}$  via addition of waste rock to the mixtures, shear behavior transitioned from a contractive, strain-softening response to a more dilative, strain-hardening response. This transition was attributed to more pronounced interaction between waste

rock inclusions in a fine-dominated structure and shows potential to mitigate development of flow behavior.

- Effective stress friction angles for WR&T mixtures increased as  $R$  increased toward  $R_{opt}$ : mixtures of AST yielded  $\phi'_t = 48^\circ$  for  $R = 2.5$  and  $\phi'_t = 44^\circ$  for  $R = 1.4$ , whereas mixtures of FST yielded  $\phi'_t = 38^\circ$  for  $R = 2.5$  and  $\phi'_t = 32^\circ$  for  $R = 1.8$ . Tailings composition and void ratio within fine-dominated WR&T mixtures affects  $\phi'_t$ . Larger tailings void ratios for FST mixtures resulted in lower  $\phi'_t$  compared to pure FST.
- The largest  $\phi'_t$  and most pronounced strain-hardening response during undrained shear were observed for WR&T mixtures prepared with  $R \approx R_{opt}$ . This behavior was attributed to tailings filling the void space between waste rock particles without compromising the waste rock skeleton, which provides resistance against rearrangement of waste rock particles and yields increased shear resistance.
- Equivalent void ratios computed for WR&T mixtures can be used to evaluate the steady state of mixtures regardless of  $R$ . An analysis of steady state behavior can be used to predict undrained behavior of a mixture with respect to the void ratio and mean effective stress (i.e., state) of the mixture. The steady-state analysis for WR&T mixtures suggests that liquefaction assessments commonly conducted on mixtures of silty sands can be extended to evaluate liquefaction potential of fine-dominated WR&T mixtures.

## 5.2 Future Research

This study was a step toward understanding the shear behavior of different WR&T mixtures such that guidelines and target mixtures can be developed for engineering applications. Further research is needed on the effects of mixture ratio on the shear behavior of WR&T to determine a practical range of mixture ratios that enhance undrained shear behavior and shear strength of mine tailings. There is a need to develop an effective method for mixing

WR&T, both at laboratory and large scale, to assess field-scale application of WR&T. Research on unsaturated properties (e.g., moisture retention) of WR&T mixtures is also needed to assess the applicability for WR&T mixtures as water storage layers in final cover systems. Finally, further testing and data compilation are needed to confirm that steady-state analysis is an effective method to evaluate flow potential of WR&T mixtures.

## REFERENCES

- ASTM D2487 (2011) Standard Practice for Classification of Soil for Engineering Purposes (USCS), *ASTM*
- ASTM C127 (2015) Standard Test Method for Relative Density (Specific Gravity) and Absorption of Coarse Aggregate, *ASTM*
- ASTM D4253 (2016) Standard Test Methods for Maximum Index Density and Unit Weight of Soils Using a Vibratory Table, *ASTM*
- ASTM D4254 (2016) Standard Test Methods for Minimum Index Density and Unit Weight of Soils and Calculation of Relative Density, *ASTM*
- ASTM D4767 (2011) Standard Test Method for Consolidated Undrained Triaxial Compression Test for Cohesive Soils, *ASTM*
- ASTM D698 (2012) Standard Test Methods for Laboratory Compaction Characteristics of Soil Using Standard Effort, *ASTM*
- ASTM D854-(2014) Standard Test Methods for Specific Gravity of Soil Solids by Water Pycnometer, *ASTM*
- ASTM D422-(2007) Standard Test Method for Particle-Size Analysis of Soil, *ASTM*
- ASTM D4318-(2010) Standard Test Methods for Liquid Limit, Plastic Limit, and Plasticity Index of Soils, *ASTM*
- Been, K. and Jefferies, M.G. (1985). A state parameter for sands, *Géotechnique*, 35(2), 99-112.
- Been, K., Jefferies, M. G., and Hachey, J. (1991). The critical state of sands. *Géotechnique*, 41(3), 365-381.
- Blight, G. (2010). *Geotechnical Engineering for Mine Waste Storage Facilities*, CRC Press, Taylor & Francis Group, London, UK.
- Bobei, D. C., Lo, S. R., Wanatowski, D., Gnanendran, C. T., & Rahman, M. M. (2009). Modified state parameter for characterizing static liquefaction of sand with fines. *Canadian Geotechnical Journal*, 46(3), 281-295.
- Boger, D.V., (2009), Rheology and the resource industries. *Chemical Engineering Science*, 64 (09) 4525 – 4536
- Brandon, T.L., Rose, A.T., and Duncan, J.M. (2006). Drained and undrained strength interpretation for low-plasticity silts, *Journal of Geotechnical and Geoenvironmental Engineering*, 132(2), 250-257.
- Bussièrè, B. (2007). Colloquium 2004: Hydrogeotechnical properties of hard rock tailings from metal mines and emerging geoenvironmental disposal approaches, *Canadian Geotechnical*

*Journal*, 44(9), 1019-1052.

- Casagrande, A., (1975), Liquefaction and Cyclic Deformation of Sands: a Critical Review. *Harvard University, Cambridge, Mass, Harvard Soil Mechanics Series No. 88.*
- Chapuis, R.P. 1990. Sand-bentonite liners: predicting permeability from laboratory tests. *Canadian Geotechnical Journal*, 27(1): 47–5.
- Clayton, S., Grice, T.G., Boger D.V. (2003). Analysis of the slump test for on-site yield stress measurement of mineral suspensions. *International Journal of Mineral Processing*. 70(3) 3-21.
- Davies, M., McRoberts, E., and Martin T. (2002). "Static liquefaction of tailings—fundamentals and case histories." AMEC Earth & Environmental, Vancouver and Edmonton, Canada.
- Finno, R.J., Harris, W.W., Mooney, M.A., and Viggiani, G. (1996), Strain Localization and Undrained Steady State Of Sand. *Journal of Geotechnical Engineering*, ASCE, 122(6): 462-473.
- Frossard, E., Hu, W., Dano, C., and Hicher, P. Y. (2012). Rockfill shear strength evaluation: a rational method based on size effects. *Géotechnique*, 62(5), 415.
- Gorakhki, M.H., and Bareither, C.A. (2016). Compressibility behavior of synthetic mine tailings amended with fly ash, *ASCE Geo-Chicago 2016*, 255-266.
- Guitierrez, M. (2003). Mixture theory characterization and modeling of soil mixtures, *Geomechanics*, 172 (34), 600-616.
- Howell, J. L., Shackelford, C. D., Amer, N. H., and Stem, R. T. (1997). Compaction of Sand-Processed Clay Soil Mixtures. *Geotechnical Testing Journal*, 20(4), 443-458.
- Jehring, M.M. and Bareither, C.A. (2016). Tailings composition effects on shear strength behavior of co-mixed mine waste rock and tailings, *Acta Geotechnica*, 1-20, online 23 Jan. 2016.
- Jennings, S.R., Neuman, D.R., and Blincker, P.S. (2008). Acid Mine Drainage and Effects of Fish Health and Ecology: A review, *Reclamation Research Group Publication*, Bozeman, MT.
- Khalili, A. and Wijewickreme, D. (2008). New slurry displacement method for reconstitution of highly gap-graded specimens for laboratory element testing, *Geotechnical Testing Journal*, 31(5), 424-432.
- Khalili, A., Wijewickreme, D., and Wilson, G.W. (2005). Some observations on the mechanical response of mixtures of mine waste and tailings. *Proc. 58th Canadian Geotechnical Conference*.
- Khalili, A., Wijewickreme, D., and Wilson, W. (2010). Mechanical response of highly gap-graded mixtures of waste rock and tailings. Part I: Monotonic shear response, *Canadian Geotechnical Journal*, 47(5), 552-565.

- La Rochelle, P., Leroueli, S., Trak, B., Blais-Leroux, L., and Tavenas, F. (1988). Observational Approach to Membrane and Area Corrections in Triaxial Tests, *Advanced Triaxial Testing of Soils and Rock*, ASTM, STP 977, 715-731.
- Leduc, M., Backens, M., and Smith, M.E. (2004). Tailings co-disposal at the Esquel gold mine Patagonia, Argentina, *Proc. SME Annual Meeting, Denver, Colorado*, 5 pp.
- Marachi, N.D., Chan, C.K., and Seed, H.B. (1972). Evaluation of properties of rockfill materials, *Journal of Soil Mechanics and Foundation Engineering*, 98(SM1), 95-114.
- Matyas, E.L., Welch, D.E., and Reades, D.W. (1984). Geotechnical parameters and behaviour of uranium tailings, *Canadian Geotechnical Journal*, 21(3), 489-504.
- MMSD, (2002), Breaking New Ground: the Report of the Mining, Minerals and Sustainable Development Project, *Earthscan Publications, Ltd.*, London, UK.
- MEND (2001). List of Potential Information Requirements in Metal Leaching/Acid Rock Drainage Assessment and Mitigation Work. *Mine Environment Neutral Drainage Program*. W. A. Price, CANMET, Canada Center for Mineral and Energy
- Morris, P.H. and Williams, D.J. (1997). Results of field trials of co-disposal of coarse and fine coal waste, *Transactions of the Institution of Mining and Metallurgy*, 106, A38-A41.
- Ni, Q., Tan, T. S., Dasari, G. R., and Hight, D. W. (2004). Contribution of fines to the compressive strength of mixed soils. *Géotechnique*, 54(9), 561-569.
- Olson, S. M., & Stark, T. D. (2003). Yield strength ratio and liquefaction analysis of slopes and embankments. *Journal of Geotechnical and Geoenvironmental Engineering*, 129(8), 727-737.
- Qiu, Y. and Sego, D.C. (2001). Lab properties of mine tailings, *Canadian Geotechnical Journal*, 38(1), 183-190.
- Rahman, M. M., Lo, S. R., and Gnanendran, C. T. (2008). On equivalent granular void ratio and steady state behavior of loose sand with fines. *Canadian Geotechnical Journal*, 45(10), 1439-1456.
- Thevanayagam, S. (1998). Effect of fine and confining stress on undrained shear strength of silty sands, *Journal of Geotechnical and Geoenvironmental Engineering*, 124(6), 479-491.
- Thevanayagam, S., Shenthan, T., Mohan, S., and Liang, J. (2002). Undrained fragility of clean sands, silty sands, and sandy silts, *Journal of Geotechnical and Geoenvironmental Engineering*, 128(10), 849-859.
- Thevanayagam, S. (2007). Intergrain contact density indices for granular mixes I - Framework, *Journal of Earthquake Engineering and Engineering Vibrations*, 6(2), 123-134.
- Wang, S., Luna, R., and Stephenson, R.W. (2011). A slurry consolidation approach to reconstitute low-plasticity silt specimens for laboratory triaxial testing, *Geotechnical Testing Journal*, 34(4), 1-9.

- Wickland, B.E., and Wilson, G.W. (2005). Self-weight consolidation of mixtures of mine waste rock and tailings, *Canadian Geotechnical Journal*, 42(2), 327-339.
- Wickland, B.E., Wilson, G.W., Wijewickreme, D., and Klein B. (2006). Design and evaluation of mixtures of mine waste rock and tailings, *Canadian Geotechnical Journal*, 43, 928-945.
- Wickland, B.E., Wilson, G.W. and Wijewickreme, D. (2010). Hydraulic conductivity and consolidation response of mixtures of mine waste rock and tailings, *Canadian Geotechnical Journal*, 47(4), 472-485.
- Williams, D.,J., Wilson, G.W., and Panidis, C. (2003). Waste rock and tailings mixtures as a possible seal for potentially acid forming waste rock, *Proc. 6th Intl Conf. on Acid Rock Drainage*, Cairns, QLD, 427-435.
- Yang, S.L., Sandven, R., and Grande, L., (2006). Steady-state lines of sand-silt mixtures. *Canadian Geotechnical Journal*, 43(11): 1213-1219.
- Zuo, L., & Baudet, B. A. (2015). Determination of the transitional fines content of sand-non plastic fines mixtures. *Soils and Foundations*, 55(1), 213-219.

## APPENDIX A: SAMPLE VOID RATIO CALCULATION

The objective of this appendix is to document a systematic procedure, accounting for measured data, background theory and assumptions to calculate equivalent void ratio for waste rock and tailing (WR&T) mixtures. An example calculation is presented with the objective of clarifying each step of the procedure. The WR&T mixture with average synthetic tailings prepared at a mixture ratio ( $R$ ) of 2.22 and tested in a CU triaxial compression at  $\sigma'_c = 100$  kPa was chosen for this example. Weight-volume relationships were used to determine global void ratio ( $e_g$ ), fraction void ratios ( $e_r$  and  $e_t$ ). Equations 2.7 and 2.8 were used to calculate equivalent void ratios ( $e^*_r$  and  $e^*_t$ ).

Measurements conducted at the end of each experiment include the mass of waste rock ( $M_r$ ), mass of tailings ( $M_t$ ) and mass of water tailings ( $M_{water}$ ). All water within the WR&T mixture was assumed to be retained within the finer (i.e. tailings) matrix. Ratio of  $M_r$  to  $M_t$  were used to define true  $R$  of the specimens, as shown in Eq. A.1. Water content of tailings ( $w$ ) was defined as the ratio of ( $M_{water}$ ) to  $M_t$ , seen in Equation A.2. For this example, measurements were  $M_r = 6879$  g,  $M_t = 3096.7$  g, and  $M_{water} = 836$  g.

$$R = \frac{M_r}{M_t} = \frac{6879}{3096.7} = 2.22 \quad (\text{A.1})$$

$$w = \frac{M_{water}}{M_t} = \frac{836}{3096.7} = 27\% \quad (\text{A.2})$$

Once  $R$  and  $w$  were defined, every specimen was standardized by defining volume of rock ( $V_r$ ) was 1 volume unit. This facilitates following volumetric calculations. Volume of voids of waste rock ( $V_{v,r}$ ) for mixtures before shear was assumed be equal to the  $V_{v,r}$  for tests at pure

SWR consolidated to the same  $\sigma'_c$ . This assumption was made based on data from Wickland et al. (2006) that shows equivalency on consolidation of pure waste rock and mixtures at  $R_{opt}$ . For this example at  $\sigma'_c = 100$  kPa,  $V_{v,r} = 0.68$  (Table 4.1).

Equations A.3 and A.4 re-calculate new values for  $M_r$  and  $M_t$  based on assumed  $V_r = 1$ , known specific gravity of SWR ( $G_{swr} = 2.7$ ), and  $R$  from on Eq. A.1. Volume of tailings ( $V_t$ ) based on known specific gravity of tailings ( $G_{ast} = 2.66$ ) and volume of water ( $V_{water}$ ) based on calculated  $w$  are shown in Eqs. A.5 and A.6 respectively. Volume of the slurry ( $V_{slurry}$ ) will be the sum of  $V_{water} + V_t$ , in Eq. A.7

$$M_r = V_r * G_{swr} = 1 * 2.7 = 2.7 \quad (\text{A.3})$$

$$M_t = \frac{M_r}{R} = \frac{2.7}{2.22} = 1.22 \quad (\text{A.4})$$

$$V_t = \frac{M_t}{G_{ast}} = \frac{1.22}{2.66} = 0.457 \quad (\text{A.5})$$

$$V_{water} = M_t * w = 1.22 * 0.27 = 0.329 \quad (\text{A.6})$$

$$V_{slurry} = V_t + V_{water} = 0.457 + 0.328 = 0.785 \quad (\text{A.7})$$

Global void ratio ( $e_g$ ) is defined as the ratio between volume of voids ( $V_v$ ) and volume of solids ( $V_s$ ), whereby  $V_s = V_r + V_t$  and  $V_v = V_w + V_{air}$ . Volume of air ( $V_{air}$ ) has to be considered if mixture has  $R > R_{opt}$  (i.e., coarse-dominated structure). For coarse dominated structures  $V_{air} = V_{v,r} - V_{slurry}$ , but this example shows a fine-dominated structure (i.e.,  $R < R_{opt}$ ), therefore  $V_{air} = 0$

Results for  $V_s$  and  $V_v$  are in Eqs. A.8 and A.9. The calculation of  $e_g$  is shown subsequently in in Eq. A.10.

$$V_s = V_r + V_t = 1 + 0.457 = 1.457 \quad (\text{A.8})$$

$$V_v = V_w = 0.328 \quad (\text{A.9})$$

$$e_g = \frac{V_v}{V_s} = \frac{0.328}{1.457} = 0.23 \quad (\text{A.10})$$

Calculation of fraction void ratios (i.e.,  $e_r$  and  $e_t$ ) are presented on Section 2.2. Fraction void ratios are only relevant for respective structure, such that for fine dominated structure has  $e_t$  and for coarse dominated structure has  $e_r$ . According to Thevanayagam (1998), the  $e_t$  for a fine dominated structure is calculated as  $e_t = V_v / V_t$ , neglecting the volume of rock. This assumes that structure will be controlled by fine fraction and void ratio of the tailings fraction will better describe the behavior. For this example, calculation of  $e_t$  is shown in Eq. A.11

$$e_t = \frac{V_v}{V_t} = \frac{0.328}{0.457} = 0.72 \quad (\text{A.11})$$

Thevanayagam (2007) provide the equations, shown in Section 2.2., for calculation of equivalent void ratios (i.e.  $e_r^*$  and  $e_t^*$ ). This example will focus on the calculation of  $e_t^*$  for a fine dominated structure. In the event of a coarse dominated structure, equivalent coarse void ratio is calculated according to Eq. 2.8. The calculation for a  $e_t^*$  is extracted from in Eq. 2.7. Further parameters needed to calculate  $e_t^*$  are  $d_r$ ,  $f_c$  and  $m$ . Calculation of  $d_r$  and  $f_c$  are shown in Eq. A.12 and A.13 following guidelines of Section 2.2. Parameter  $m$  is a coefficient ranging between 0 and 1 that depends on particle characteristics and packing of the finer fraction. Definition of  $m$  is based on best fitting of a SSL and common ranges found in literature (Thevanayagam 2007; Rahman et al 2008). For fine dominated structure of AST, regardless of R, this research found  $m=0.28$  to be statistically significant (Table 4.3). Final calculation of  $e_t^*$  is shown in Eq. A.14.

$$d_r = \frac{D_{10}}{d_{50}} = \frac{6}{0.015} = 400 \quad (\text{A.12})$$

$$f_c = \frac{V_t}{V_r + V_t} = \frac{0.457}{1.457} = 0.31 \quad (\text{A.13})$$

$$e_g^* = \frac{e_g}{f_c + \frac{1-f_c}{d_r^m}} = 0.52 \quad (\text{A.14})$$

The calculation for equivalent tailings void ratio shown above is example calculation following guidelines found in the literature represented on Section 2.2.. A fine dominated structure was chosen as an example once the majority of mixtures in this study were found to be fine dominated structures. Calculation of equivalent rock void ratio differs little, and guidelines presented in Section 2.2. Results for all mixtures is shown in Fig 4.3.

## REFERENCES

- Rahman, M. M., Lo, S. R., and Gnanendran, C. T. (2008). On equivalent granular void ratio and steady state behavior of loose sand with fines. *Canadian Geotechnical Journal*, 45(10), 1439-1456.
- Thevanayagam, S. (1998). Effect of fine and confining stress on undrained shear strength of silty sands, *Journal of Geotechnical and Geoenvironmental Engineering*, 124(6), 479-491.
- Thevanayagam, S. (2007). Intergrain contact density indices for granular mixes I - Framework, *Journal of Earthquake Engineering and Engineering Vibrations*, 6(2), 123-134.